SECURITY MARKING

The classified or limited status of this report applies to each page, unless otherwise marked.
Separate page printouts MUST be marked accordingly.

THIS DOCUMENT CONTAINS INFORMATION AFFECTING THE NATIONAL DEFENSE OF THE UNITED STATES WITHIN THE MEANING OF THE ESPIONAGE LAWS, TITLE 18, U.S.C., SECTIONS 793 AND 794. THE TRANSMISSION OR THE REVELATION OF ITS CONTENTS IN ANY MANNER TO AN UNAUTHORIZED PERSON IS PROHIBITED BY LAW.

NOTICE: When government or other drawings, specifications or other data are used for any purpose other than in connection with a definitely related government procurement operation, the U. S. Government thereby incurs no responsibility, nor any obligation whatsoever; and the fact that the Government may have formulated, furnished, or in any way supplied the said drawings, specifications, or other data is not to be regarded by implication or otherwise as in any manner licensing the holder or any other person or corporation, or conveying any rights or permission to manufacture, use or sell any patented invention that may in any way be related thereto.

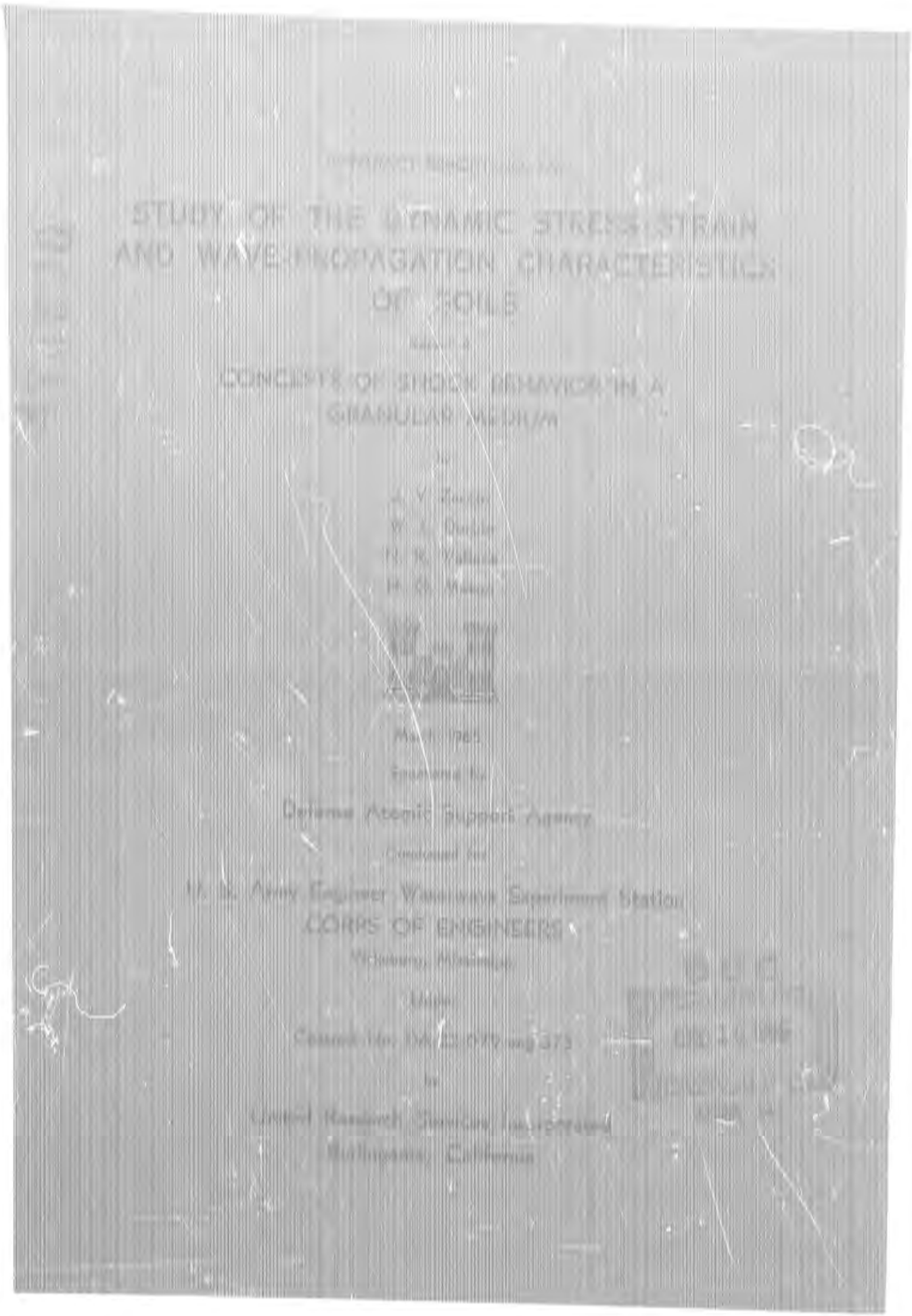

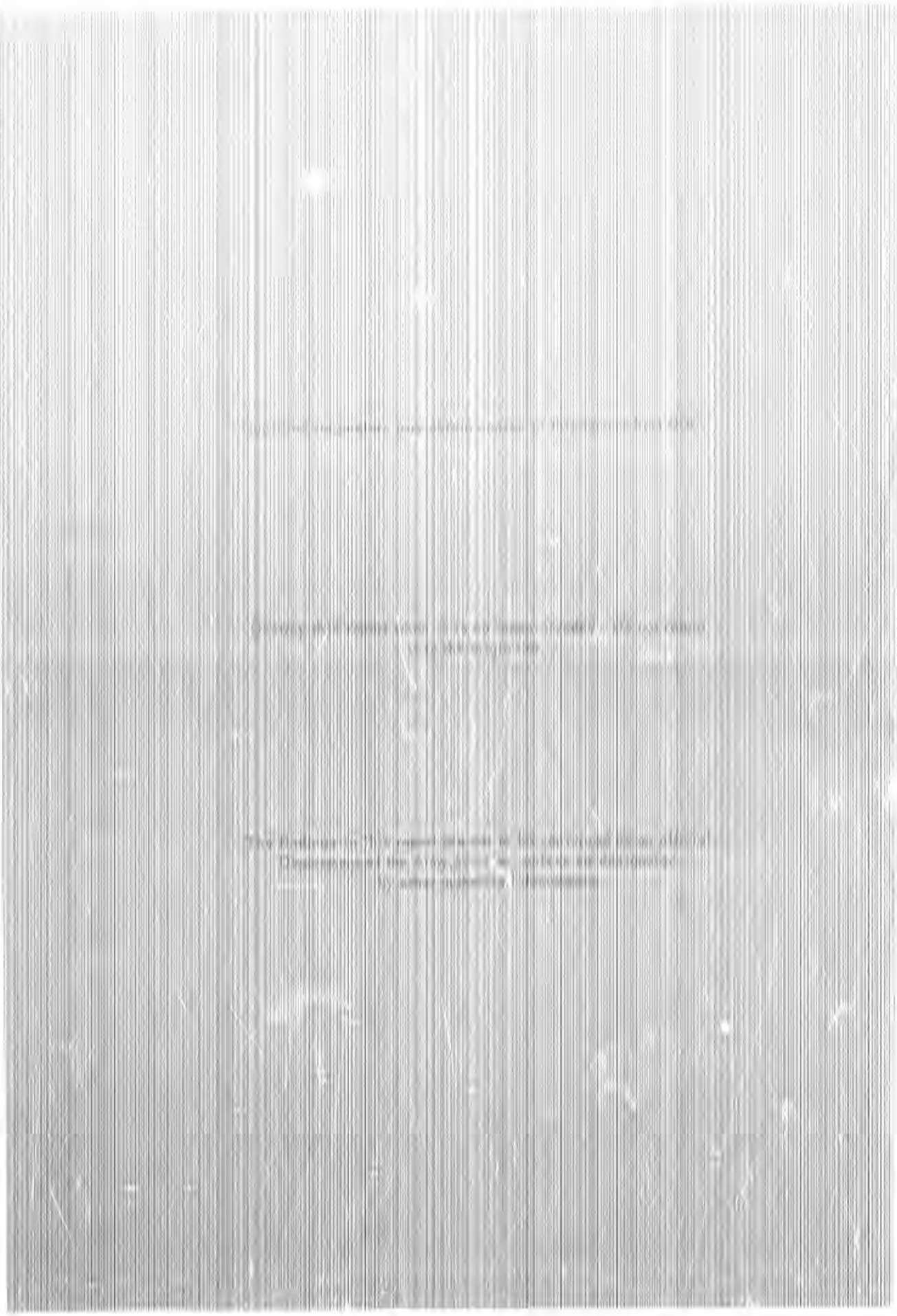

Contract Report No. 3-91

STUDY OF THE DYNAMIC STRESS–STRAIN AND WAVE-PROPAGATION CHARACTERISTICS OF SOILS

Report 4

CONCEPTS OF SHOCK BEHAVIOR IN A GRANULAR MEDIUM

by

J. V. Zaccor
W. L. Durbin
N. R. Wallace
H. G. Mason

March 1965

Sponsored by

DEFENSE ATOMIC SUPPORT AGENCY

Conducted for

U.S. ARMY ENGINEER WATERWAYS EXPERIMENT STATION
CORPS OF ENGINEERS
Vicksburg, Mississippi

Under
Contract No. DA-22-079-eng-373

by

UNITED RESEARCH SERVICES, INC.
Burlingame, California

(URS 637-25)

CONTENTS

Contents (Continued)

ILLUSTRATIONS

Illustrations (Continued)

Illustrations (Continued)

Illustrations (Continued)

ABSTRACT

This report summarizes current URS understanding of wave propagation in a cohesionless dry granular material in response to loadings suddenly applied and held at constant magnitude.

Experimental studies of propagating waves were conducted in which measurements were made of stress and displacement, as a function of time and position along a column of granular material, so that the stress–strain relationship, and wave and particle velocities could be determined. The latter quantities, thus obtained from experimental measurements, have been compared with values obtained from applicable equations of state. A number of equations of state are considered.

Two equations of state appropriate to rigid-pack conditions have been discussed. They apply to very different, but regular, packings of equi-radii elastic spheres where Hertz-type contact forces prevail and rearrangement of particles under loading is not allowed. These two equations of state were derived only from material properties of the individual particles and the packing arrangement. In addition, equations of state appropriate to conditions where particle relocations occur during loading have also been developed from the measured stress–strain relationship.

From the equations of state, shock, sound, and particle velocities have been obtained as derived quantities and compared with those obtained from experiment.

Excellent agreement has been found between experiment and theory. Experimentally it has been found that where no initial stress exists prior to dynamic loading, the behavior is governed entirely by particle-relocation phenomena. Where an initial-stress condition exists prior to loading, elements of response that are characteristic of a rigid-pack condition may be found to be superimposed on the response associated with particle relocation.

With regard to damage, the pertinent response is that governed by particle-relocation phenomena.

Pertinent to the subject of sidewall friction, a number of observations have been made during the course of this study. These observations, and others drawn from the literature, have been summarized in an appendix in a form which provides a relationship between pressure and depth of cover for the static case. Observations of some of the effects of dynamic behavior of sidewall friction are discussed.

NOTATION

The following symbols have been adopted for use in this report:

A	A constant, characteristic of the packing
B	One-half the span of the container
C	Velocity of sound in the material behind the shock front
C_o	Velocity of sound in the material ahead of the shock front
c	In the text: normal compliance; In Appendix A: cohesion
D	Diameter of the container
E	Internal energy/unit mass
e	Natural logarithm
e_o	Initial void ratio
f	Coefficient of friction
g	Acceleration due to gravity
K	Ratio of the horizontal (lateral) to the vertical (axial) stress
N	Normal force
n_o	Initial porosity
q	Surcharge per unit area
R	Radius of a particle
RD	Relative density
T	Kinetic energy per unit mass

Notation (Continued)

t	Time
U	Shock-wave velocity
u	Particle velocity (incident wave)
u_r	Particle velocity (reflected wave)
V	Volume
Z	Depth of the soil
γ_o	Initial bulk density or unit weight
ϵ	Strain
$\Delta\epsilon$	Strain increment (corresponding to $\Delta\sigma$)
$\Delta\epsilon_r$	Peak strain increment (corresponding to $\Delta\sigma_r$)
μ	Shear modulus of the material
ν	Poisson ratio of the material
ρ	Mass density (γ_o/g)
ρ_o	Mass density ahead of the front
ρ_i	Mass density for the particular condition that $\sigma = 0 = \sigma_o$
ρ_f	Final mass density (in the limit of rigid pack)
ρ^*	Mass density function
σ	Absolute stress
σ_o	Initial stress
σ_1	In the text: a parameter in the equation of state of the material; in Appendix A: axial stress

Notation (Continued)

σ_3	Lateral stress
σ_r	Reflected (absolute) stress
σ_v	Vertical stress on a horizontal section at depth Z
$\Delta\sigma$	Stress increment ($\sigma - \sigma_o$)
$\Delta\sigma_r$	$\sigma_r - \sigma_o$
φ	Angle of internal friction
$\tan \varphi$	Coefficient of internal friction of the soil

Section 1
INTRODUCTION

In underground protective construction, effective use of earth media as a shield against nuclear weapons depends on learning how to predict media response to nuclear weapons loading characteristics. As part of a long-range study program at United Research Services (URS), specialized equipment and techniques were developed that have made possible a laboratory study of soil response to certain nuclear weapons loading characteristics. The subsequent step has been to learn the general nature of the significant effects associated with material response. These effects should be predictable through use of the conservation laws of mechanics once an applicable equation of state is identified. An applicable equation of state will be identified when stress—strain behavior is related to characteristics of propagating waves, in particular those that define the momentum transfer process and hence determine the deliverable impulse. If for one material the salient features having to do with determining the impulse deliverable at any point in a medium can be determined, the same procedures might be applied to other materials, and finally, it might be possible to learn how to make more general extrapolations to a wide range of materials, perhaps from simply measured parameters of the soil itself. A series of four reports dealing with the more important contributions to date of the long-range program summarized above is completed with this report. A brief summary of the individual report contributions follows.

PROGRAM REVIEW (Reports)

Report 1 of this series provides a current review of concepts relating to soil behavior, evolved at URS, that led to development of the present techniques and equipment used in this program and describes that equipment. Report 2 demonstrates some implicit wave-propagation relationships, in the form of graphical summaries, for several granular materials. Report 3 contains an explicit graphical summary of the relationship between stress–strain behavior and measured wave and particle velocities for several granular materials, including some of those employed in obtaining the results of Report 2. The present report (Report 4) contains additional information for a dry granular cohesionless material concerning parameters that are indicative of the deliverable impulse.

The information contained in this report is in the nature of an extension of previously presented ideas and information in order to include variations in initial stress among the conditions under which it is possible to make predictions of the deliverable impulse (i.e., determine distribution of stress and particle velocity as a function of position and time) in laboratory systems. It is anticipated that with additional study on unloading aspects, on time-dependent effects associated with initial stress conditions (in essence overburden stresses), and on boundaries, it should be possible to arrive at a fairly complete understanding of the behavior of one dry granular cohesionless material and,

hence, methods for a complete evaluation of any other. When that point is reached, application of similar procedures might be expected to enable field predictions to be made from laboratory studies of site material and from a knowledge of the applicable loading geometry and field boundary conditions.

APPROACH

Current URS understanding of wave propagation in a dry granular cohesionless material, in particular 20 – 30 Ottawa sand, has been derived from an experimental program in which measurements were made of the distribution of momentum and impulse as a function of position and time along a column for certain loading and boundary conditions. In order to simplify the problem, stepped shock loadings have been used in a system in which lateral confinement is generated as a result of particle relocations that occur under the axial loading resulting in a stress – strain ($\sigma - \epsilon$) behavior characterized by $d^2\sigma/d\epsilon^2 > 0$. Only first loadings have been considered in order to determine the behavior associated with irreversible processes. The objective has been to learn how to predict the impulse delivered at a given location as a function of source and medium properties. Equations governing the conservation of mass and momentum have been applied, and the stress – strain relationship has been used, in effect, as the equation of state for the material. The net result of using this approach and applying constant conditions ahead of and behind the wave front has been to

arrive at an understanding of the stress-strain-initial-stress relationships as they apply to propagating waves.

Section 2
BACKGROUND

As stated earlier, in order to predict soil response to an applied dynamic loading it is necessary to determine what constitutes an applicable equation of state for the conditions of interest so that the conservation laws of mechanics may be applied. Such an "applicable equation of state" (dynamic in this case) is merely a governing relationship that has been shown to link the state of the medium uniquely to the loading and boundary conditions of interest. The point, is that once identified, the dependence of the equation of state on medium and boundary properties may be studied, and then this information may be used to predict dynamic phenomena. An equation of state may take the form of a pressure–density (pressure–volume) or stress–strain relationship. A relationship defined quantitatively implies quantitative prediction of behavior. Naturally, qualitative predictions are possible simply from the general form of an equation of state. For example, the existence of stress–strain behavior characterized by $d^2\sigma/d\epsilon^2 > 0$ carries with it the implication that induced stress waves having slowly increasing stress fronts should exhibit a tendency for their fronts to steepen. This situation arises because higher stress portions of the pulse propagate with higher velocities and thus "catch up" to the lower stress portions. If this type of process is continued, eventually a shock wave will result (Ref. 1, pp. 21–23).

Thus the form of stress—strain behavior indicated above implies formation of shock waves, and hence it is instructive to examine waves propagating in soils under these conditions in order to discover more about shock-wave properties. Some similarities in characteristics of waves and similarities in the behavior of various media may be expected. Nevertheless, preconceived notions about just what these similarities should be can seriously impede their identification and, hence, their constructive use.

It is important to realize that the form of stress — strain behavior indicated above ($d^2\sigma/d\epsilon^2 > 0$) is a "sufficient condition", to provide a tendency to form shocks, and that it may or may not involve the existence of real boundaries. As an example of each possibility, studies conducted in the laboratory in columns of granular media have shown the "sufficient condition" to be dependent on the actual sample boundary conditions (since they greatly influence the shape of the stress—strain curve). In another medium, i.e., the atmosphere, the "sufficiency" prevails even though the wave is spherically expanding. It may be noted the term "shock" wave is applied to waves that develop in free air from detonation of explosives or simply from rapidly moving objects, even though these are not conditions that lead to <u>stable</u> shocks. So also, shock fronts may develop from point source loadings in other media, and, thus, conceivably in soil.

Whether they do depends on the form of the applicable equation of state. The object of this discussion is to establish that the restrictive terminology of shock, as it applies to propagation of stable shocks,* is not the connotation intended here.** Furthermore, there is no requirement that strains be precluded in directions other than that of the propagating wave in order for shocks to develop. Steepening of wave fronts can also occur under conditions wherein lateral strains are permitted. Provided constant conditions are maintained ahead of and behind the wave front, even stable shocks may be propagated under these less restrictive boundary conditions.

In view of the fact that many experimental programs to investigate soil response have been undertaken in granular media under conditions in which stress–strain behavior has been characterized throughout some or all of the range investigated by $d^2\sigma/d\epsilon^2 > 0$***, it is surprising that shock wave concepts have not received much more than cursory recognition.

---

* With the requirement for constant conditions ahead of and behind the wave front.

** If reference to a stable shock is intended, it will be stated.

*** This condition has been maintained by a number of investigators, at least under some circumstances (Refs. 2–6).

There are a number of reasons why this has occurred; but perhaps the most important is that there has been a general lack of appreciation of the fact that a shock wave need not have an abrupt front, but may actually be required to have a finite transition zone.

The reason a finite transition zone might occur is discussed in Section IV of Ref. 7, which contains a brief discussion on the influence of time-dependent stress–strain behavior on shock propagation in porous media. It is stated there that when a shock in the form of a discontinuity is induced in media that display latent straining, it will have to degrade to a finite rise time. For simplicity it might be envisioned that stable shocks that have finite rise times are a consequence that stems from certain kinds of unloading processes, i.e., those that have a finite duration. Unloading sources of this type can derive from boundary or material properties (or both) as a direct result of the loading, and their origin, in effect, also propagates with the wave front. In general terms, we refer to such behavior as a "stress relaxation." The term "stress relaxation" is descriptive of the type of phenomenon but does not at all give insight into its source. However, when reference is made to viscous effects, it is likely to indicate a belief that it is a behavior that stems from the sample properties only. Thus, we believe that such behavior derives from latent relocation of particles, but have yet to answer the question "in what manner?"

It is postulated that the answer lies in the following time-dependent behavior. It is clear that wave propagation is the process of the transmission of information and that this process always takes a finite time. Therefore, if we were to physically remove a particle from the sample* (or simply relocate one), it would result in the propagation of an unloading wave from that disturbance which would "inform" the surrounding sample. The effect would be to cause additional particle relocations to take place in the surrounding region. These new relocations result in propagation of similar information, of ever-decreasing magnitude, until a stable condition is attained. In essence this is a description applicable to the state of affairs in the loading front of a wave propagating in an assemblage of granular particles. During the passage of material through the changing stress region at the front, adjustments occur very rapidly, but, nevertheless, require a finite time. Thus, it appears that this sort of time-dependent behavior, i.e., that due to particle relocations, might well account for observed short-term (several hundred microseconds) relaxation** effects.

---

* For a realistic process that is effectively the equivalent of such an action, see a discussion of bridging arrays, pp. A-10, 11 of Ref. 8.

** Ref. 9, p. 5.

Additional short-term relaxation effects are likely to be engendered by other events leading subsequently to particle relocation. For example, a similar type of behavior is to be expected where particle fracturing occurs. Intuitively, it would seem the addition of another process, i.e., the fracturing process, would result in somewhat longer relaxation times. Finally, variations in restraint, provided by the boundary perpendicular to the wave front, should again result in a similar initiation of unloading waves as the particles relocate due to lateral displacement. These relocations might also be expected to change the nature of the front, and the change would depend on the time required to reach an equilibrium condition for this process. A longer transition zone at the wave front would be expected to coincide with larger lateral displacements.*

The particular relaxation effects just described, two material and one boundary, derive from the loading as a result of "failure" of particular grain assemblages to support the load and so appear to be in a nature of "plastic deformation." Nevertheless, the "failure" processes are finite in duration and must eventually lead to a stable front

---

* Since lateral displacement at a boundary causes an unloading wave to propagate, it is clear that a gauge located in a column will be affected, insofar as recording rise times is concerned, by the time required for news of this adjustment to be transmitted to the gauges. Full adjustment is likely to require more than one round trip. Observation of this behavior is dependent, of course, on-gauge resolution.

(provided constant conditions are maintained in the material ahead of the front and in the applied loading). We term the above-described propagating wave a stable shock, even though behavior at that front appears to include delayed particle relocations (with its semblance of plastic behavior).

Consider, for a moment, an experiment in which an impulsive load is applied to a column of granular material in which the pore air space is partially evacuated to produce pressures less than ambient. In this case, the constant confining pressure developed through evacuation would be sufficient to prevent lateral deformation from continuing to failure, provided the constant confining pressure is not exceeded by the lateral pressure generated in the soil by the impulsive load. The maximum load that can be supported in this fashion may be estimated from observed ratios of lateral to axial stress. Since this ratio is approximately one-half (depending on material and density), an axial stress increment slightly less than the confining pressure might be stably supported. Thus, when overpressures in excess of this amount are applied, the behavior of the higher stress portion of the front would then be plastic. However, the portion of the overpressure below the supportable amount will propagate with a constant velocity characteristic of a shock. In this case (contrary to the one in which the entire front is a shock) the rise time to the peak stress would appear to increase with distance

propagated.* Unfortunately, this "shock-plastic" behavior appears no different from what is called elasto-plastic, in that the lower stress regions propagate with constant velocity while the higher stress portion is seen to spread out with distance propagated.

The behavior in the constant confining pressure experiment is of this form because the lateral displacements do not cease during the period of examination. However, had these displacement and, hence, this plastic failure been limited as they are in the wave-propagation containment devices of Seaman (Ref. 4), Stoll and Ebeido (Ref. 6), and URS (Ref. 3), it would appear simply as a relaxation effect.** Thus, the entire front, from the first disturbance to the peak stress, would propagate unchanged as long as the "constant conditions" requirement for a shock is maintained. Examples of the sorts of things that can prevent maintaining such constant conditions are sidewall friction,*** and increasing geostatic stress (Ref. 4).

---

* This behavior can be clearly seen in measurements made by Selig all along a 64-in. column (Ref. 5, p. 49) and by Whitman (Ref. 2) at the reaction end of a sample.

** These relaxation effects are of short duration and vary in amount in the different devices cited because of variations in the degree of confinement and diameter of the container.

*** See Appendix A. Sidewall friction is the cumulative resistance, as a result of boundary constraints, to free displacements of the body of the sample in the direction of the propagating wave.

Although the former is, in effect, also an unloading source, it continually generates unloading waves throughout the period of load application that are variable in magnitude all along the column, so that it is indeed impossible to achieve a steady state under such boundary conditions.

The phenomenological picture has been presented as an attempt to construct a physical counterpart of the mathematical representations (to be discussed later) that have been found to describe the observed behavior and also to explain how this behavior is related to observations of other investigators. There are a number of important conclusions to be drawn from the foregoing views. Stable shocks will not be observed where sidewall friction occurs. Stable shocks in granular soil media will not be characterized by an abrupt front, but will have finite transition zones. The length of the transition zones will at least be a function of both material properties and the lateral restraint. Consequently, it should not be surprising that this zone has been found to be different in the same material, at the same density, under the same loading condition by different investigators, all of whom were using devices having different forms of lateral containment.

For some of the <u>experimental</u> difficulties in identifying stable shocks, see Appendix B. A formal mathematical development which describes some of the properties of steady one-dimensional shock waves appears in the next section.

Section 3
SHOCK WAVES IN GRANULAR MEDIA

It is well known that under certain conditions of concavity and monotonicity in the equation of state of a medium, a compression wave will steepen into a shock wave.* These conditions simplify when the equation of state consists of a relation between the pressure and density with little or no dependence on the entropy (Ref. 10). Then the essential requirement is that the compressibility decrease with pressure, i.e., that the stress−strain curve be concave about the stress axis. Under certain circumstances, this condition is satisfied. Of particular interest is the case of a plane-fronted stress wave propagating in a dry, granular medium. For such a wave, of infinite extent in the plane of the wave front, the condition established on every element of the medium behind the wave front is that of zero strain in any direction parallel to the plane of the front. The distortion which an element of the medium undergoes in passing through the wave front is determined by only a single relationship connecting the axial strain in the direction of wave propagation with the axial stress.

Laboratory studies of dry, granular samples subjected, in essence, to a one-dimensional compression (i.e., substantially laterally confined)** have indicated that for some

---

* This has been shown to apply to a porous medium (Ref. 7).

** For example, Ref. 11.

initial void ratio, zero initial stress, and steadily increasing applied stress, the shape of the stress–strain curve is basically determined by three separate regions of behavior. (See Fig. 1.)* As already indicated a qualitative description of behavior can be deduced from the general form of a stress–strain relationship such as depicted. Thus, from a stress of zero to some value σ_A, the particles move relative to each other in such a way as to decrease the void ratio while at the same time experiencing contact forces between particles. In going from stress σ_A to some value σ_B, relative motion of the granules and the change of void ratio with increasing stress is negligible, and the strain as a function of stress depends almost entirely on the elastic compression at the points of contact. The stress–strain behavior in this region derives from elastic theory as given by Hertz (Ref. 12) for the normal forces and by Mindlin (Ref. 13) for the shear forces at the contact points.

Beyond the stress σ_B, the particles undergo crushing and further relocation. Whereas the phenomena in the first two regions of Fig. 1 produce a stress–strain curve concave (upwards) about the stress axis, the stress–strain in the region of crushing is concave about the strain axis.

---

* For the defined conditions experimental observations yield the general form shown. However, for conditions other than those defined, in particular for a finite, large initial stress, a more general behavior may be observed which includes another knee (i.e., such as that shown in Fig. 1 in region III) closer to the origin. Such behavior is at present excluded from the discussion in order to get at shock wave behavior (associated with any portion of a stress–strain curve such as regions I and II of Fig. 1).

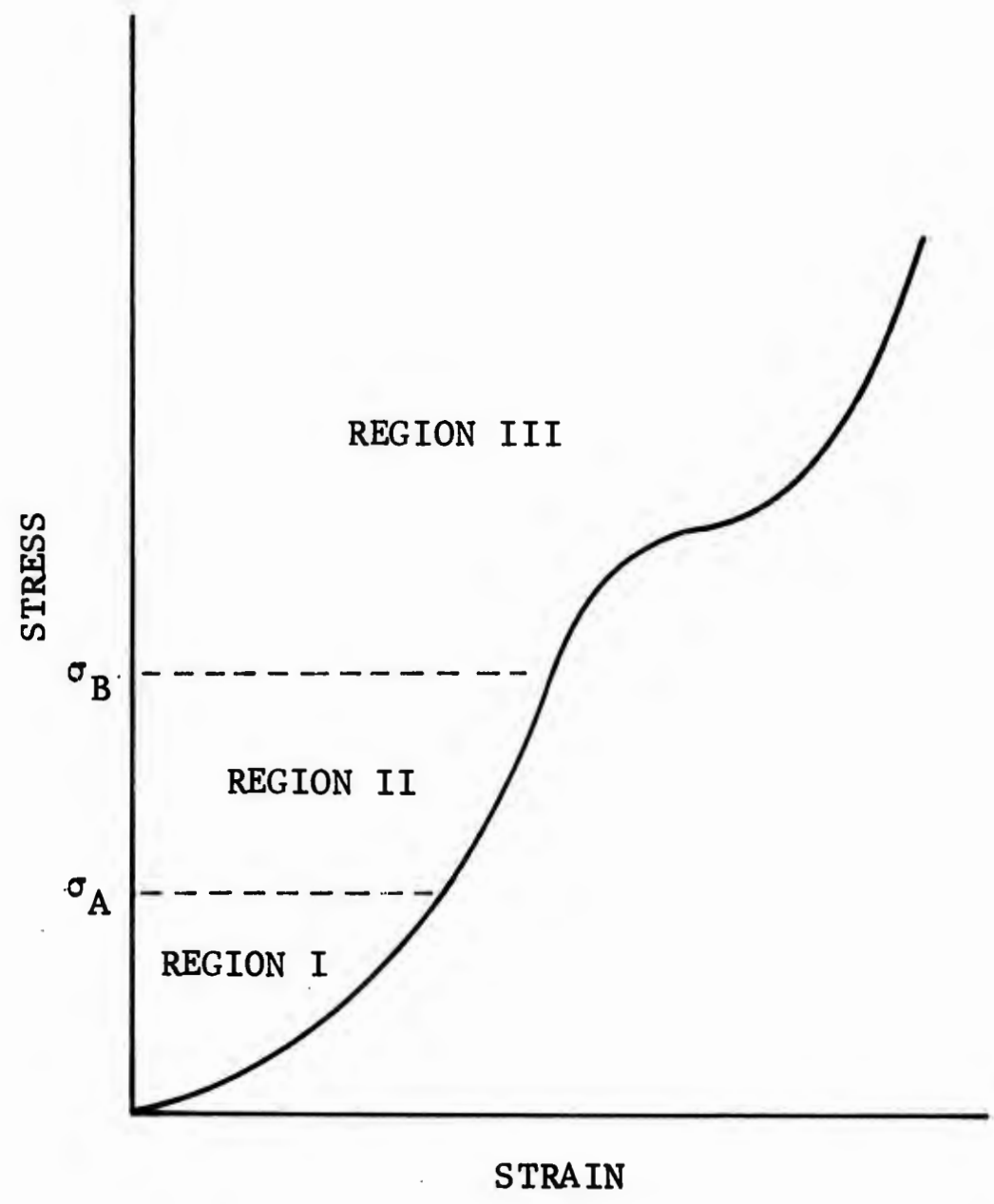

Fig. 1. Typical Stress—Strain Curve for One-Dimensional Loading of a Fully Confined Granular Medium With no Initial Stress

As long as the stress–strain curve has a single curvature concave about the stress axis, a plane-fronted compression wave will steepen into a shock wave. If the stress behind the front is a constant independent of distance from the front, the shock front will eventually achieve a steady-state condition. That is, the shape of the stress–distance curve as measured in a coordinate system moving with the front will remain unchanged in time. The steady shock in a granular medium is not characterized by discontinuities in the pressure–distance curve or any of its derivatives, but rather by the time invariance of this curve as seen from the moving coordinate system. The shock-wave transition zone connecting the two states of constant stress ahead of and behind the shock may have any shape, depending on the relaxation behavior of the granules in passing through the zone. It is, however, the time-steady property of this zone which makes possible application of conservation conditions of mass, momentum, and energy, i.e., the Rankine-Hugoniot conditions; and this property, in turn, depends upon the upward concavity of the stress–strain curve. Therefore, the stress region of crushing is excluded from the following discussion. To simplify still further, the particles will at first be assumed to be spheres of uniform size in some initial state of close packing. This merely combines the stress of both regions I and II into a single region dominated by elastic contact forces characteristic of region II and makes possible computation of the stress–strain curve from the elastic constants of the particles themselves. Subsequent to analysis of the close-packed aggregate, modifications will be

made in the equation of state to account for particle relocation typifying region I.

SHOCK WAVES IN CLOSE-PACKED GRANULAR MEDIA

For certain regular packings of uniform, elastic spheres under complete lateral confinement, the Hertz theory of contact forces can be shown to give as the functional form for the stress – strain curve

$$\sigma = A\epsilon^{3/2} \tag{1}$$

A will be taken here to be a constant whose value depends on the geometry of packing and the elastic constants of the spheres.

As shown in Fig. 2, the shock wave is presumed to be a transition region separating two regions of constant state. The granular material ahead of the shock is under a uniform initial load, σ_o, and the shock compresses this material to the state of uniform stress, σ.

The Rankine-Hugoniot equations (e.g., Ref. 32, p. 38) for conservation of mass, momentum, and energy through the shock are:

Conservation of mass: $$\rho_o U = \rho(U - u) \tag{2}$$

Conservation of momentum: $$\sigma - \sigma_o = \rho_o U u \tag{3}$$

Conservation of energy: $$E - E_o = \frac{1}{2}(\sigma + \sigma_o)\left(\frac{1}{\rho_o} - \frac{1}{\rho}\right) \tag{4}$$

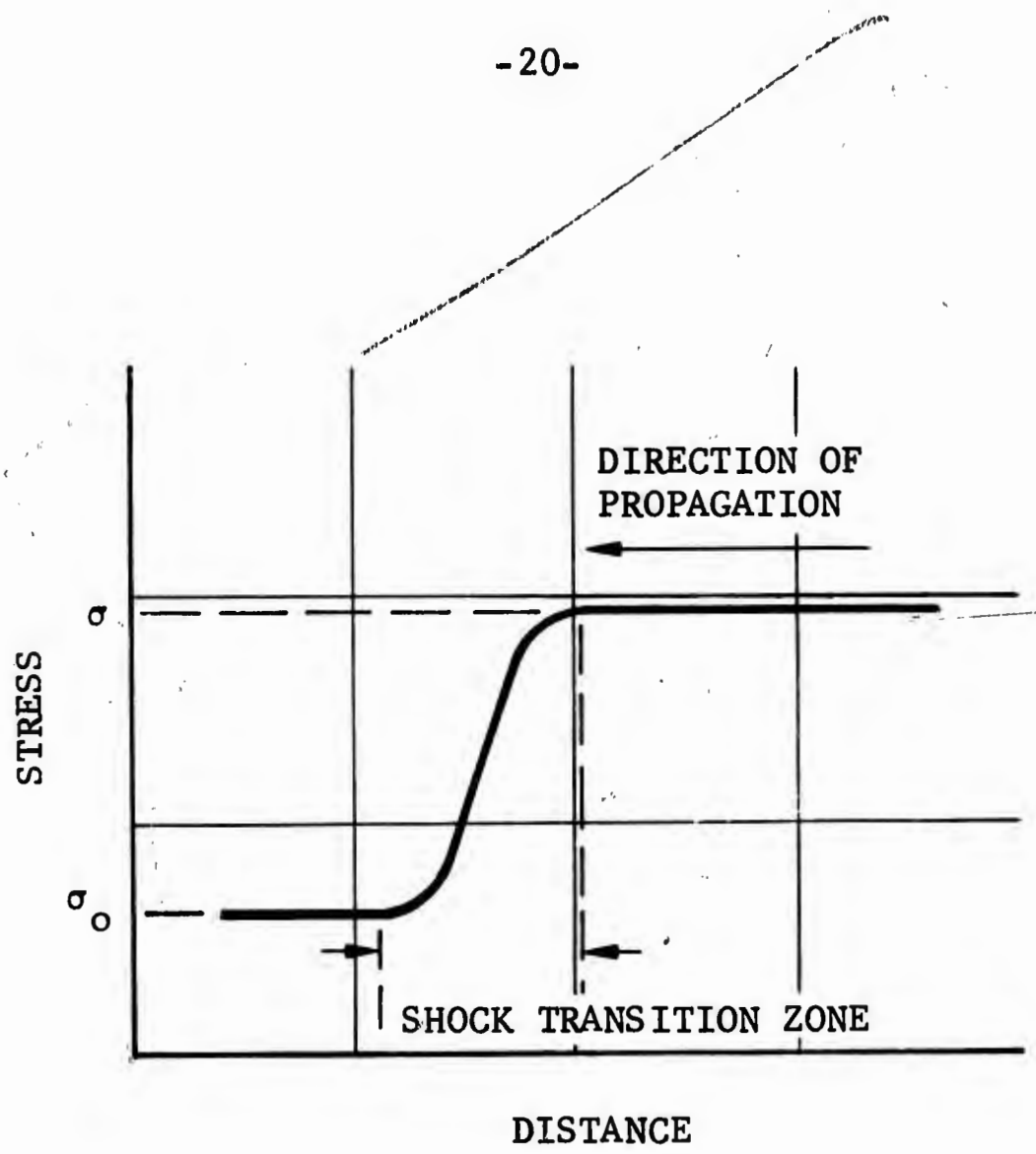

Fig. 2. Stress—Distance Diagram of a Stable Shock (Time-Independent Transition Zone) Connecting Two Regions of Uniform Stress

where

ρ = mass unit density

σ = absolute stress

E = internal energy

U = shock-wave velocity

u = particle velocity

The subscript 0 refers to conditions ahead of the shock, no subscript refers to conditions behind the shock, and the subscript i will apply to the mass density, or volume V per unit mass, for the particular condition that $\sigma = 0 = \sigma_o$.

Since the spheres have, for this discussion, been defined as perfected elastic and no redistribution of the sphere packing is to occur during loading, there is no entropy change, and the first two conditions alone determine the shock process.

The strain ϵ may be expressed in terms of the constant A [from Eq. (1)], the volume, or (since $V = 1/\rho$) the density change of an element of the medium by

$$\epsilon = \left(\frac{\sigma}{A}\right)^{2/3} = \frac{V_i - V}{V_i} = \left(1 - \frac{V}{V_i}\right) = \left(1 - \frac{\rho_i}{\rho}\right) \qquad (5)$$

and, hence

$$\frac{\rho_i}{\rho} = \left[1 - \left(\frac{\sigma}{A}\right)^{2/3}\right]$$

$$\frac{\rho_i}{\rho_o} = \left[1 - \left(\frac{\sigma_o}{A}\right)^{2/3}\right] \qquad (5a)$$

Equation (1) gives as the equation of state of the medium (taking into account the initial conditions)

$$\sigma - \sigma_o = A\left(\epsilon^{3/2} - \epsilon_o^{3/2}\right) \tag{6}$$

which on substituting from Eq. (5) becomes

$$\sigma - \sigma_o = A\left[\left(1 - \frac{\rho_i}{\rho}\right)^{3/2} - \left(1 - \frac{\rho_i}{\rho_o}\right)^{3/2}\right] \tag{6a}$$

The ambient speed of sound C_o may be determined from this equation. The sound speed C_o is defined as the speed with which an infinitesimal pressure wave will propagate through the material when subjected to uniform initial conditions. In this case a load σ_o. It is given (e.g., Ref. 10, Appendix to Chapter III) by

$$C_o^2 = \left.\frac{d\sigma}{d\rho}\right|_{\sigma = \sigma_o} \tag{7}$$

On differentiating Eq. (6a), and substituting from Eqs. (5) and (5a)

$$C^2 = \frac{d\sigma}{d\rho} = \frac{3}{2}A\left(1 - \frac{\rho_i}{\rho}\right)^{1/2} \frac{\rho_i}{\rho^2} = \frac{3}{2}A\left(\frac{\sigma}{A}\right)^{1/3} \frac{\rho_i}{\rho_i^2}\left[1 - \left(\frac{\sigma}{A}\right)^{2/3}\right]^2$$

and

$$C^2 = \frac{3}{2}\frac{A^{2/3}}{\rho_i}\sigma^{1/3}\left[1 - \left(\frac{\sigma}{A}\right)^{2/3}\right]^2 \tag{8}$$

and also from Eq. (7)

$$C_o^2 = \frac{3}{2}\frac{A^{2/3}}{\rho_i}\sigma_o^{1/3}\left[1 - \left(\frac{\sigma_o}{A}\right)^{2/3}\right]^2 \qquad (8a)$$

This is the "seismic" or "Hertzian" velocity in the granular array. It is not, in general, independent of direction through a regular packing of spheres. For one-dimensional loading considered here, the velocity of sound defined by Eq. (8) applies only in the direction of the loading.

By eliminating the particle velocity u from Eqs. (2) and (3) the shock-wave velocity is obtained as

$$U^2 = \frac{1}{\rho_o^2}\left(\frac{\sigma - \sigma_o}{\frac{1}{\rho_o} - \frac{1}{\rho}}\right) \qquad (9)$$

Using Eq. (5a), both ρ and ρ_o of Eq. (9) can be written in terms of a single density, i.e., ρ_i, to give

$$U^2 = \frac{A^{2/3}}{\rho_i}\left[1 - \left(\frac{\sigma_o}{A}\right)^{2/3}\right]^2\left(\frac{\sigma - \sigma_o}{\sigma^{2/3} - \sigma_o^{2/3}}\right) \qquad (10)$$

Figure 3 shows a plot of the velocity of sound C obtained from Eqs. (8), and from Eq. (10) plots of U for $\sigma_o = 0$ and $\sigma_o = 40$ psi. Evaluation of the constants A and ρ_i for the

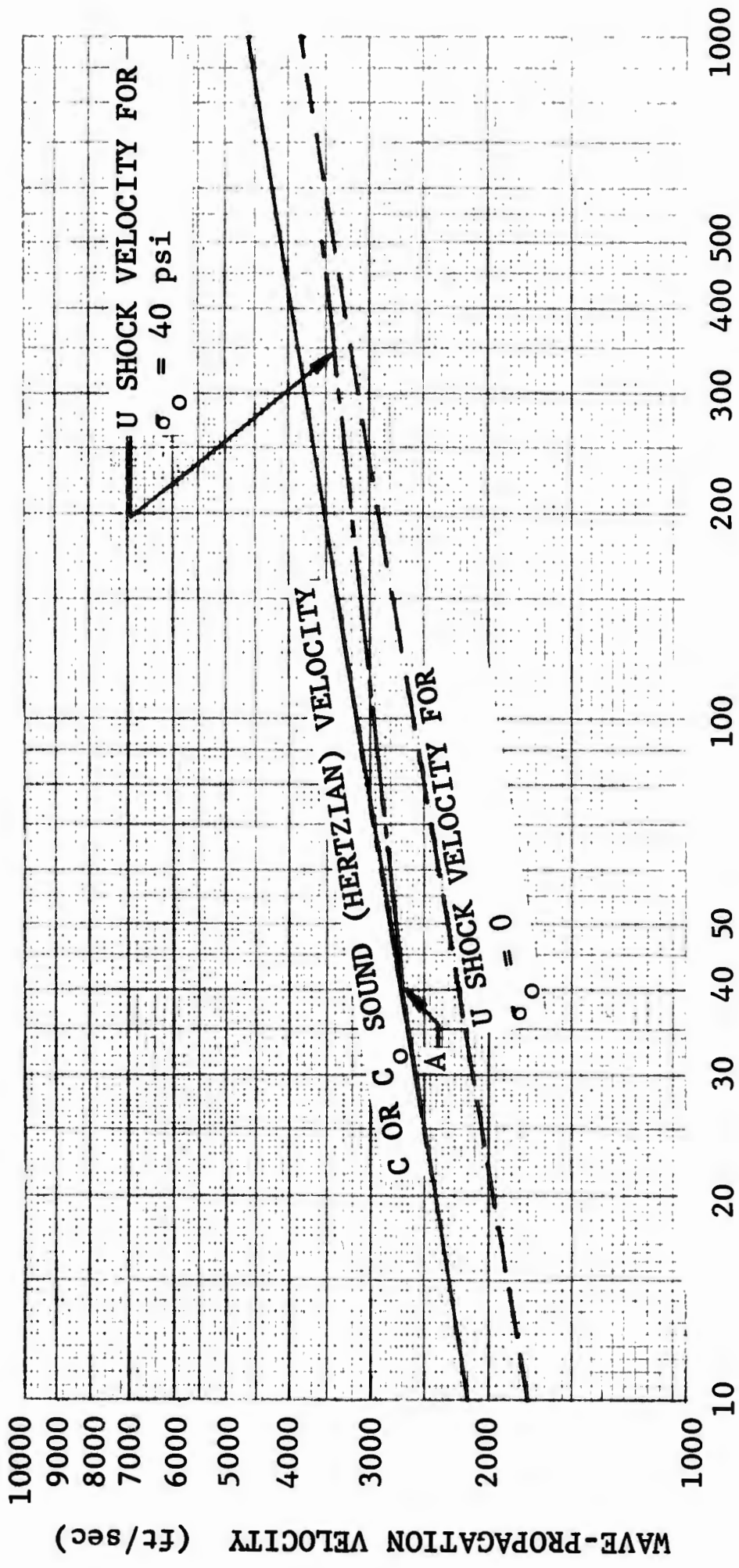

Fig. 3. Sound and Shock Velocities According to Eqs. (8) and (10)

example will be discussed later in the text ($A = 5.75 \times 10^6$ psi and $\rho_i = 122.4$ pcf). It can be seen that A is much larger than any stress depicted in Fig. 3. Consequently, the squared terms in brackets in Eqs. (8), (8a), and (10) are very nearly equal to unity. The ratio of U^2/C^2 appears to range from 2/3 to 1 as σ_o ranges from 0 to σ. The shock velocity is seen to decrease as the stress jump across the shock is decreased, and the three velocities C_o, U, and C become equal only in the limit of an infinitesimal stress difference on the two sides of the shock transition. (See point A, Fig. 3.)

The particle velocity behind the shock front is from Eq. (2):

$$u = U\left(\frac{\rho - \rho_o}{\rho}\right)$$

Substituting stress for density by means of Eqs. (5a) there obtains

$$u = U\left[\frac{\sigma^{2/3} - \sigma_o^{2/3}}{A^{2/3} - \sigma_o^{2/3}}\right] \tag{11}$$

On the other hand, from Eqs. (3) and (5a) u can be expressed by

$$u = \frac{\Delta\sigma}{\rho_o U} = \frac{\Delta\sigma}{\rho_i U}\left[1 - \left(\frac{\sigma_o}{A}\right)^{2/3}\right] \tag{12}$$

and since it has been stated $A >> \sigma_o$

$$u \sim \frac{\Delta\sigma}{\rho_i U} \tag{13}$$

For waves of finite amplitude, the particle velocity should always be determined from Eq. (12) or Eq. (13).

REFLECTIONS

When a one-dimensional wave of constant stress behind the front impinges on a perfectly rigid surface aligned normal to the direction of propagation, a reflected wave is produced which propagates back upstream through material at the state of stress established by the incident wave. For a linear equation of state, such as results from Hooke's law forces in linear elasticity, the ratio of reflected wave overstress to incident overstress has the specific value of 2. Nonlinear equations of state in which the stress–strain relation is concave upwards characteristically produce overstress ratios greater than 2, with the value of 2 achieved only in the limit of infinitesimal incident overstress.

The boundary conditions on reflection require that the granules' motion be stopped at the rigid wall. This is equivalent to superimposing a particle velocity for the reflected shock u_r equal in magnitude but opposite in direction to the particle velocity of the incident shock, i.e., $|u| = |u_r|$, where state variables behind the reflected

shock waves will be indicated by the subscript r. Across the reflected shock, the absolute stress goes from σ to σ_r. Thus from Eq. (11), substituting the appropriate subscripts to reflect the new conditions ahead of and behind the front,

$$u = U\left[\frac{\sigma^{2/3} - \sigma_o^{2/3}}{A^{2/3} - \sigma_o^{2/3}}\right] = U_r\left[\frac{\sigma_r^{2/3} - \sigma^{2/3}}{A^{2/3} - \sigma^{2/3}}\right] = u_r \qquad (14)$$

and there obtains from Eq. (14)

$$\frac{U^2}{U_r^2} = \left(\frac{\sigma_r^{2/3} - \sigma^{2/3}}{\sigma^{2/3} - \sigma_o^{2/3}}\right)^2\left(\frac{A^{2/3} - \sigma_o^{2/3}}{A^{2/3} - \sigma^{2/3}}\right)^2 \qquad (15)$$

Equation (10) gives

$$\frac{U^2}{U_r^2} = \left(\frac{A^{2/3} - \sigma_o^{2/3}}{A^{2/3} - \sigma^{2/3}}\right)^2\left(\frac{\sigma - \sigma_o}{\sigma_r - \sigma}\right)\left(\frac{\sigma_r^{2/3} - \sigma^{2/3}}{\sigma^{2/3} - \sigma_o^{2/3}}\right) \qquad (16)$$

Eliminating the wave velocities of Eqs. (15) and (16)

$$\left(\frac{\sigma_r}{\sigma} - 1\right)\left[\left(\frac{\sigma_r}{\sigma}\right)^{2/3} - 1\right] = \left(\frac{\sigma}{\sigma_o} - 1\right)\left[\left(\frac{\sigma}{\sigma_o}\right)^{2/3} - 1\right] \qquad (17)$$

This gives σ_r/σ as a fifth order polynomial in terms of σ/σ_o. Note that Eq. (17) is independent of A and, therefore, of the particular packing arrangement of the spheres. The curve of σ_r/σ versus σ/σ_o is shown in Fig. 4.

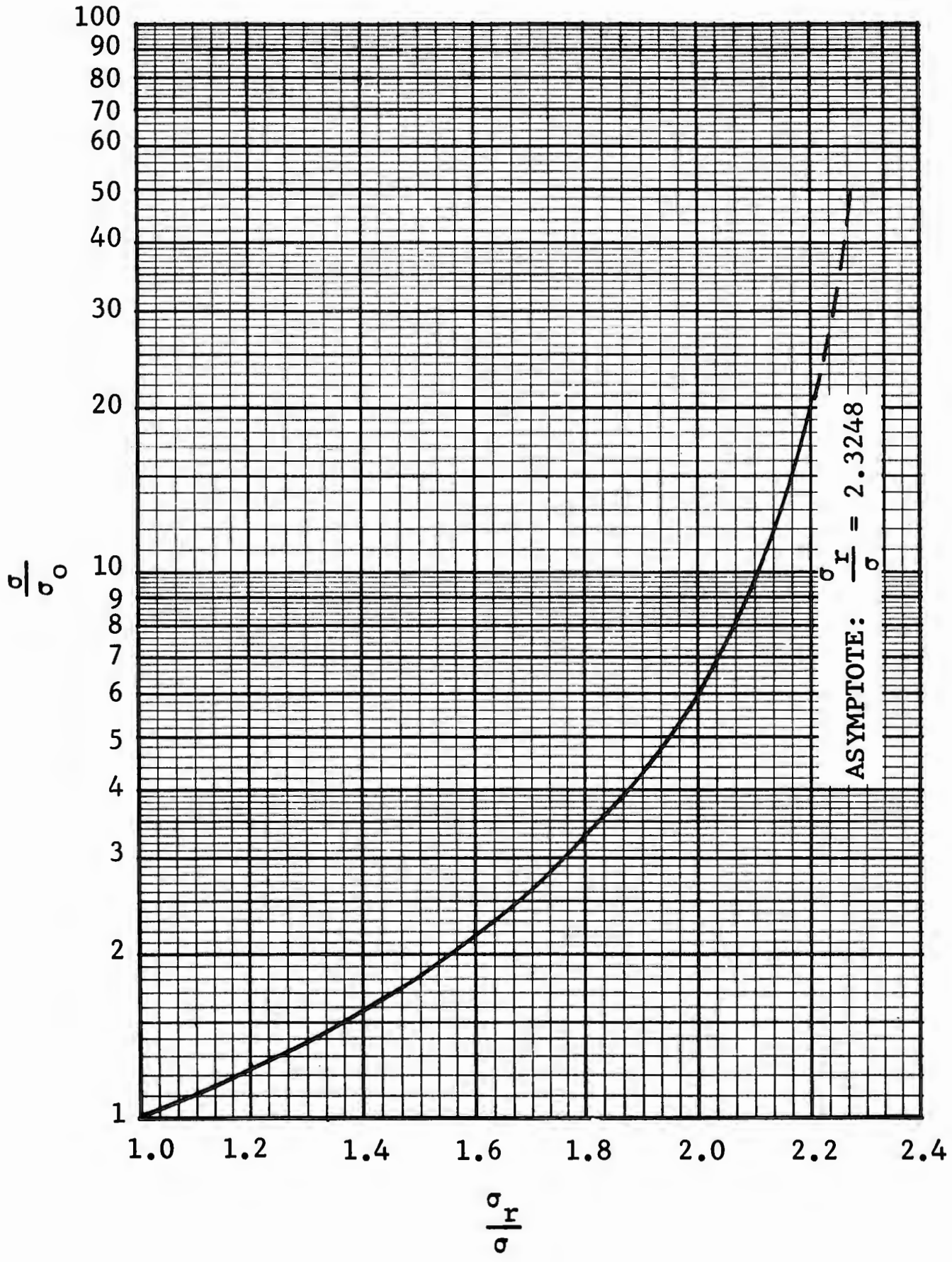

Fig. 4. Incident-Absolute-Stress Ratio Versus Reflected-Absolute-Stress Ratio for a Rigid Pack

ENERGY CONSIDERATIONS

It is also of interest to determine how the total energy is partitioned between kinetic and potential energy in the compressed region behind the steady-state shock front.

The internal energy (the same as the potential energy for this equation of state) of a unit mass of granules is

$$E = -\int_{V_i}^{V} \sigma' dV' \tag{18}$$

where the primes indicate the variable (and V becomes a fixed state). Substituting the equation of state, Eq. (6a),

$$E = -A\int_{V_i}^{V}\left(1 - \frac{V'}{V_i}\right)^{3/2} dV' = \frac{2}{5}\frac{A}{\rho_i}\left(1 - \frac{\rho_i}{\rho}\right)^{5/2} \tag{19}$$

Consequently the internal energy change per unit mass across the shock transition is

$$E - E_o = \frac{2}{5}\frac{A}{\rho_i}\left[\left(1 - \frac{\rho_i}{\rho}\right)^{5/2} - \left(1 - \frac{\rho_i}{\rho_o}\right)^{5/2}\right] \tag{20}$$

The kinetic energy per unit mass, T, behind the shock with respect to a coordinate system fixed in the undisturbed material ahead of the shock is given by

$$T = \frac{1}{2}u^2 \tag{21}$$

Using Eqs. (3), (9), and (6a) in Eq. (21) to eliminate u, U, and $\sigma - \sigma_o$

$$T = \frac{1}{2} A \left[\left(1 - \frac{\rho_i}{\rho} \right)^{3/2} - \left(1 - \frac{\rho_i}{\rho_o} \right)^{3/2} \right] \left(\frac{1}{\rho_o} - \frac{1}{\rho} \right) \qquad (22)$$

Writing both Eqs. (20) and (22) in terms of the stresses through Eqs. (5a) and forming the ratio of kinetic to potential energy

$$\frac{T}{E - E_o} = \frac{5}{4} \frac{(\sigma - \sigma_o)\left(\sigma^{2/3} - \sigma_o^{2/3}\right)}{\sigma^{5/3} - \sigma_o^{5/3}} \qquad (23)$$

This is again independent of the coefficient A. Although dimensionless quantities, such as the reflected-to-incident-pressure ratio and the kinetic-to-potential-energy ratio have been shown to depend only on the functional form of the equation of state, determination of absolute values of quantities of interest, U, u, and C, requires knowledge of the magnitude of A. For simple, regular packings of uniform spheres which satisfy the assumptions of the Hertz theory of contact forces, this coefficient can be determined directly from the packing geometry and the elastic constants of the spheres.

Consider the cubic lattice of spheres all of radius R, for which a unit cell is shown in Fig. 5b. This is the simplest lattice to discuss analytically, provided the applied forces are required to be parallel to the major axes. In one-dimensional loading along the axis indicated in Fig. 5b,

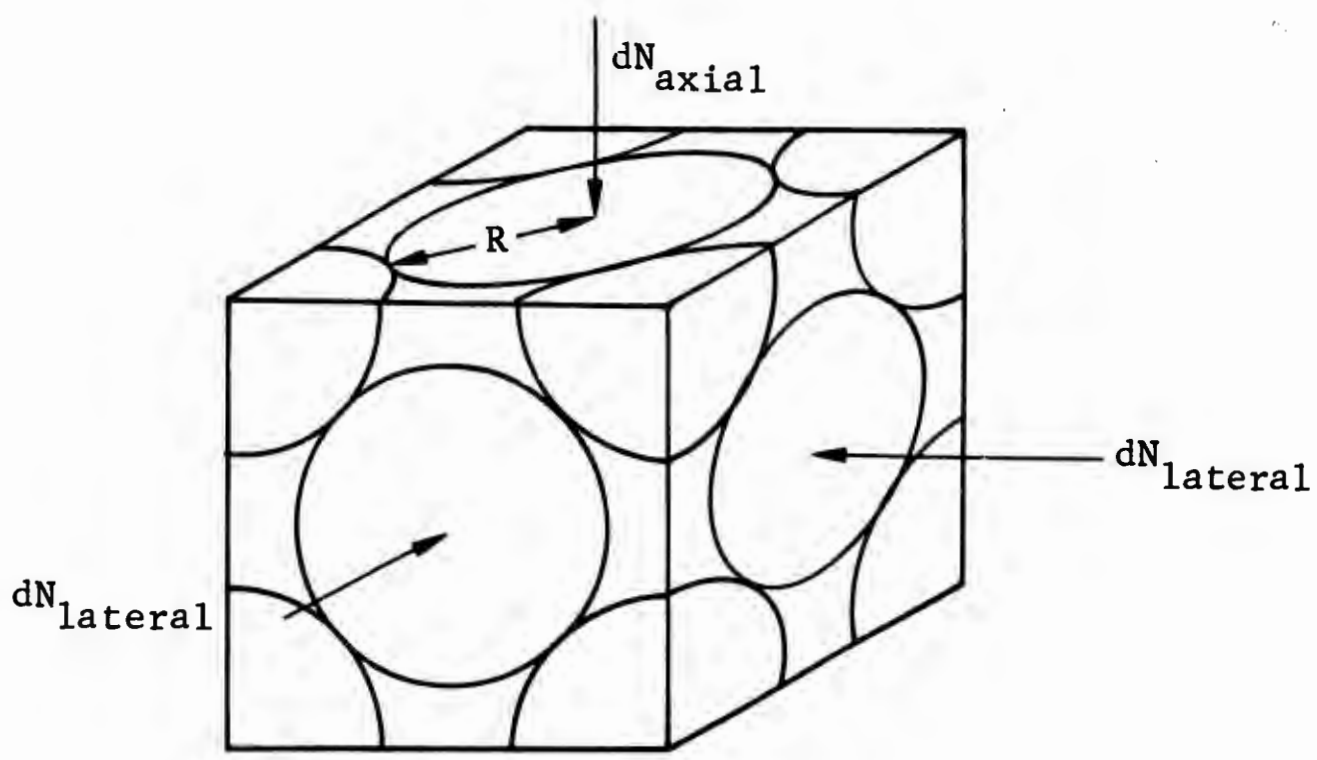

Fig. 5a. Unit Cell - Face-Centered Cubic Packing

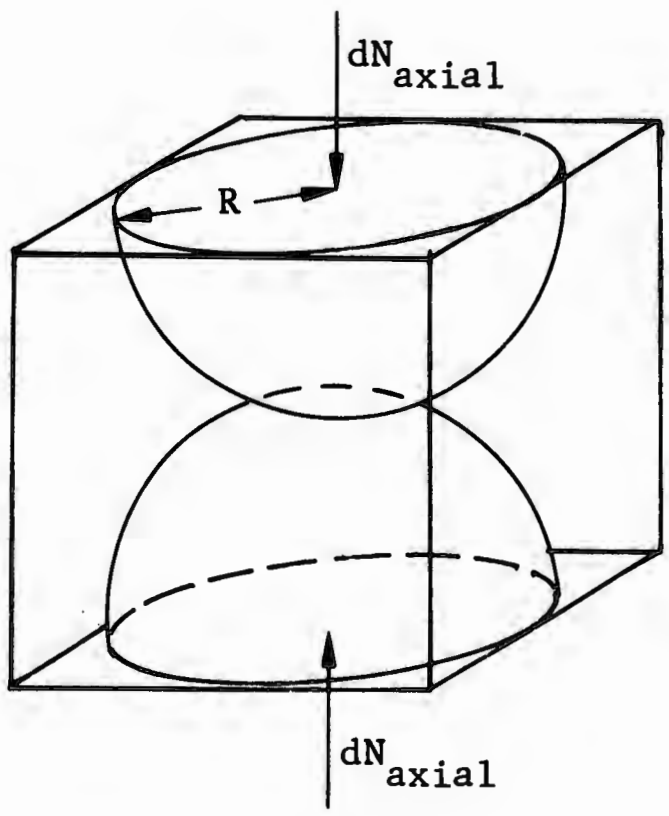

Fig. 5b. Unit Cell - Simple Cubic Packing

the constraint of zero lateral strain is automatically satisfied, and only normal forces appear at the circle of contact. The applied forces are related to the incremental stress by

$$dN = 4R^2 d\sigma \tag{24}$$

The relative displacement $d\alpha$ of the sphere centers is related to the normal forces by

$$d\alpha = c\,dN \tag{25}$$

where c is the normal compliance (see, for example, Ref. 14),

$$c = \frac{1 - \nu}{2\mu a} \tag{26}$$

μ is the shear modulus, ν is the Poisson ratio of the material comprising the spheres, and a is the radius of the circle of contact given by

$$a = \left[\frac{3(1 - \nu)NR}{8\mu}\right]^{1/3} \tag{27}$$

Combining Eqs. (24), (25), (26), and (27), one obtains

$$d\epsilon = \left(\frac{2}{3}\right)^{1/3}\left(\frac{1 - \nu}{\mu}\right)^{2/3}\sigma^{-1/3}d\sigma \tag{28}$$

Integrating and setting the constant of integration equal to zero

$$\sigma = \frac{2}{3}\,\frac{\mu}{1 - \nu}\,\epsilon^{3/2} \tag{29}$$

and therefore for the cubic packing

$$A = \frac{2}{3}\frac{\mu}{1 - \nu} \tag{29a}$$

The cubic packing with forces applied parallel to a major axis is incapable of physical realization, for the equilibrium is unstable. In the Hertz theory, distortion of a sphere in the neighborhood of the circle of contact produced by applied forces does not produce distortion over the entire sphere. The lateral contacts of spheres along a direction normal to that of the applied forces experience no strain and, therefore, no stress. Each column of spheres whose axis is in the direction of the applied force deforms axially, independent of adjoining columns. Lateral perturbations are not balanced by a restoring force. As a result, the cubic packing would collapse into a more stable, but not necessarily regular, packing geometry.

The cubic packing provides an interesting example of the anisotropy of seismic-wave propagation mentioned earlier. Under a static stress, σ_o, along a principal axis, the seismic-wave velocity is given by Eq. (8a), provided the wave is propagated along the axis; but in any direction normal to that axis, the velocity is a minimum corresponding to $\sigma_o = 0$. The "ellipsoid of sound wave normals" in this special case has maximum eccentricity. Put another way, the ratio of velocity in the direction of the applied load to that in the transverse direction is a maximum as compared to the ratio of any other pair of orthogonal velocities.

A more stable arrangement of spheres is the face-centered cubic packing in which each sphere is in contact with twelve others. The constant A for this assemblage was determined by Hendron et al. (Ref. 11, p. 38) to be

$$A = \frac{2\mu(1 + f)}{3(1 - \nu)} \tag{30}$$

where f is the coefficient of static friction which relates the shearing force to the normal force at the circle of contact. Representative values of f, μ, and ν for quartz particles were cited by Hendron (Ref. 11, p. 180) to be

$$\begin{aligned} f &= 0.15 \\ \mu &= 6 \times 10^6 \text{ psi} \\ \nu &= 0.20 \end{aligned} \tag{31}$$

There is only a 15 percent increase in the force constant associated with this face-centered cubic packing over the cubic packing arrangement previously discussed. Comparison of Eq. (30) with Eq. (29a) suggests that for frictionless spheres of uniform size, the equation of state of a granular medium is independent of the packing geometry, i.e., arrangement and number of contact points, as long as they do not change during loading, with the result that strains are still ascribable entirely to deformation of the individual particles and not relocation. The most important consequence of this comparison between simple cubic packing and face-centered cubic packing of spheres is the set of observations that the power law, $\sigma = A\epsilon^{3/2}$, appears to hold whatever the

packing arrangement and that the multiplicative constant, A, can be expected to change very little as the composition of the granular material* and the distribution of contact points are varied. For the calculated sound and shock velocities shown in Fig. 3, the granular sample is presumed to be in a face-centered cubic array, in which no increase in initial sample density is possible except for compression as a function of stress given by Eq. (5a). A is calculated from Eq. (30) and from the values given in Eq. (31) to be

$$A = 5.75 \times 10^6 \text{ psi} \tag{32}$$

For the face-centered cubic packing of uniform spheres, the ratio of the volume occupied by the spheres to the total volume is 0.74. Hence if Ottawa sand is assumed to be represented by uniform spheres, then

$$\rho_i = 0.74 \times 2.65 \text{ gm/cc} = 1.96 \text{ gm/cc} = 122.4 \text{ pcf} \tag{33}$$

Equations (32) and (33) were used in Eqs. (8a) and (10) to give the three curves shown in Fig. 3. Two curves are shown for shock velocity, i.e., for $\sigma_o = 0$ and for $\sigma_o = 40$ psi.

It is worth noting from the figure that

$$C_o < U < C \tag{34}$$

---

* Since μ and ν will not change greatly.

where C is the velocity of sound in the uniform region behind the shock. This is unlike shocks in a perfect gas because in this case, small signals can catch up with the shock front without the assistance of a particle velocity behind the front. As can be seen in a perfect gas

$$C_{o_{(\text{perf. gas})}} < C_{(\text{perf. gas})} < U_{(\text{perf. gas})}$$

but (35)

$$U_{(\text{perf. gas})} < u_{(\text{perf. gas})} + C_{(\text{perf. gas})}$$

This fact expressed by Eq. (34) would appear to have important implications with regard to unloading behavior.

SHOCK WAVES IN GRANULAR MEDIA UNDERGOING PARTICLE RELOCATION

For a random collection of granules it must be presumed that particles will relocate under applied load so as to increase the density of the packing. As suggested in Fig. 1, this relocation would finally become insignificant, and there may exist a region (region II) where only the stress–strain law of $\sigma = A\epsilon^{3/2}$ predominates, provided the particles do not begin to fracture before relocation ceases. Relocation of particles from some initial packing density ρ_i to some final density ρ_f is expected to be reasonably insensitive to the choice of functional form connecting ρ, ρ_i, ρ_f, and σ in region I, provided observed stress–strain curves can be matched satisfactorily and, further, provided functional continuity between regions I and II is obtained. That is,

values of u, U, C, and C_c obtained from the conservation relations are expected to be insensitive to the form of the function

$$\rho = F(\rho_i, \rho_f, \sigma) \tag{36}$$

but the shape of the shock front connecting the two regions of stress is not. In fact, the form of the function F in Eq. (36) probably controls the shape of the smooth stable shock transition; or, conversely, experimental determination of the shape of the stable-shock transition would serve as a constraint on the choice of functions, $F(\rho_i, \rho_f, \sigma)$. But for now, any reasonable choice of F will suffice to generate values of u, U, C, and C_o from an experimental stress–strain curve. The most likely choice is an exponential law common to most statistical processes wherein the rate of an event is proportional to the number of events (relocations) that have not yet taken place. Therefore, take as the functional form of Eq. (36)

$$\rho^* = (\rho_f - \rho_i)\left(1 - e^{-\frac{\sigma}{\sigma_1}}\right) + \rho_i \tag{36a}$$

where ρ^* is the change in density due to particle relocation, and σ_1 is a stress parameter identifying the particular exponential curve between the limits

$$\rho^* = \rho_i \quad \text{at} \quad \sigma = 0$$

$$\rho^* = \rho_f \quad \text{as} \quad \sigma \to \infty$$

Throughout the process of particle relocation Hertz-type contact forces still act.

The equations relating ρ, ρ_o, and ρ_i in terms of the new parameters ρ_f and σ_1 may be generated by substitution of the more general ρ^* from Eq. (36a) for ρ_i in Eqs. (5a). (ρ_i, of course, maintains its original connotation.) Thus

$$\rho = \frac{\rho_f + (\rho_i - \rho_f)e^{-\frac{\sigma}{\sigma_1}}}{1 - \left(\frac{\sigma}{A}\right)^{2/3}} \tag{37}$$

$$\rho_o = \frac{\rho_f + (\rho_i - \rho_f)e^{-\frac{\sigma_o}{\sigma_1}}}{1 - \left(\frac{\sigma_o}{A}\right)^{2/3}} \tag{37a}$$

Rearranging Eqs. (37) and (37a) and subtracting gives the equation of state in the form

$$\sigma - \sigma_o = A\left\{1 - \frac{\rho_i}{\rho}\left[\frac{\rho_f}{\rho_i} + \left(1 - \frac{\rho_f}{\rho_i}\right)e^{-\frac{\sigma}{\sigma_1}}\right]\right\}^{3/2} - A\left\{1 - \frac{\rho_i}{\rho_o}\left[\frac{\rho_f}{\rho_i} + \left(1 - \frac{\rho_f}{\rho_i}\right)e^{-\frac{\sigma_o}{\sigma_1}}\right]\right\}^{3/2} \tag{38}$$

$$\sigma = A\left\{1 - \frac{\rho_i}{\rho}\left[\frac{\rho_f}{\rho_i} + \left(1 - \frac{\rho_f}{\rho_i}\right)e^{-\frac{\sigma}{\sigma_1}}\right]\right\}^{3/2} \qquad (38a)$$

Performing the differentiation as in Eq. (7) and taking $1 - (\sigma/A)^{2/3} \approx 1$ [because Eq. (32) shows A to be large compared with σ] wherever it occurs after differentiating, one gets

$$C^2 = \frac{\frac{3}{2\rho_i} A^{2/3}\sigma^{1/3}}{\frac{\rho_f}{\rho_i} + e^{-\frac{\sigma}{\sigma_1}}\left(\frac{\rho_f}{\rho_i} - 1\right)\left(\frac{3}{2\sigma_1} A^{2/3}\sigma^{1/3} - 1\right)} \qquad (39)$$

Substituting Eqs. (37) and (37a) into Eq. (9) and again taking

$$1 - \left(\frac{\sigma}{A}\right)^{2/3} \approx 1 - \left(\frac{\sigma_o}{A}\right)^{2/3} \approx 1$$

one obtains after some algebra

$$U^2 = \frac{\frac{A^{2/3}}{\rho_i}(\sigma - \sigma_o)\left[\frac{\rho_f}{\rho_i} - \left(\frac{\rho_f}{\rho_i} - 1\right)e^{-\frac{\sigma}{\sigma_1}}\right]}{\left\{\frac{\rho_f}{\rho_i} - \left(\frac{\rho_f}{\rho_i} - 1\right)e^{-\frac{\sigma_o}{\sigma_1}}\right\}\left\{\frac{\rho_f}{\rho_i}(\sigma^{2/3} - \sigma_o^{2/3}) + A^{2/3}\left(\frac{\rho_f}{\rho_i} - 1\right)\left(e^{-\frac{\sigma_o}{\sigma_1}} - e^{-\frac{\sigma}{\sigma_1}}\right)\right\}} \qquad (40)$$

The equation of state for $\sigma_o = 0$, i.e., Eq. (38a), was fitted to two experimentally determined stress–strain curves, using the ratio ρ_f/ρ_i and σ_1 as parameters. The constant A was taken from Eq. (32), and the actual densities ρ_i were taken as 1.76 and 1.64 gm/cc, i.e., 110.0 and 102.2 pcf for curves B and C, respectively, in Fig. 6. These analytical curves are shown in Fig. 6 together with the values of σ_1 and ρ_f/ρ_i, which identify them through Eqs. (38) and (38a). Curve A in Fig. 6 was drawn from the equation of state for the face-centered cubic pack [Eq. (5a) or (6)]. In view of the very small total axial strain of curve A, it is not surprising to find that the excess strain of samples B and C are almost numerically equal to the excess over 1 of the ratio, ρ_f/ρ_i. That is, the total axial strain of a laterally confined granular sample stressed into region II of Fig. 1 is almost numerically equal to the sum of the strains produced by the elastic compression of the granules and the incremental compaction due to relocation of the granules.

Figures 7 and 8 show sound and shock velocities in the material plotted versus total stress, σ, behind the shock in the case of shock-wave propagation; and in the case of sound-wave propagation ($\Delta\sigma << \sigma_o$), the sound-velocity curves are in terms of the initial stress, σ_o. Sound velocity was obtained from Eq. (39) and shock velocity from Eq. (40). It is seen that both sound velocity and shock velocity are depressed at the lower stresses, where significant particle relocation is going on, and that shock velocity is slower to reach the limit of rigid pack, also shown (as curve A) on each figure as replotted from Fig. 3.

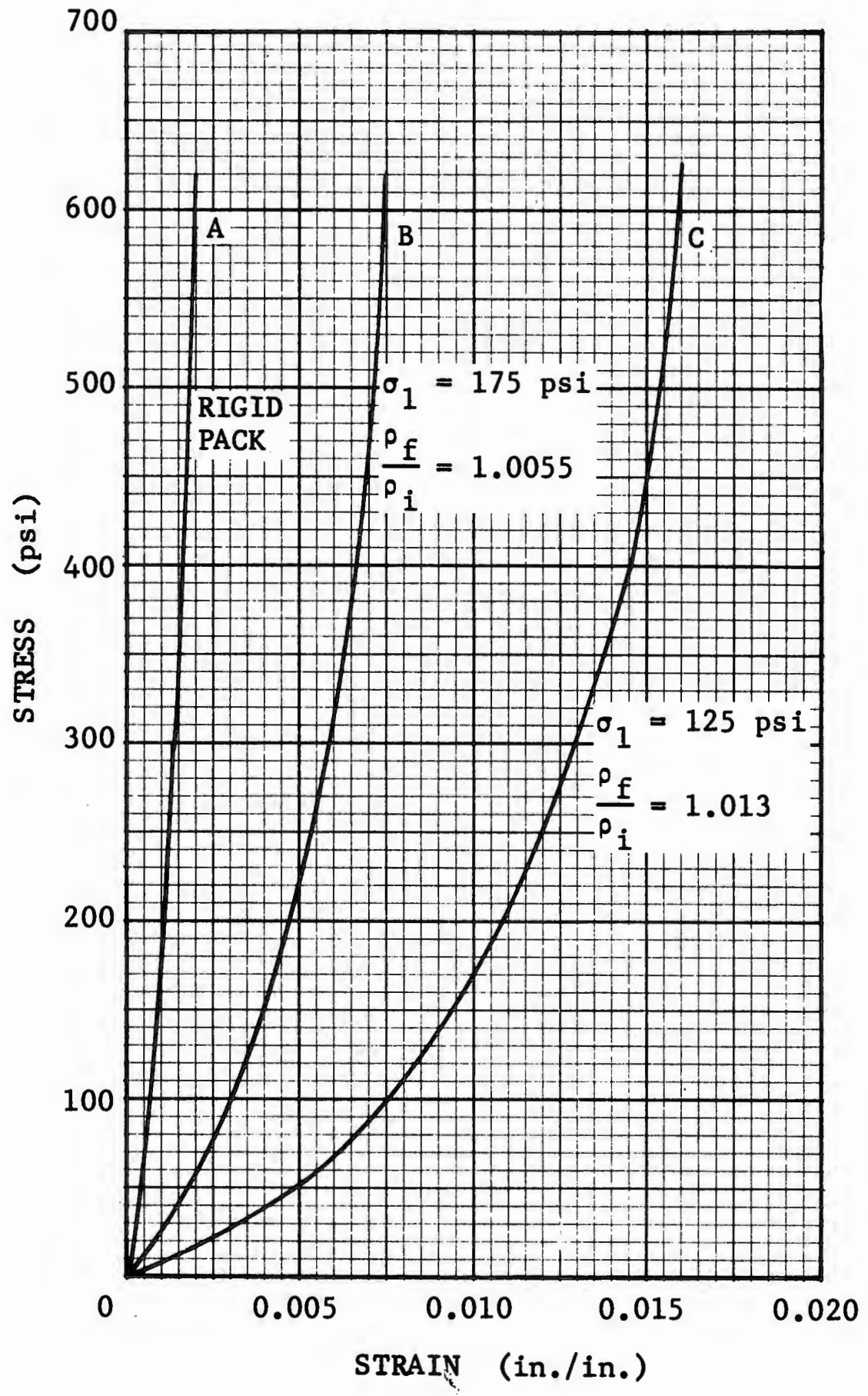

Fig. 6. Stress—Strain Curves for Representative Samples of Ottawa Sand Under Confined Compression

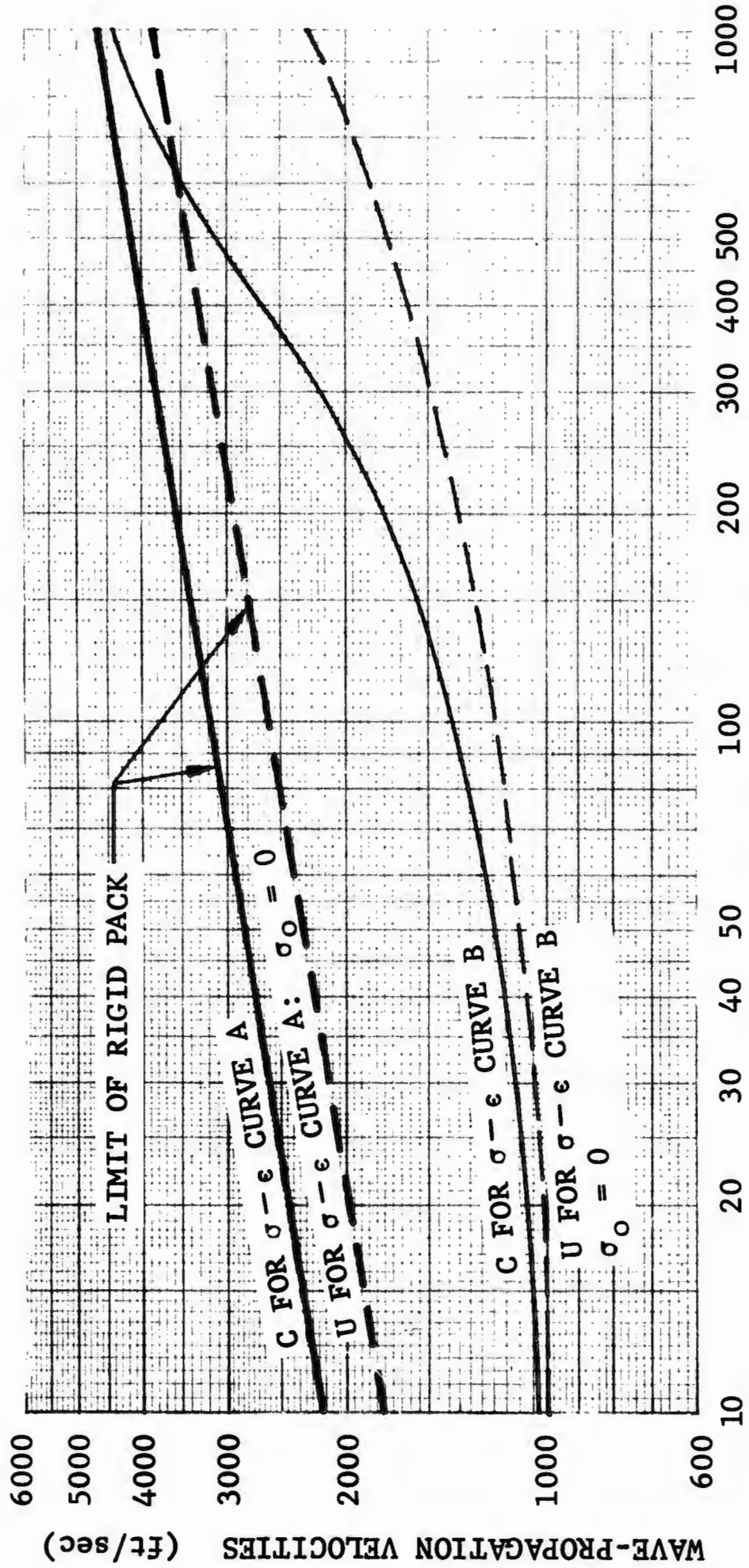

Fig. 7. Sound and Shock Velocities Appropriate to Stress—Strain Curve B
(σ_1 = 175 psi, ρ_f/ρ_i = 1.0055)

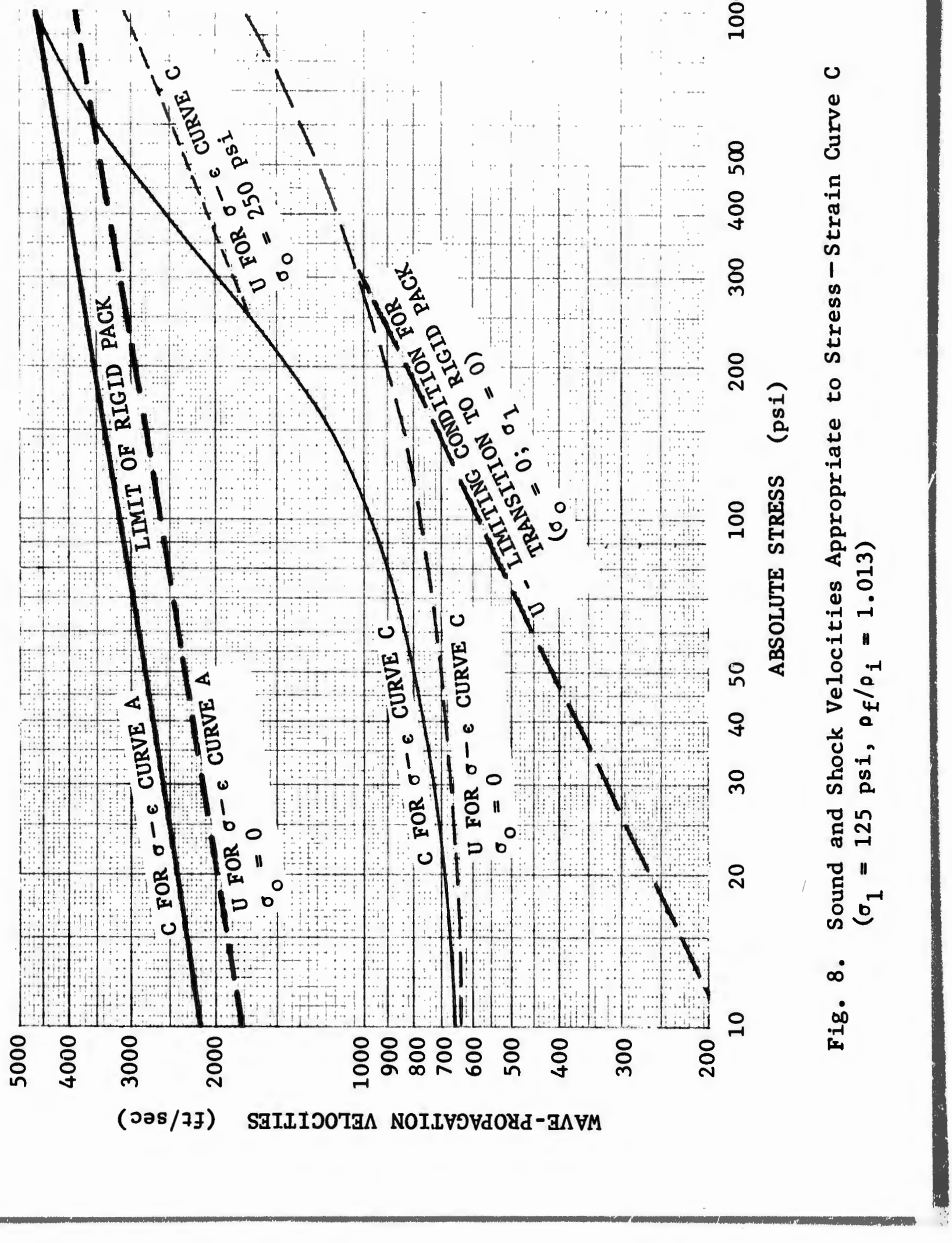

Fig. 8. Sound and Shock Velocities Appropriate to Stress—Strain Curve C
(σ_1 = 125 psi, ρ_f/ρ_i = 1.013)

Figure 8 includes the lower-limit curve to the shock velocity (with $\sigma_o = 0$), which occurs when the limit of $\sigma_1 \to 0$ is taken in Eq. (40). This curve is equivalent to the limiting case No. 2 discussed by Weidlinger and Matthews (Ref. 15). All shock-velocity curves of the family depending parametrically on σ_o are contained between this limiting line and the line indicating the limit of rigid pack. One member of this family, that for $\sigma_o = 250$ psi, is also shown in Fig. 8.

It may be observed that the algebraic expressions [Eqs. (39) and (40)] were not necessary to the construction of the particular sound- and shock-velocity curves shown in Figs. 7 and 8. If an experimentally determined stress—strain curve for a granular sample under complete lateral confinement were replotted on a σ-versus-ρ diagram, then the sound velocity at each value of stress is just the tangent to this curve at that stress, and the shock velocity may be obtained from the secant between two points, σ_o and σ, on the same curve. [See Eq. (9).] Although a complete graphic solution is possible from the stress—strain curve alone, it is useful to match an algebraic expression to the observed stress—strain curve in order to determine the behavior of the material under change of the governing parameters. Thus it may be seen, for example, that as little as a 1-percent change in packing density during loading of the sample changes the shock velocity by a factor in excess of 3. For example, Fig. 6 shows about a 1-percent change in packing density (i.e., 0.01 in./in. difference in strain) between curves A and C under a load of 200 psi. An

examination of the ratio of shock velocities in Fig. 8 at this same 200-psi load is seen to be about 3.1/1 (2950 ft/sec divided by 900 ft/sec). Also of interest is the ratio of sound velocity, given by curve A, to the shock velocity given by curve C. In Fig. 8, at a load of 200 psi, this ratio is 4.0/1. In a material with a very short relaxation time, this indicates that unloading waves would be 4 times faster than loading waves at this level of stress.

Section 4
GEOMETRICAL INTERPRETATION

The derivations have been directed towards exposition of the sound velocity and the velocity of a stable shock in a granular medium. It is now quite simple to make a geometrical interpretation of these quantities in terms of a stress–density diagram. Stress–strain curve B of Fig. 6 is replotted in Fig. 9, where ρ is the abscissa. Rewriting Eq. (5), ρ is given by

$$\rho = \frac{\rho_i}{1 - \epsilon} \tag{41}$$

From Eq. (7) it is clear that the value of the tangent to every point on this curve is numerically equal to the square of the velocity of sound at the corresponding stress. The secant connecting the two points $\sigma_o = 10^4$ lb/ft^2 (a nominal 70 psi) and $\sigma = 5 \times 10^4$ lb/ft^2 (a nominal 350 psi) is related to the square of the shock velocity. This is the graphical equivalent of the analytical expression, i.e., Eq. (9)

$$U^2 = \frac{\rho}{\rho_o}\left(\frac{\sigma - \sigma_o}{\rho - \rho_o}\right) \tag{9}$$

Thus the numerical value of the square of the shock velocity of stress σ propagating into material at an initial stress σ_o is obtained from the curve by multiplying the secant connecting these points by the density ratio. This value is always

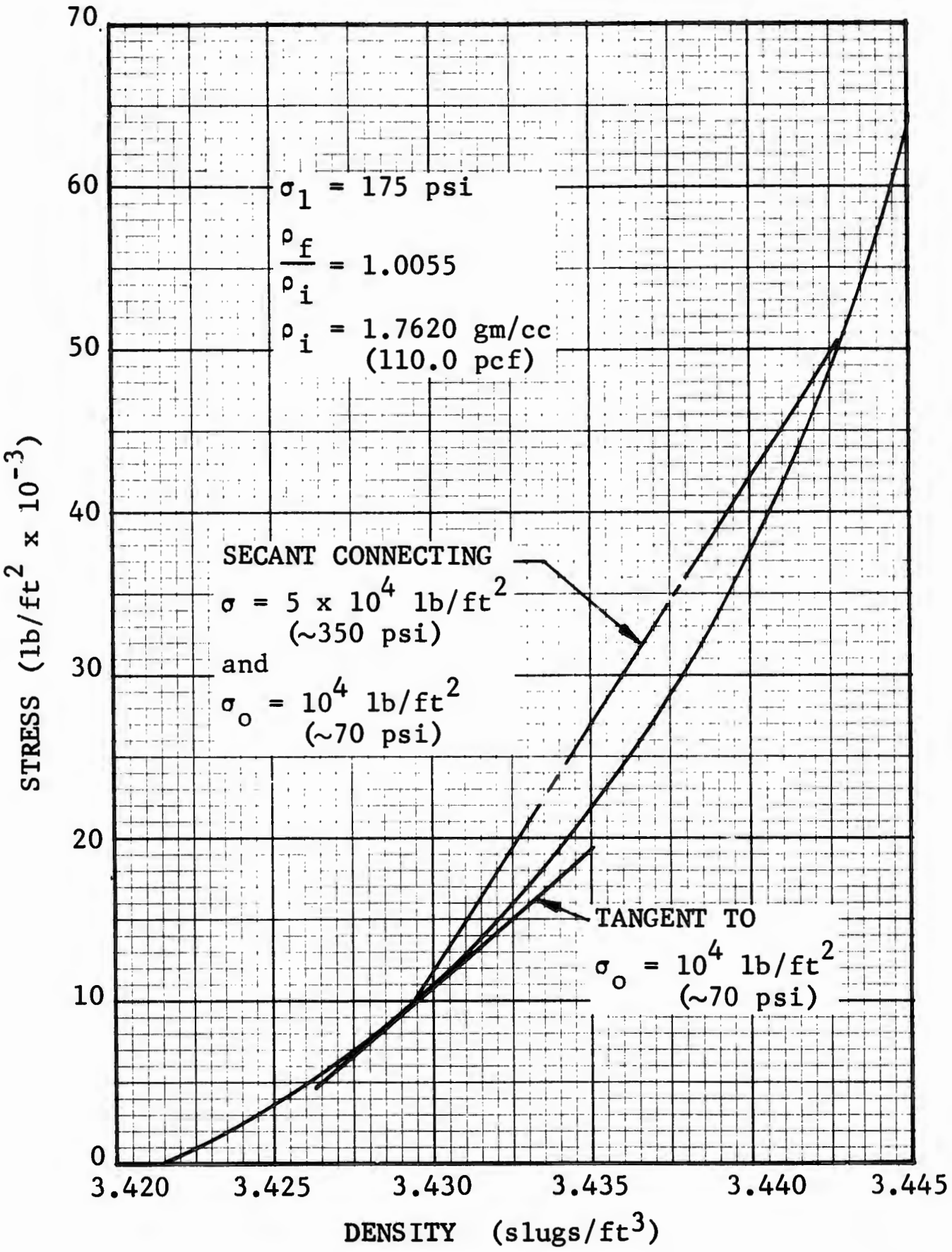

Fig. 9. Stress—Density Curve Replotted From Curve B of Fig. 6

greater than the tangent at σ_o, showing the shock to be always supersonic with respect to conditions ahead of the shock. Holding σ_o fixed and letting σ approach σ_o, one finds that the secant approaches continuously the tangent at σ_o. This is in agreement with the fact that a sound wave is an infinitesimally weak shock.

Section 5
COMPARISON OF CONCEPTS TO OBSERVATIONS OF RECORD

It should be noted that two of the stress-wave velocity curves calculated from the elastic properties of the individual particles correspond very closely with a band of velocities measured and reported by Lawrence (Ref. 16). A comparison is made in Fig. 10. From the foregoing section, it should be remembered that the calculated velocities were for the rigid-pack condition, in which the loading wave is propagated without particle relocations. It might, therefore, be inferred that the Lawrence band is somehow the empirical counterpart of a theoretical "no particle relocation" case such as region II. Several related points that bear on this subject are discussed below.

The process of vibrating samples and cycling loadings is a familiar way to obtain more reproducible results.* In the case of an assemblage of granular particles, such an elimination of irreversible processes, accomplished by cycled loadings (with a more or less fixed amplitude) is synonomous with relocating virtually all particles ordinarily subject to relocation under that loading, so that no new and different

---

* Stated another way, these are methods of eliminating irreversible processes. If there are no irreversible processes left, then the only processes that remain are reversible, which by definition guarantees that on repeating the process it is reproducible.

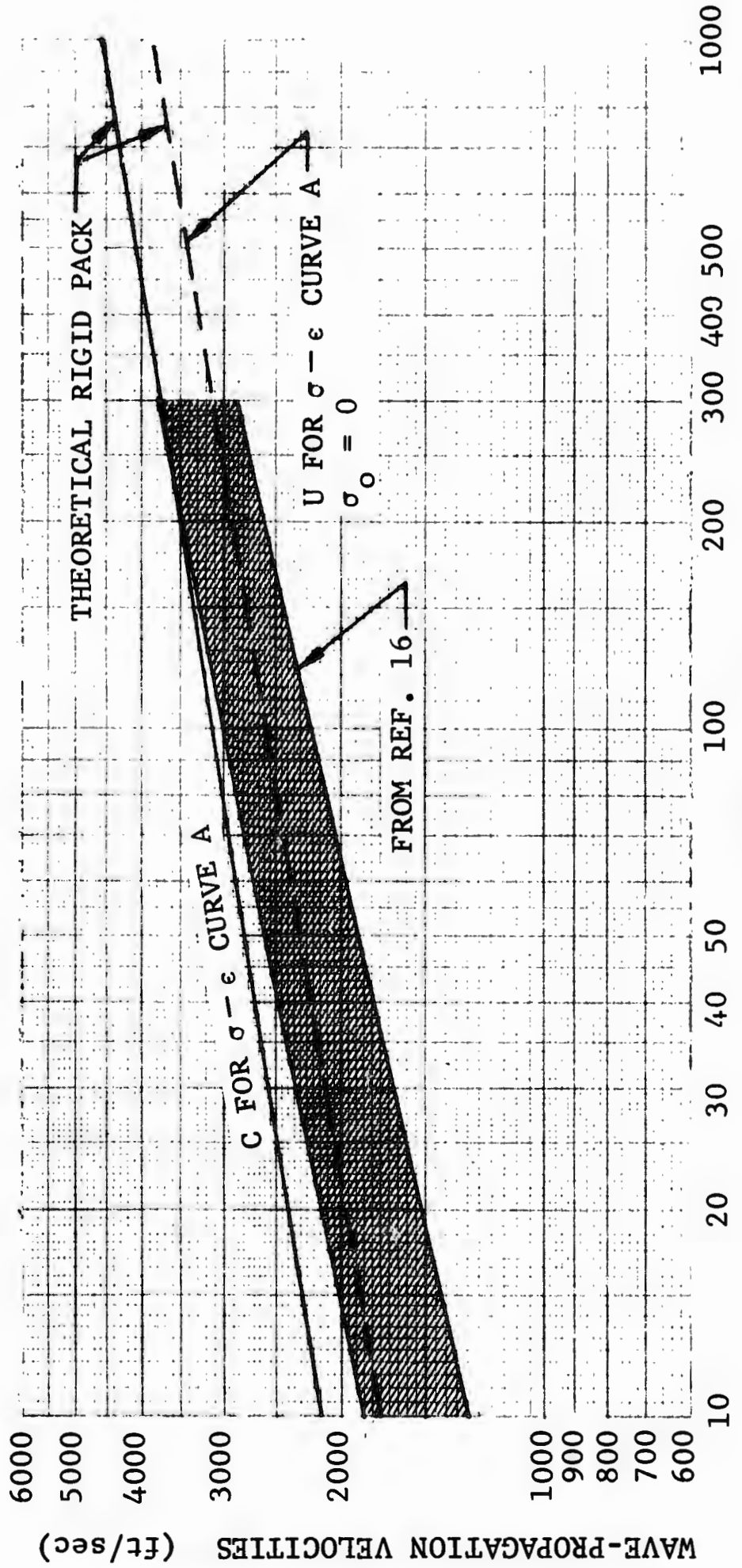

Fig. 10. Comparison of Theoretical Wave Velocities and Experimental Results From Ultrasonic Tests

relocations are left to occur on the next cycle. Thus a loading on a sample with a history of many cycles of loading is just the experimental counterpart to the mathematical "no particle relocation" (or rigid-pack) case, provided the amplitude of the cycled loadings is not exceeded.

Whitman (Ref. 17) has already shown that loadings as high as 5 psi in amplitude, repeated 500 times, result in a modulus comparable to that determined from the wave velocities (of much smaller amplitude) measured by Lawrence.*

In summarizing, it would appear that the experimentally measured response (from Ref. 16) of a granular assemblage to a loading with an amplitude that does not exceed what has already been felt some 500 times will be just the rigid-pack Hertzian elastic response as calculated theoretically and shown in Fig. 3 (cf. Fig. 10). However, it should be noted that the very first loading to an amplitude never before applied** requires consideration of the irreversible behavior of the medium. Thus the stress of any amplitude that is cycled will still propagate with the rigid-pack velocity, but another behavior is associated with the particle-relocation phenomenon

---

* Although Lawrence does not state the number of cycles to which his samples were subjected, it might be inferred that they were a number comparable to 500, or more. Since the frequencies Lawrence used were on the order of 0.1 to 0.5 Mc/sec, even a 5-ms warm-up of the equipment would result in over 500 cycles of loading.

** As might be expected in an analogous field problem for nuclear weapons loadings.

that plays its role at all higher stresses. This higher stress portion of the response might be expected to follow the behavior treated semiempirically in the previous section and summarized graphically (and compared with the rigid-pack elastic response) in Figs. 7 and 8.

An example of both types of behavior in a single loading has been reported in Refs. 9 and 19. Described therein were laboratory tests made at URS in which initial pressures were applied prior to application of a dynamic loading. In this case the loadings were the first application. Nevertheless, when the dynamic increment was applied, the first disturbance was observed to propagate with the particular rigid-pack velocity indicated as being characteristic of the initial stress conditions that prevailed (Fig. 10). In accordance with the previous paragraph, the propagation velocity of the peak disturbance was observed to correspond to the much lower velocity characteristic of the particle relocation behavior as indicated in Fig. 8.

In these experiments, which did not involve cycled loadings either of the initial pressure or of a small-amplitude dynamic load above the initial pressure, the first arrivals were still equivalent to the cycled load values inferred from stress—strain behavior by Whitman and measured as propagating pulses by Lawrence. The source of the effect in the URS test is not known. It seems likely to be the result of having to overcome friction forces (excluded from consideration in Section III), but it is possible that it might be related statistically to fewer opportunities

for relocation of particles or to the existence of background "noise" that provides many cycles of low-amplitude loading of the same magnitudes as the first disturbances. The latter two effects may simply be facets of the former.

In the field problem, those waves of an amplitude commensurate with the cycling of background noise or seismic disturbances will propagate with the rigid-pack velocity. However, any wave having a higher amplitude of stress will have a different behavior, one analogous to the particle relocation phenomenon presented in the previous section and which was compared graphically in Figs. 7 and 8 with the rigid-pack elastic response.

Section 6
EXPERIMENTAL RESULTS

A description of the apparatus employed and the sample material used in these studies is presented in Appendix C.

The experiments described were aimed primarily at examining the momentum distribution process when dynamic loadings* are applied to granular material under the influence of varying conditions of initial stress.

ZERO-INITIAL-STRESS CONDITIONS ($\sigma_o = 0$)

In order to provide a limiting reference condition, results of tests conducted with an initial stress of 0 psi are included in the following paragraphs.

Quasi-Static Tests**

The stress—strain curve for the test sand (20—30 Ottawa) in a quasi-static constrained compression test under essentially zero initial stress has the characteristic curvature, concave to the stress axis. In this study a series of such tests was conducted at an initial unit weight, γ_o, of 110 pcf

---

* That is of a type that have nuclear weapons loading characteristics (Ref. 3, Section 3).

** For definitions of the terms "quasi-static" and "wave propagation," as used here, see Ref. 18, pp. 4 and 5.

(RD ≃ 75%). A summary of the resulting curves is presented in Fig. 11.

Wave-Propagation Tests

The stress–strain relationship obtained as a result of applying impulsive loadings to this same material at the same density are presented in Fig. 12. This is a plot of peak incident stress, $\Delta\sigma$, versus the strain, $\Delta\epsilon$, at the same time the stress level $\Delta\sigma$, reaches the base of the sample, i.e., $\Delta\epsilon$ is the strain corresponding to a sample uniformly stressed to $\Delta\sigma$. In addition, values of peak reflected stress $\Delta\sigma_r$ versus its peak strain $\Delta\epsilon_r$ are also included. The difference in strain $(\Delta\epsilon_r - \Delta\epsilon)$, of course, can be considered to result from an overstress $(\Delta\sigma_r - \Delta\sigma)$ propagating into a material (of slightly increased density) under an initial stress $\Delta\sigma + \sigma_o$.*

In Fig. 13 the stress–strain data from the wave-propagation tests has been compared with that from quasi-static tests. From that comparison it appears as though there are no measurable time-dependent effects in this material.

In addition to the stress–strain relationship obtained in the wave-propagation tests, relationships of peak particle

---

* For the special case of $\sigma_o = 0$, the above equations could be simplified somewhat. See Fig. 12 for a graphical description of these terms. See Refs. 18 and 19 for additional information on stress and strain measurements.

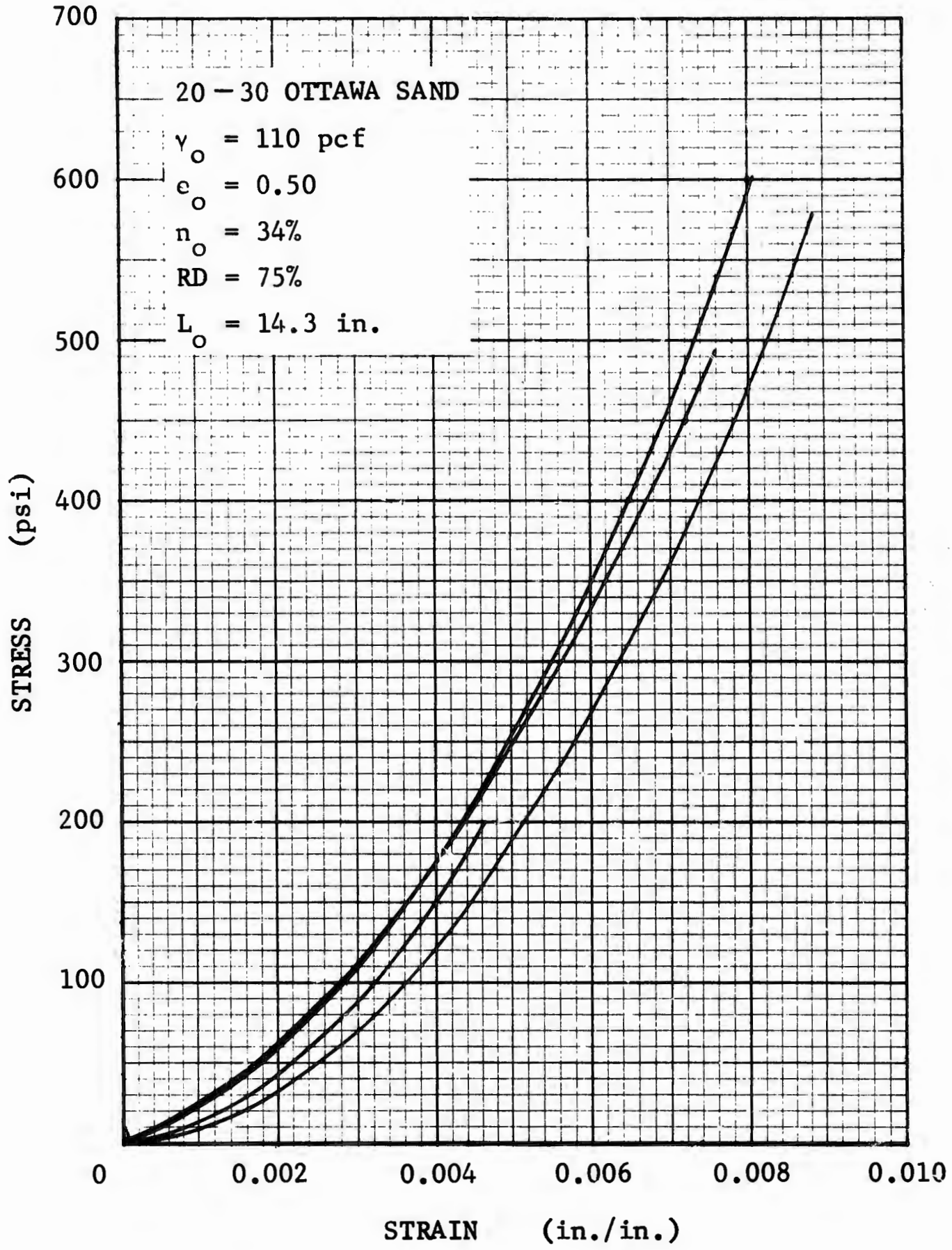

Fig. 11. Summary of Quasi-Static Stress – Strain Curves With $\sigma_o \simeq 0$

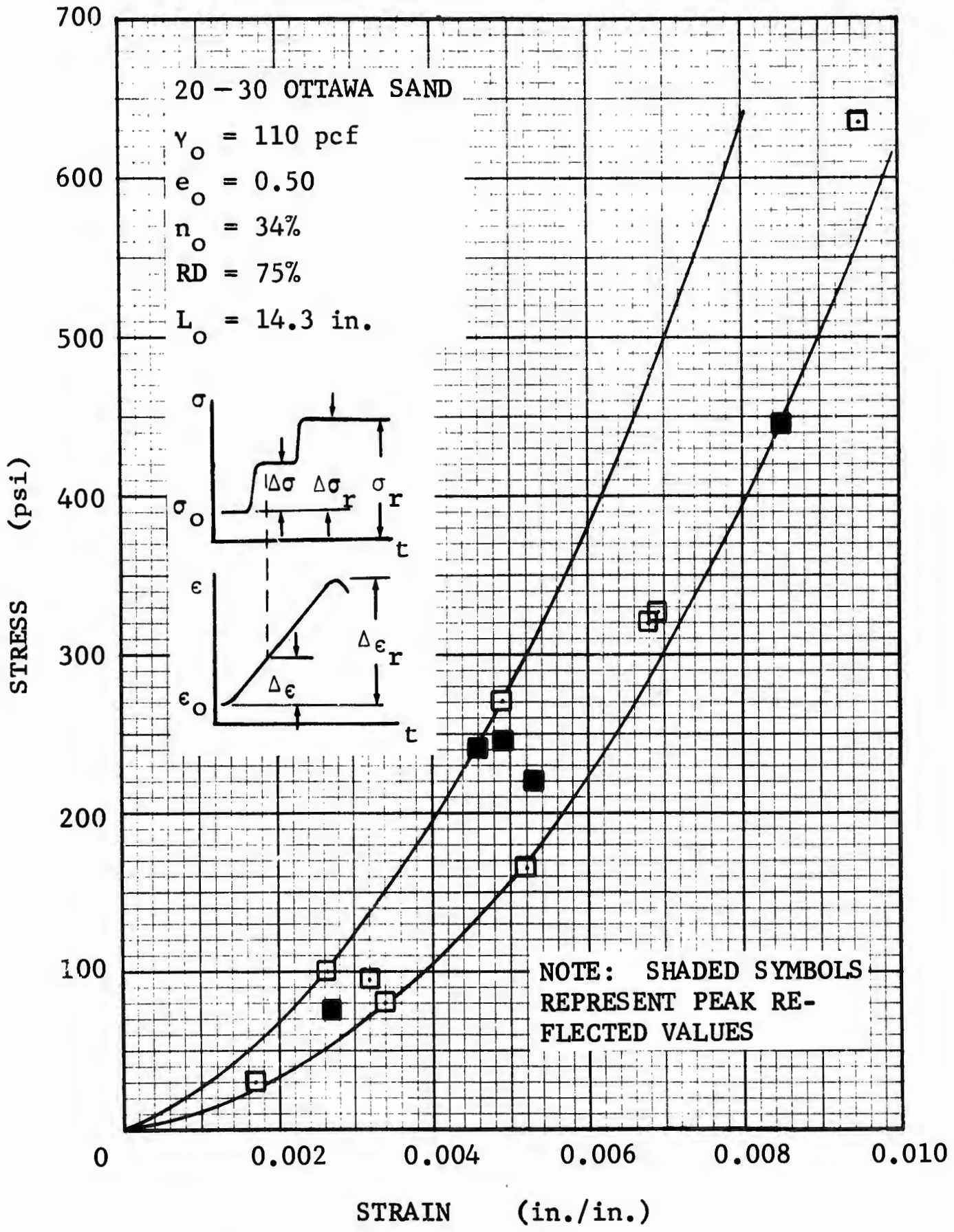

Fig. 12. Stress – Strain Data From Wave-Propagation Tests

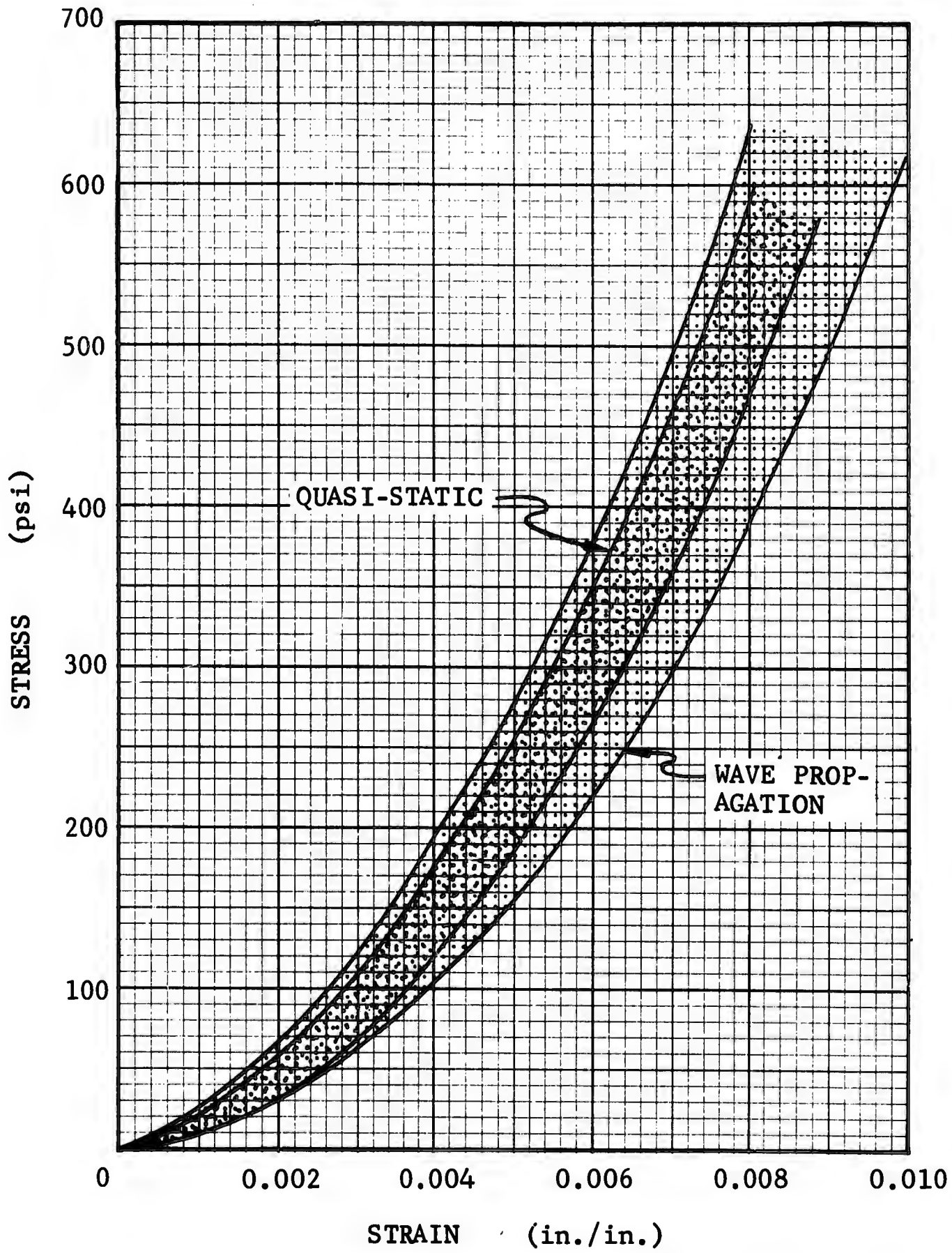

Fig. 13. Comparison of Results From Quasi-Static and Wave-Propagation Tests

velocity versus stress and wave-propagation velocity versus stress have also been obtained as measured quantities.

The data on peak particle velocity are presented in Fig. 14, where they are compared with values calculated from equations developed (in Section 3) to describe shocks propagating in a rigid pack of granular material. The form of the equations used embodies as parameters stress—strain behavior and the placed density (in effect ρ_i). Thus the equations have been related to standard engineering parameters, which are readily measured, in order to make appropriate comparisons for the circumstance that particle relocations occur. The computed values were calculated from the equation of state, using Eqs. (5), (9), and (12) combined to give

$$u = \left[\frac{\sigma - \sigma_o}{\rho_i}\right]^{1/2} \left[\left(\frac{\sigma}{A}\right)^{2/3} - \left(\frac{\sigma_o}{A}\right)^{2/3}\right]^{1/2}$$

$$= \left[\frac{(\sigma - \sigma_o)(\epsilon - \epsilon_o)}{\rho_i}\right]^{1/2} \qquad (42)$$

where

u = peak particle velocity

$(\sigma - \sigma_o)$ = incident axial stress $(\Delta\sigma)$

ϵ and ϵ_o = strains corresponding to σ and σ_o

ρ_i = initial mass density

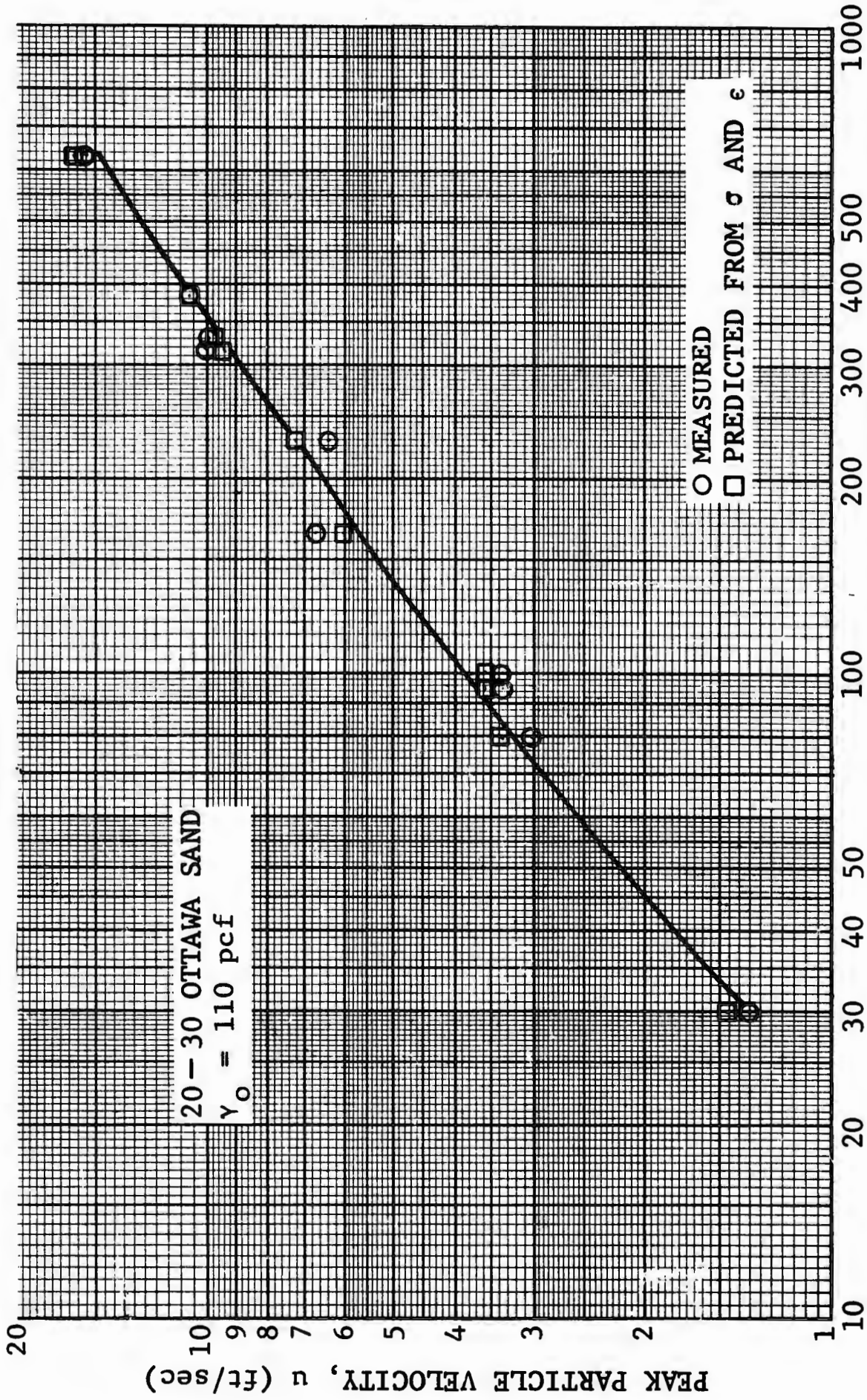

Fig. 14. Comparison of Measured and Predicted Peak Particle Velocities

In the present case, $\sigma_o = 0 = \epsilon_o$ and $\rho_o \equiv \rho_i$. The measured peak particle velocities were obtained from the slope of the displacement−time trace.

The stress-wave propagation-velocity data are presented in Fig. 15, where they are also compared with values calculated according to the equation of state, but again from the particular values of σ and ϵ measured in each dynamic load.* In this case the calculated values were obtained by combining Eqs. (5) and (9) to give

$$U = \left[\frac{\sigma - \sigma_o}{\rho_i(\epsilon - \epsilon_o)}\right]^{1/2} \tag{43}$$

where U = stress-wave propagation velocity** and the other symbols are as defined previously. In Eq. (43) the substitution $\rho_o \simeq \rho_i$ has been made. The measured particle and wave velocities appear to agree very well with the calculated values.

FINITE-INITIAL-STRESS CONDITIONS

Finite-initial-stress conditions are important from the standpoint of providing information on the role played by

---

* Since a fresh sample was used in each test, the scatter is thought to be principally due to variations in placement.

** See Appendix B of Ref. 18 for details of velocity measurements.

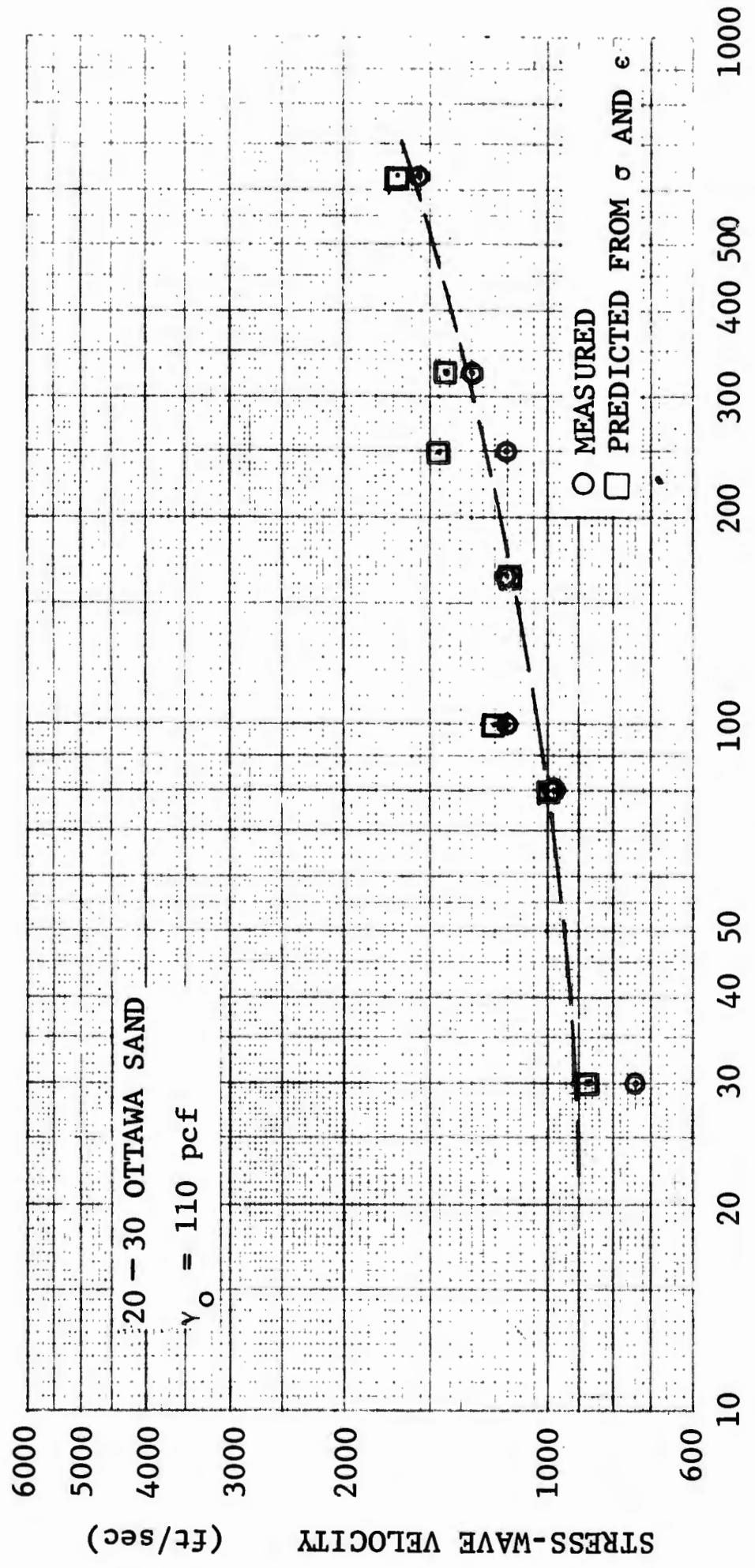

Note: Zero initial stress during test but a nominal 5 psi load used temporarily to facilitate the removal of the ring holder.

Fig. 15. Comparison of Measured and Predicted Stress-Wave Velocities With $\sigma_o \simeq 0$

overburden pressures in determining how momentum is distributed when impulsive loadings are applied. Thus, it is of value to investigate the effect of propagating stress waves on samples with significant initial stresses. As indicated earlier, information of this type is inherent in data such as those presented in Fig. 12 (and in earlier reports of this series as well as in Ref. 9).

Consider for the moment the reflected pulse generated at a rigid end-boundary and propagating back whence the incident wave came. (The incident pulse is a step pulse of constant stress.) One can appreciate then that the reflected pulse corresponds to a stress wave applied to material at an initial stress just equal to the incident stress. Certainly in order to fit the same stress—strain behavior as observed for the incident wave (which it appears to do), the stress—strain relationship of the reflected wave must be determinable by a simple origin shift of the stress—strain curve, equivalent to the magnitude of the incident stress (and, of course, its corresponding strain). (The velocity of the reflected wave also seems to be determinable from this new origin.) However, it must be admitted that this is a singular relationship in that the reflected stress wave is generated as a result of bringing the incident particle velocity to rest. Thus it has been of interest to determine if the relationship holds for other than the discussed unique stress—strain—initial-stress conditions (e.g., see Ref. 9). Of further interest on this subject are studies recently reported by Whitman et al. (Ref. 20), which have indicated that there

is also a time-dependent behavior, associated with the initial stress, which must be considered in the stress–strain–initial-stress relationship. This time-dependent behavior will be of interest with regard to its effect on momentum transfer and therefore should be determined from studies of propagating waves. It is clear that the periods of application of the "initial" stress, in the URS studies of reflected waves, amount to a matter of several hundred microseconds at the most and so are likely to be close to a minimum. Longer delays between application of the initial stress and the overstress are, therefore, desirable.

Before discussing some experimental findings on effects of initial-stress time dependence, it is important to note that the theory presented in Section 3 does not, in its present form, take into account the response associated with the initial-stress time-dependent behavior. Nevertheless, in view of the objective to discover sufficient information with regard to dynamic behavior to be able to apply it to making free-field predictions of behavior, it is of some interest to compare results of measurements from experiments which do involve such time-dependent behavior with calculations from an equation of state which, in effect, ignore that behavior to see how well we may fare. Thus the comparison is, to some extent, arbitrary. Nevertheless, the remainder of this section is such an exposition. In order to make comparisons with confidence, i.e., to establish them as fact with suitable limits rather than merely good empirical fits in some region of observed behavior, understanding of the source of

the behavior is required and hence, knowledge of the manner in which any simplified approximation differs. At present, of course, without a theory that includes observed time-dependent behavior this more desirable sort of comparison is not possible.

Quasi-Static Tests

Quasi-static tests were conducted wherein a portion of the load was applied and held for some time before the application of the second increment. The results of these tests are presented in Figs. 16–19. In Figs. 16 and 18, the entire stress–strain curve is presented, whereas Figs. 17 and 19 are enlarged plots of that behavior for the second stress increment. This latter portion was plotted from an oscilloscope record in which the gain settings were increased to allow more accurate determination of stress–strain measurements and, hence, the initial tangent modulus.

In these tests an arbitrary hold time of about 3 min was employed, during which time additional straining (creep) was recorded. Upon application of the second increment it appeared as though the curve returned to a path much as the one it would have followed had the stop not been made (e.g., compare Fig. 18 with Fig. 13). A comparison of these static results with those of Whitman (Ref. 20) clearly demonstrates qualitative agreement.

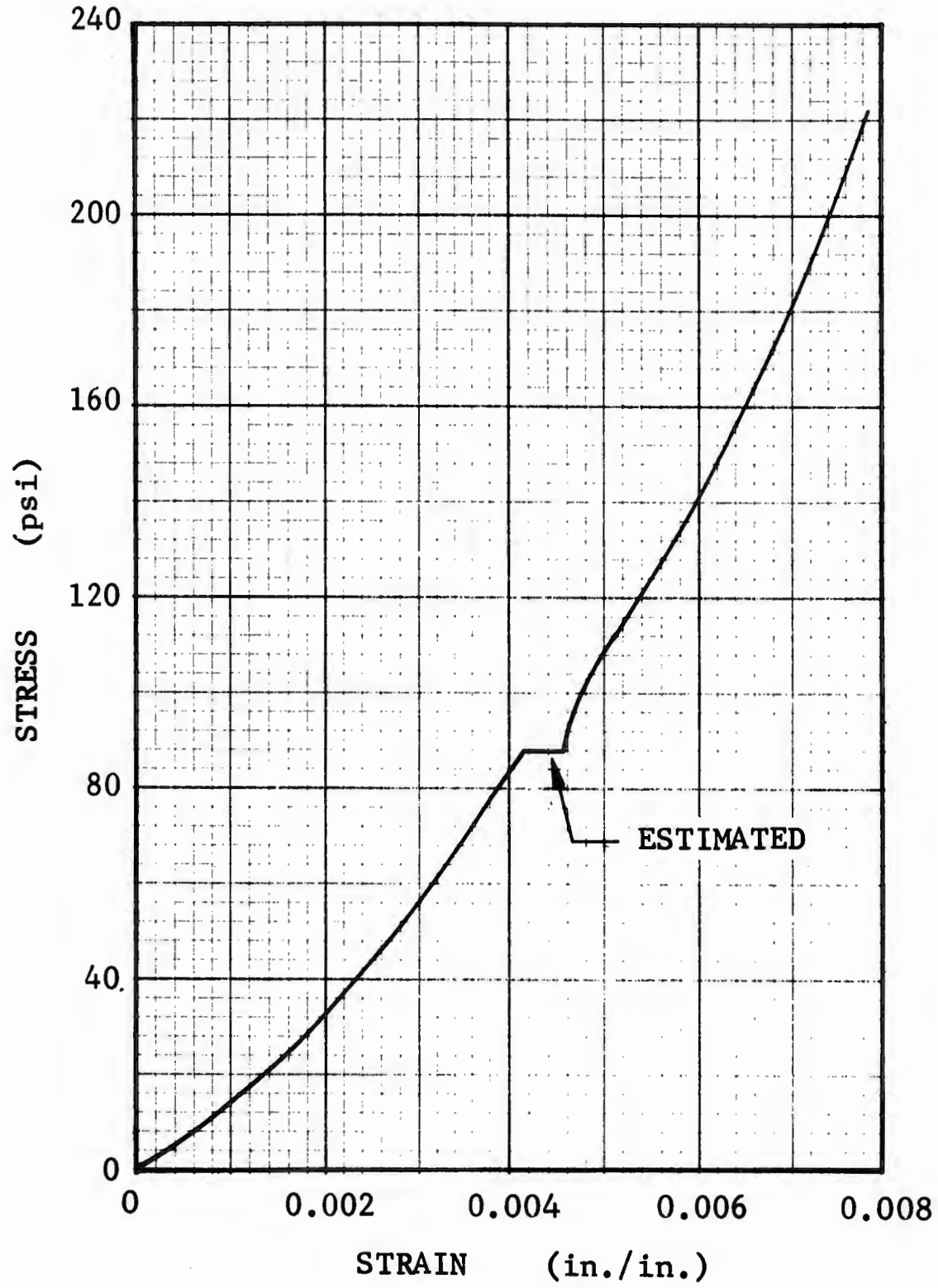

Fig. 16. Quasi-Static Stress—Strain Curve

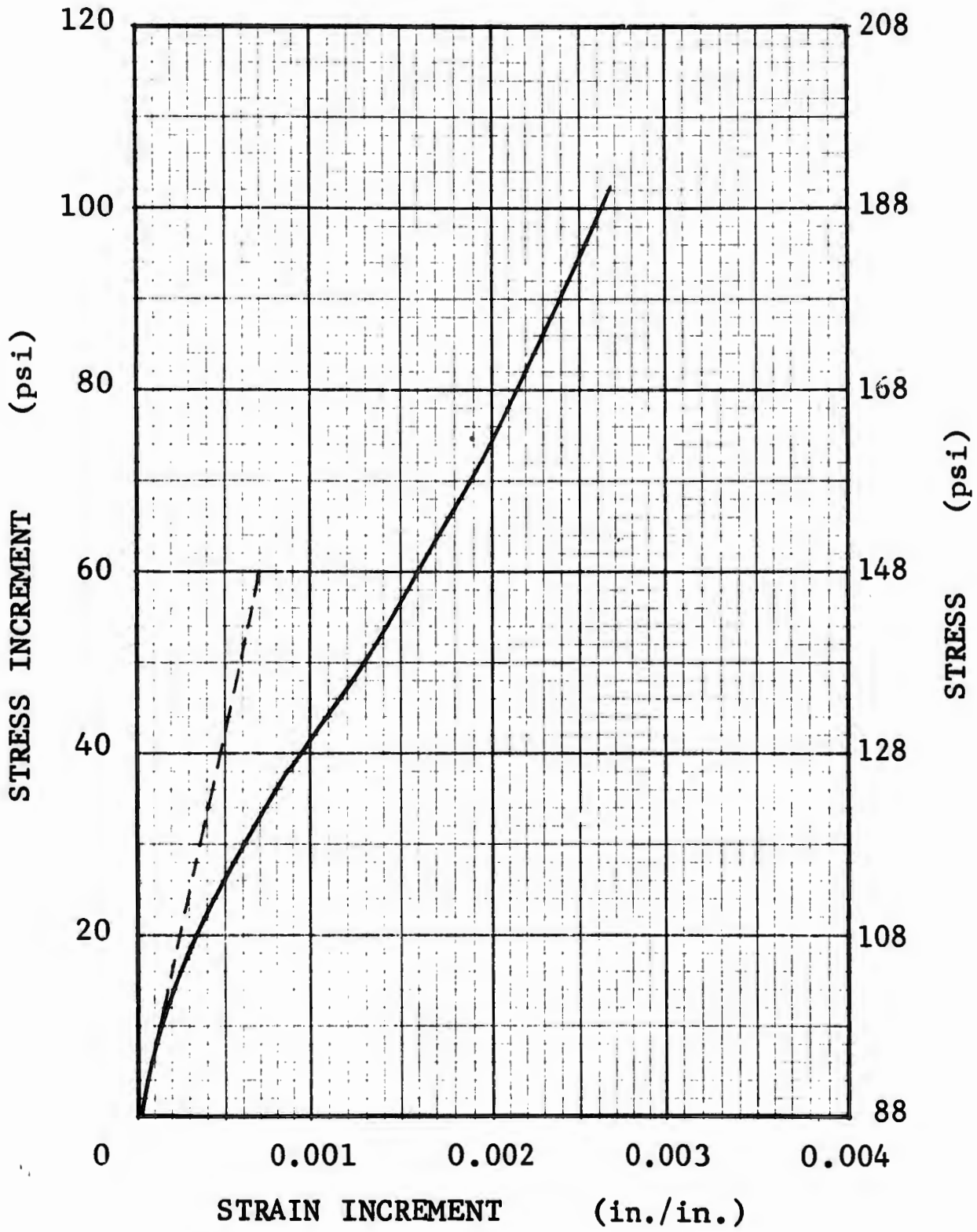

Fig. 17. Quasi-Static Stress — Strain Curve Starting From σ_o = 88 psi

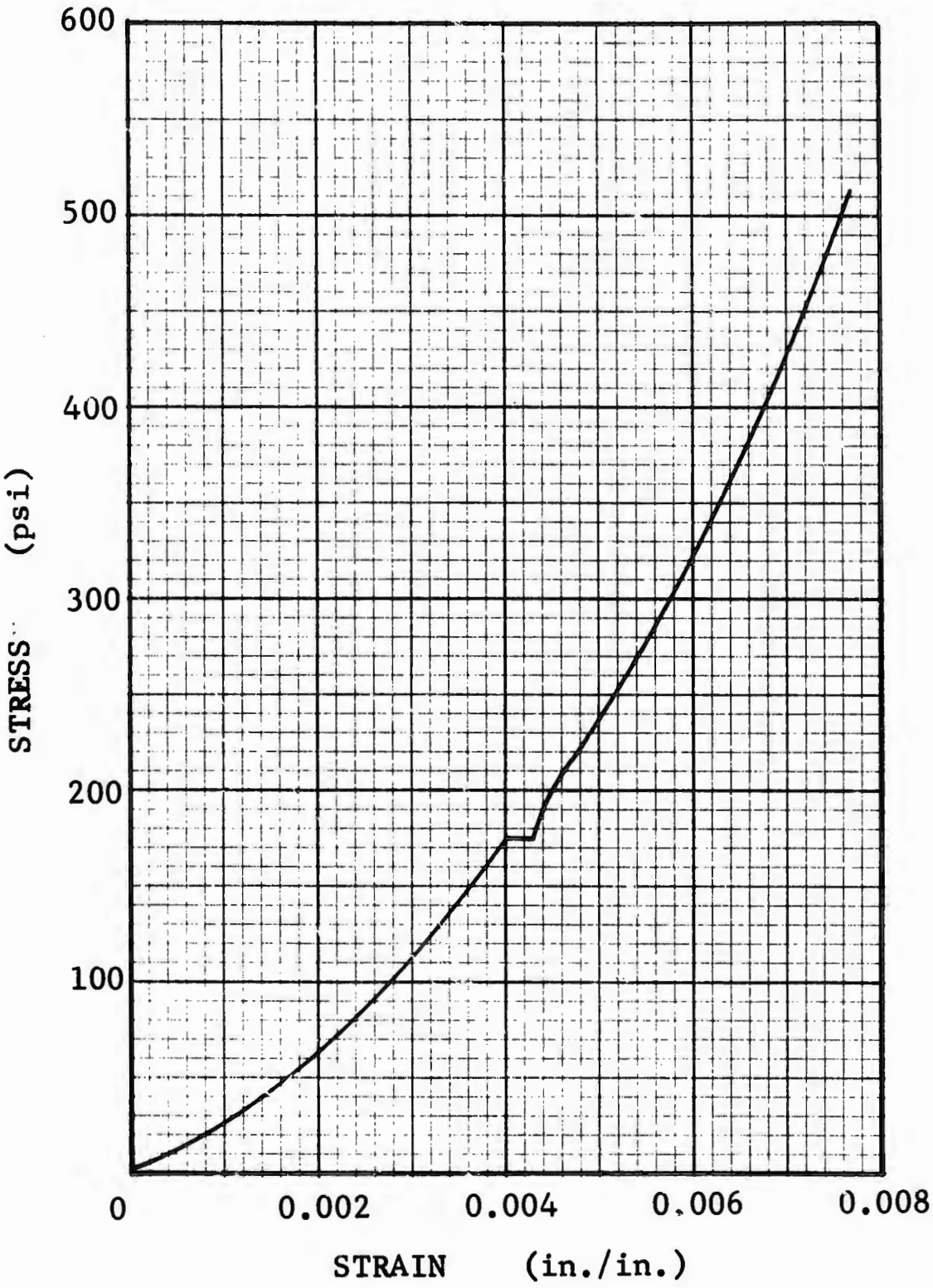

Fig. 18. Quasi-Static Stress—Strain Curve

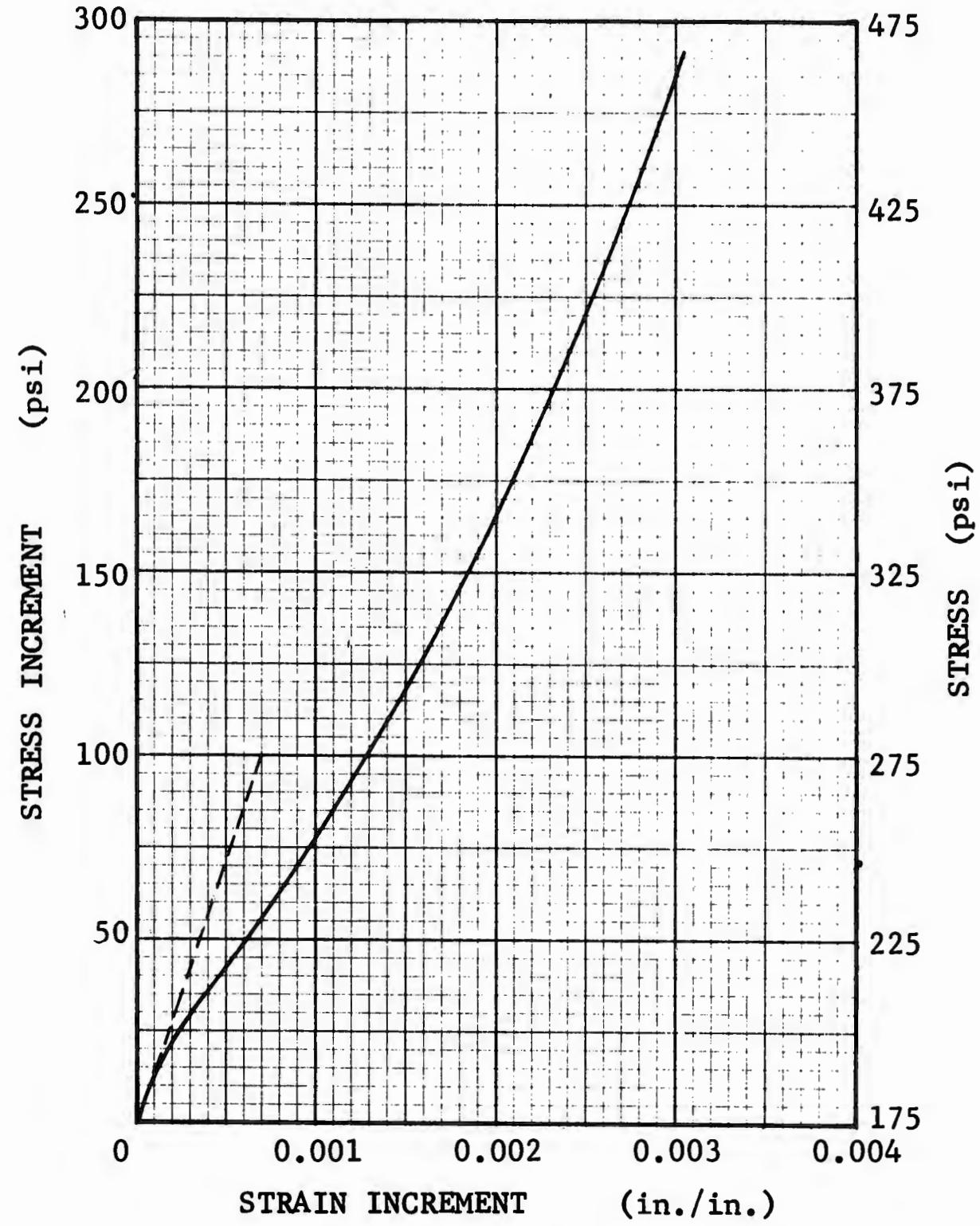

Fig. 19. Quasi-Static Stress—Strain Curve Starting From σ_o = 175 psi

Wave-Propagation Tests

It has been observed that there is a direct correspondence between characteristics of propagating waves and the equation of state (stress–strain curve). In view of observations that the stress–strain behavior is altered by a period of application of constant stress, corresponding changes are to be expected in the behavior of propagating waves. In fact, it might be reasonable to expect observed changes to be comparable in magnitude (relatively speaking) to the observed alterations in the stress–strain relationship. As an example, compare the magnitude of the time-dependent effect with the total stress–strain behavior in Figs. 16 and 18. (As indicated on p. 67, the importance of studying the behavior does not, however, rest simply in the magnitude of effects presently observed.)

At present, the experimental observations of time dependence on the initial stress with regard to wave-propagation studies are of a general nature, i.e., a parametric examination of the effect of time has not yet been undertaken. There are a number of observations, however, that bear on the subject recorded in the literature and doubtless many more not yet reported.

Observations of time-unsteady behavior of stress pulses (induced by impulsive loads) have been observed and reported by most investigators studying propagation of finite-amplitude waves. Most of these observations have been under circumstances in which constant conditions were not maintained ahead of and behind the wave front, so shock behavior

either was not observed or else obscured because only vestiges of such behavior were represented. Nevertheless, from the standpoint of application of information, it is important to place in perspective whatever observations of time-unsteady behavior are available. In that regard, Seaman and Whitman (Ref. 4) have examined changes in wave fronts for impulsive loadings in which the geostatic stress provided conditions ahead of the wave front that were not constant. In such studies, precursors were observed. Thus, since discernible increases in the time between first arrivals and the peak stress were observed to occur as a function of depth, the entire wave front was obviously lengthening.

From a graphical summation of their results, reproduced here as Fig. 20, they concluded that the transition zone between shock waves and plastic [non-shock] waves, in the range they examined, was approximately related to the dynamic stress increment by the following relationship:

$$\frac{\text{dynamic stress increment at wave front}}{\text{initial geostatic stress}} = 12$$

Nevertheless, the transition is not from pure shock to pure plastic waves, and additional considerations are required to establish the significance of such observations in determining the distribution of momentum. A key item to examine is the shape of the entire wave front. Obviously, if the precursor amplitude is very small in comparison with that of the subsequent peak stress, and if the transition zone to peak stress is sharp (several inches) and continually lags farther behind the precursor front, the most important

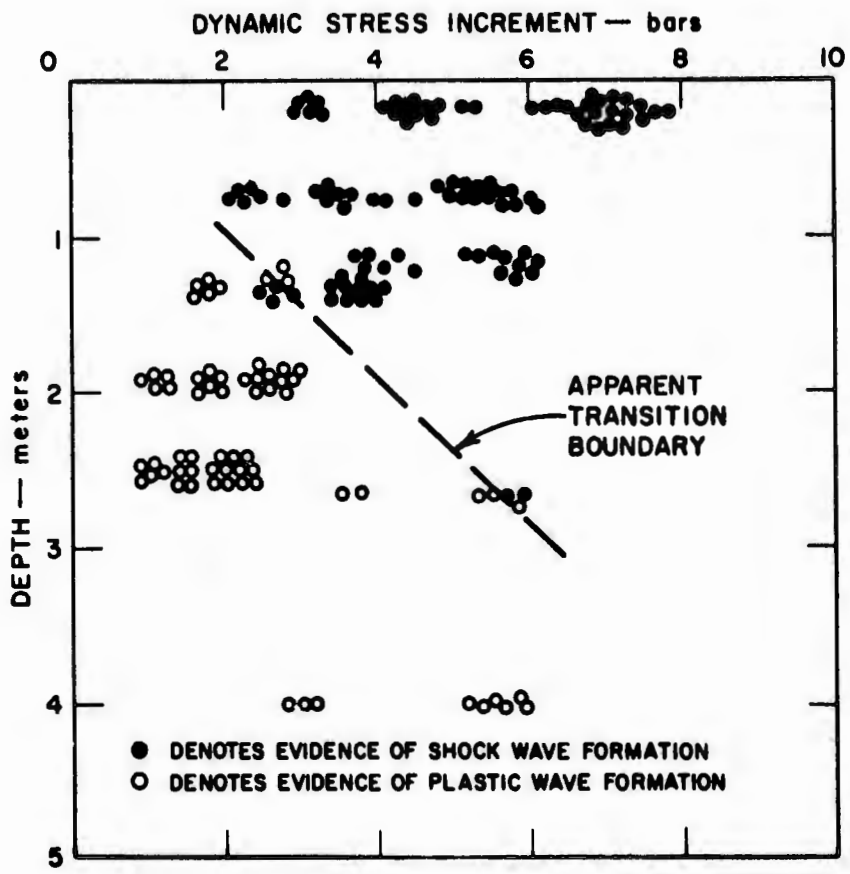

Fig. 20. Observations of Type of Wave Front As Function of Dynamic Stress and Depth (After Seaman and Whitman)

aspect of the response would be associated with the later, main wave (and its rate of propagation) rather than the precursor. Thus the question arises as how to evaluate the precursor and main wave relationship both qualitatively and quantitatively.

One qualitative concept for relating a precursor front to the location and magnitude of any knee in the applicable stress–strain relationship has been indicated in Ref. 5 and depicted here as the first two curves in Fig. 21. Curve (a) indicates an assumed equation of state (something like Fig. 17) and (b) depicts the anticipated relationship of the precursor to the main wave. Of course, the sharp front for the main wave is idealized. Curve (c) is a stress–time form typically (from a purely qualitative standpoint) measured at URS. Roughly speaking the portion of curve (c) below the lower dashed line would lengthen with distance propagated; but for one-dimensional propagation, the remainder would stay constant, provided constant conditions are maintained in the loading and ahead of the front.

As part of a quantitative study to determine the effect of initial or of geostatic stresses on propagating waves, the following observations have been made at URS. It should be noted that the length of the URS ring-boundary column was not great enough for geostatic stress to play an important part in the response, but greater amounts of geostatic stress can be simulated by the application of an initial static air pressure to the loading piston. With regard to practical application of wave-propagation phenomena, where

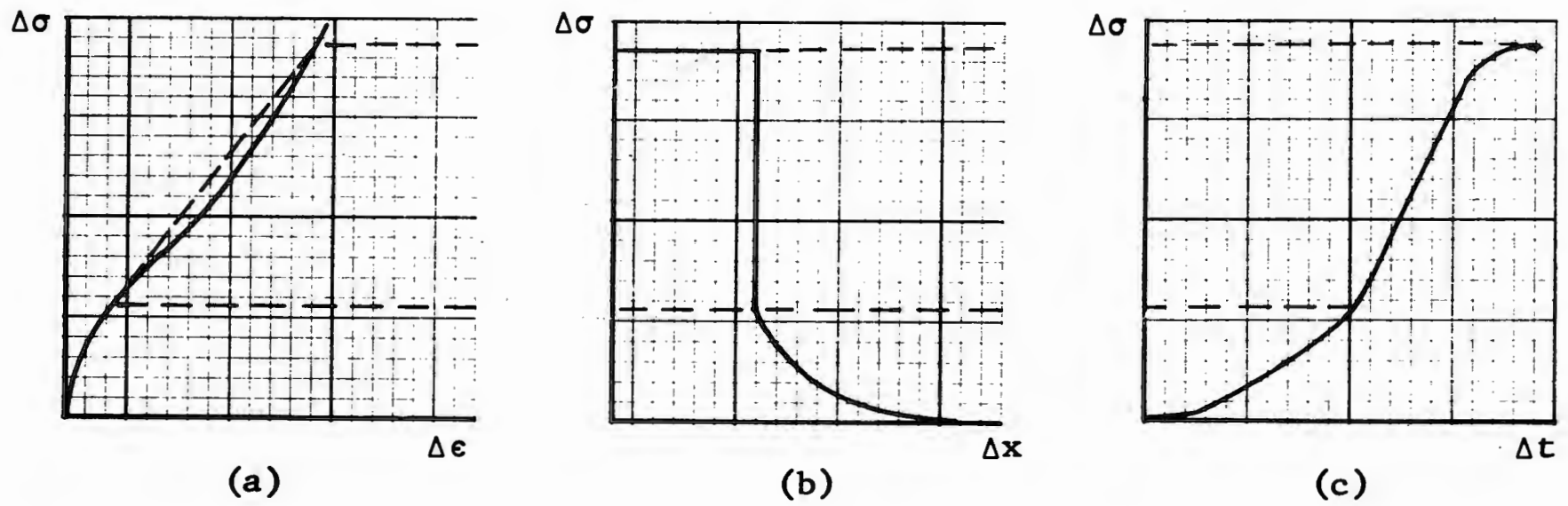

Fig. 21. Typical Stress – Strain, Stress – Distance, and Stress – Time Records for Sand

initial-stress time dependence occurs, the results tend to indicate a behavior somewhat in keeping with the description taken from Selig's survey (Ref. 5). For example, consider the stress−time records in Fig. 22, in which an overstress, $\Delta\sigma$, of 135 psi was applied to a sample with an initial stress, σ_o, of 45 psi (i.e., the ratio of $\Delta\sigma/\sigma_o = 3.0$). From the FFSG* traces it is obvious that for this particular condition, there has been a shortening of the rise time of the stress pulse, i.e., a "shocking up" even though the initial (or geostatic) stress was 45 psi. That is, after propagating a distance of 1 in., the rise** time was about 400 μsec but after propagating a total distance of 8.3 in. it was only 300 μsec.*** There is an indication of a slight precursor on the FFSG trace,**** however, its amplitude could not be more than a few percent of the peak incident stress.

As the ratio of overpressure to initial pressure is made smaller, the latter would be expected to have a greater

---

* FFSG is an abbreviation for free-field stress gauge.

** This comparison can be made using the entire wave front, i.e., from the first observable disturbance to the peak incident stress, if the peak disturbance has an apparent velocity in excess of the first disturbance.

*** At a total distance of 11.3 in., it was only 200 μsec; however, at that gauge station the reflected pulse is just beginning to interfere with the incident wave.

**** The existence of a precursor is more clearly indicated on the RSG trace, however, the character of it is distorted by the fact that the wave is reflecting into prestressed material.

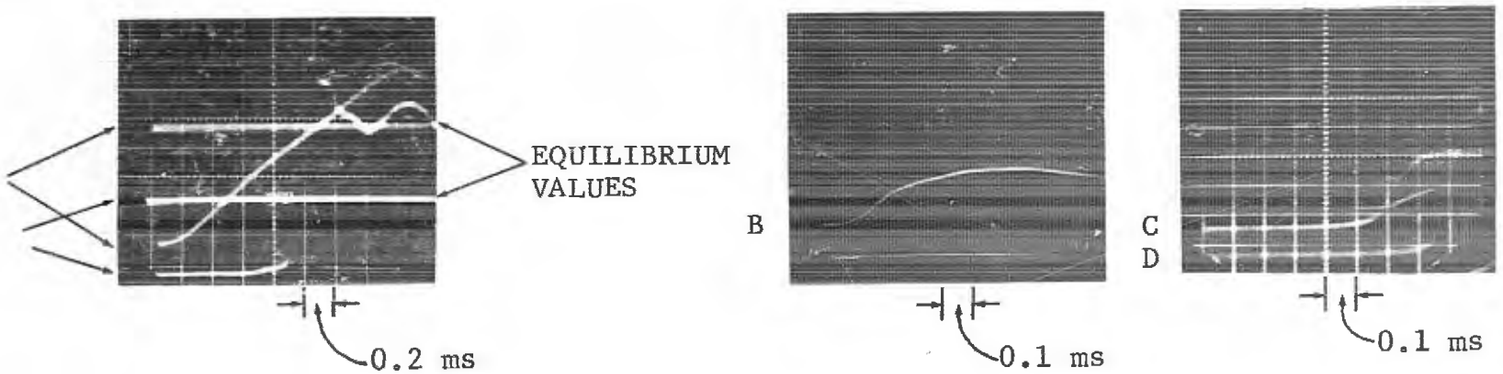

NOTES:

TEST NO.	03096501
MATERIAL	20 – 30 OTTAWA
DENSITY	110 pcf
σ_o	45 psi
$\Delta\sigma$	135 psi

TRACE	GAUGE	VERTICAL SCALE	DEPTH
A	CDT*	~0.012 in./div.	0 in.
B	FFSG 1	85 psi/div.	1.0 in.
C	FFSG 2	42 psi/div.	8.3 in.
D	FFSG 3	32 psi/div.	11.3 in.
E	RSG**	53 psi/div.	14.3 in.

* CDT is an abbreviation for capacitance displacement transducer
** RSG is an abbreviation for reflected stress gauge

Fig. 22. Displacement – Time and Stress – Time Traces From a Wave-Propagation Test

effect on the shape of the stress wave. The results of a test in which $\Delta\sigma$ = 21 psi and σ_o = 13 psi (i.e., the ratio $\Delta\sigma$ to σ_o = 1.6) are presented in Fig. 23. In this case the rise time of the entire front at a distance of 1.0 in. from the input end was about 500 μsec and the shape was similar to that of the previous results. At the time the wave passed the FFSG at a distance of 8.3 in., the rise time of the entire front was about 560 μsec, and the precursor portion (between the first two arrows on the trace) is now evident. This portion is about 280 μsec and the remainder to the peak (including relaxation) is about 280 μsec. At a distance of 11.3 in., the rise time of the entire front is about 620 μsec but now the precursor portion is about 340 μsec and the remainder is about 280 μsec.* This is qualitatively similar to the concepts depicted graphically in Fig. 21 and carries in addition the implication that the higher stress portion was traveling at a constant velocity with no change in shape within the resolving power of the equipment.

The last type of test examined is one in which the ratio of overstress to initial stress is less than 1.0. Oscilloscope records from such a test are presented in Fig. 24. In this case, $\Delta\sigma$ = 30 psi and σ_o = 48 psi ($\Delta\sigma/\sigma_o$ = 0.63). The rise time of the entire front at a distance of 1.0 in. from the input end was about the same as the previous tests, i.e.,

---

* On this last gauge station, the reflected wave is beginning to interfere with the incident wave before the period of rise is over.

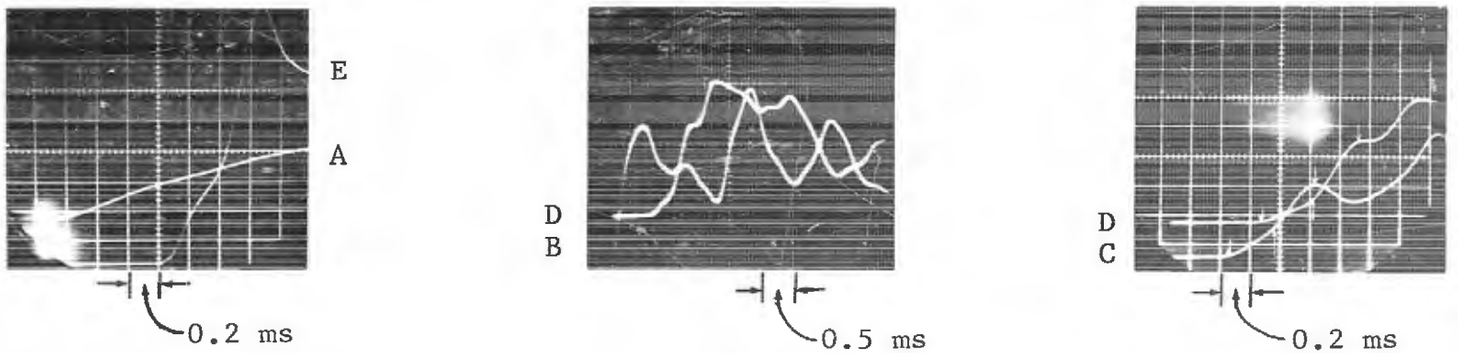

NOTES:

TEST NO.	03166501
MATERIAL	20 – 30 OTTAWA
DENSITY	110 pcf
σ_o	13 psi
$\Delta\sigma$	21 psi

TRACE	GAUGE	VERTICAL SCALE	DEPTH
A	CDT	~0.006 in./div.	0 in.
B	FFSG 1	8.5 psi/div.	1.0 in.
C	FFSG 2	13.0 psi/div.	8.3 in.
D	FFSG 3	8.5 psi/div.	11.3 in.
E	RSG	5.0 psi/div.	14.3 in.

Fig. 23. Displacement – Time and Stress – Time Traces From a Wave-Propagation Test

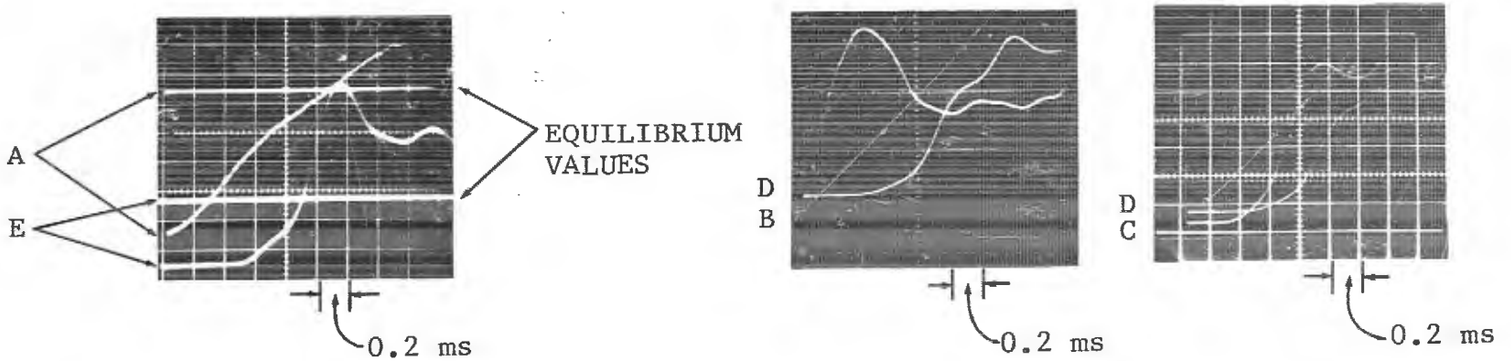

NOTES:

		TRACE	GAUGE	VERTICAL SCALE	DEPTH
TEST NO.	03226501	A	CDT	0.0025 in./div.	0 in.
MATERIAL	20 – 30 OTTAWA	B	FFSG 1	8.5 psi/div.	1.0 in.
DENSITY	110 pcf	C	FFSG 2	7.0 psi/div.	8.3 in.
σ_o	48 psi	D	FFSG 3	8.5 psi/div.	11.3 in.
$\Delta\sigma$	30 psi	E	RSG	15 psi/div.	14.3 in.

Fig. 24. Displacement – Time and Stress – Time Traces From a Wave-Propagation Test

$\simeq$ 400 μsec. At a distance of 8.3 in. this rise time had increased to about 640 μsec. It was not possible in this case to determine the rise time accurately at a distance of 11.3 in., since the reflection returned before the peak incident stress had arrived.

In summary, the following observations were made regarding stress−time records. First, for $\Delta\sigma/\sigma_o \geq 3$, the entire front rise time was observed to decrease as the stress wave propagated along the column, and the precursor appeared small (0−5%) relative to the overstress, i.e., in some cases, if a precursor was propagating faster than the peak stress, it was too small to detect. Secondly, for $\Delta\sigma/\sigma_o \simeq 1$, the rise time of the entire wave front showed a slight increase, although the increase appeared associated primarily with the precursor propagating ahead of the main wave, whereas the main wave portion appeared to propagate unchanged.

Stress−Strain Data

As stated earlier, if the stress−strain curve were continuously concave about the stress axis under all conditions of interest, then the effect of an initial pressure on the stress−strain behavior resulting from a subsequent dynamic overpressure could be accounted for by merely shifting the origin of the curve (Ref. 9). For example, from the stress−strain curve for zero initial pressure, the applicable curve for an initial pressure of 50 psi would be obtained by moving the origin of the axis to the 50-psi level on the curve for zero initial stress. Similarly,

curves for the other initial stresses could be obtained in a like manner. A family of such curves appears in Fig. 25.*

However, this procedure will not be legitimate where time dependence affects the stress−strain curve. Examination of Figs. 16−19 indicates the magnitude of the difference in response to subsequent loading for two such cases. The effect is seen to be relatively larger when the subsequent overpressure is small compared to the initial stress. It would be desirable to know under what conditions it is necessary to account for this aspect of behavior for impulsive loadings insofar as the distribution of momentum is concerned. At present, an idea of the importance in this regard may be obtained by examining stress−strain data from wave-propagation tests wherein initial pressures were applied for 1−3 min hold times. Such data (involving time dependence on initial stresses) has been compared in Fig. 26, with the simple family of curves generated in Fig. 25 (these curves portray the case wherein latent straining was not considered). From this comparison it appears as though the graphical solution, generated entirely from the equation of state for a zero-initial-stress condition, is reasonably adequate, in the range examined, for predicting the strains likely to result from dynamic overpressures, provided the initial-stress conditions are known. Through the relationship between particle velocity and stress−strain (Eq. 42), it may be inferred that

---

* These curves were derived from a single curve which is the average of the four curves in Fig. 11.

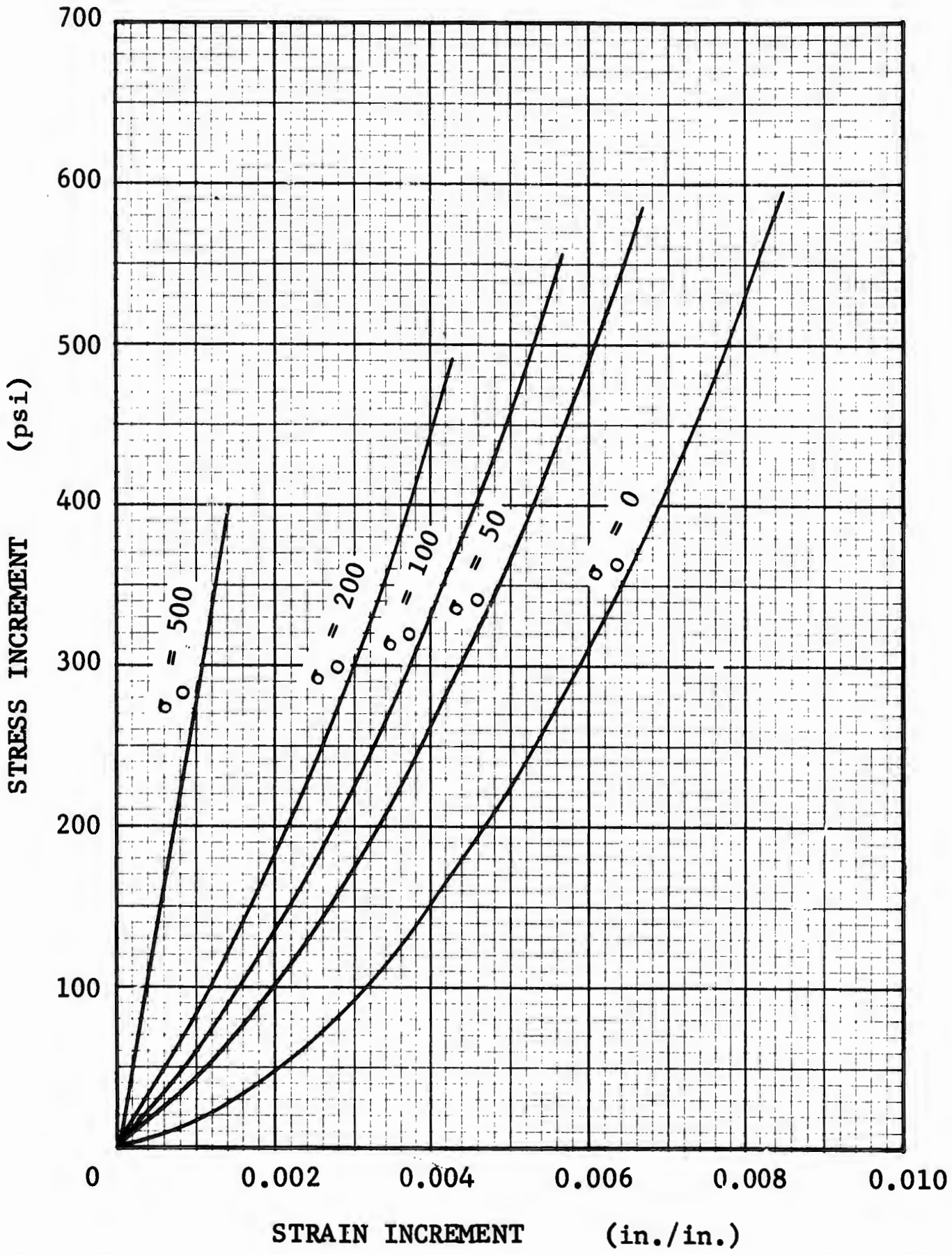

Fig. 25. Stress—Strain Curves for Various Initial Stresses Calculated From the Curve for $\sigma_o = 0$

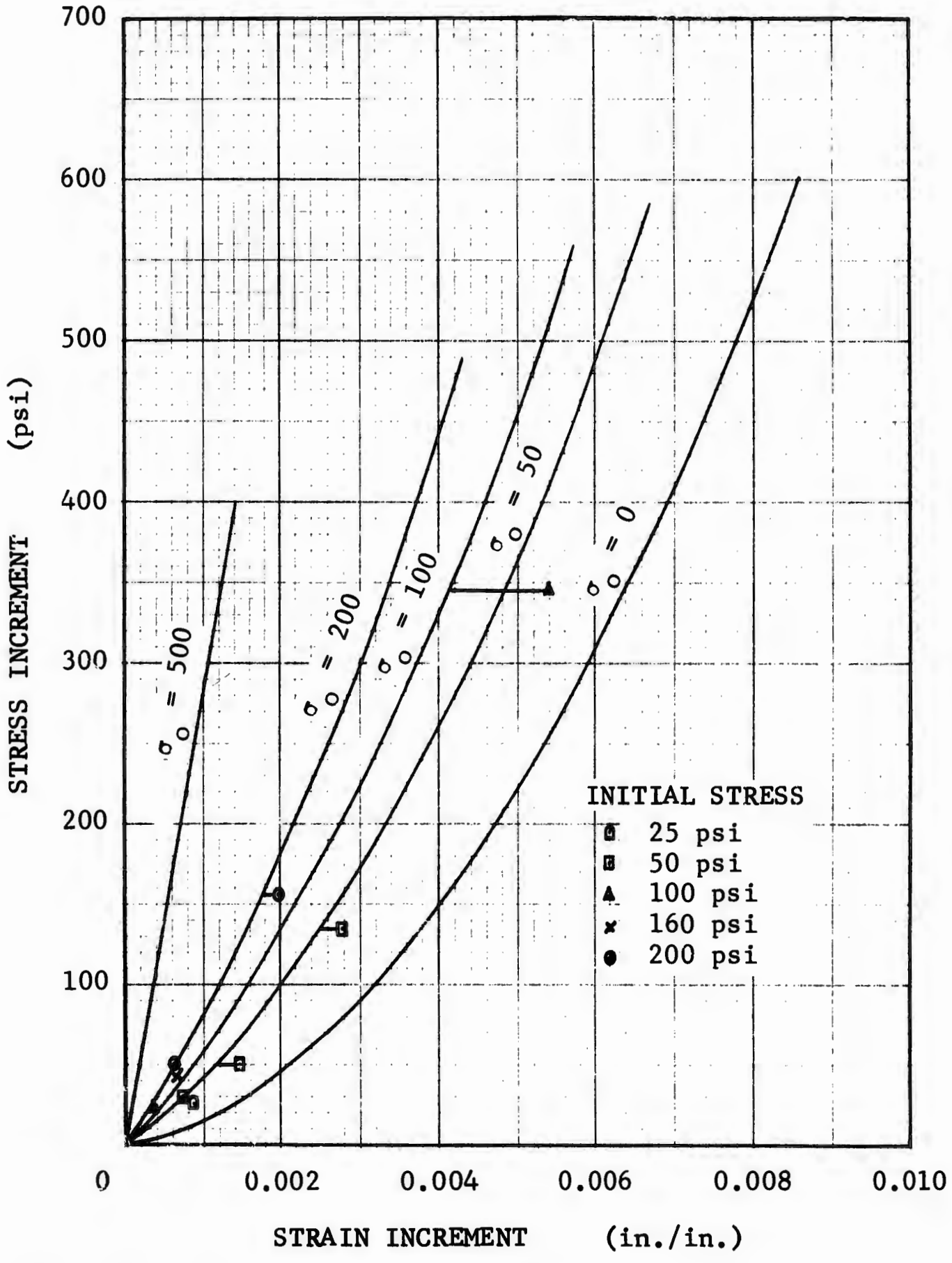

Fig. 26. Comparison of Measured Data From Wave-Propagation Tests and the Stress—Strain Curves From Fig. 25

the same is true of momentum. It will be shown below that precursor (or seismic) velocities provide a useful index of initial-stress conditions.

Stress Wave Velocities

A number of wave-propagation tests were conducted on sand specimens subjected to initial stresses, σ_o, ranging from 13 to 310 psi. In these tests, the overpressure or dynamic stress increment, $\Delta\sigma$, ranged from 21 psi to 500 psi and the ratio of overpressure to static initial stress $\Delta\sigma/\sigma_o$) ranged from 0.25 to 4.9. Constant conditions were maintained ahead of and behind the wave front. From these tests the relationship between the velocity of the first disturbance and the magnitude of the initial stress was determined and is presented in Fig. 27.* In most cases, this velocity was obtained by dividing the total sample length by the total travel time, where that time was obtained from the instant the displacement—time trace indicated motion to the time at which the first observable disturbance (in this case a precursor) was monitored by the RSG. In addition, free-field velocity measurements were obtained between corresponding points on two traces. The former measure is superior in determining velocities of first disturbances, since it has the advantage of greater resolution. This is because the stations used were farther apart and because smaller signals may be

---

* The numbers adjacent to the data points refer to over-stresses, from which it is apparent that the velocity of the first disturbance is independent of the magnitude of the dynamic increment.

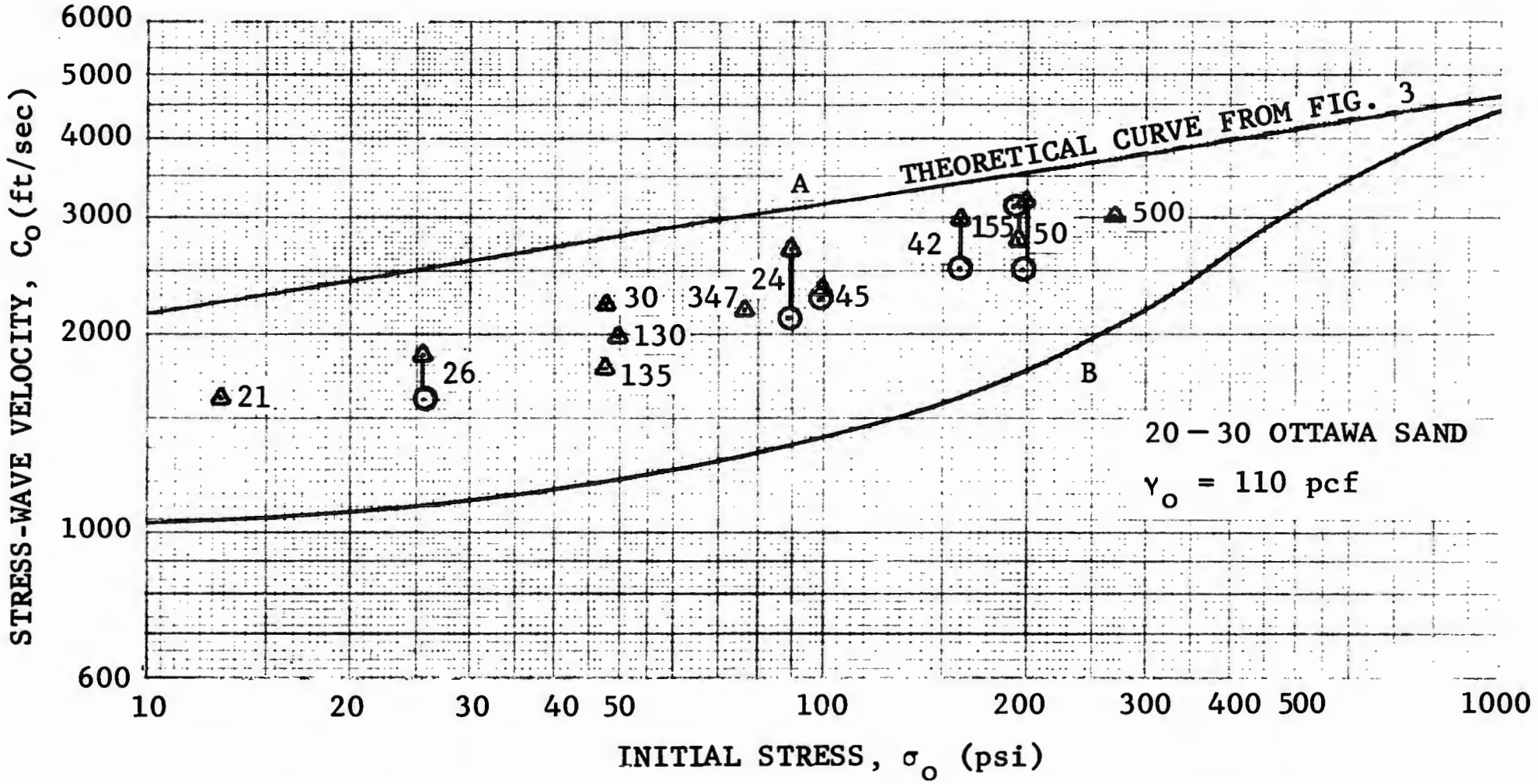

△ Velocity of the First Arrival Measured Over the Total Sample Length
○ Velocity of the First Arrival Measured Between Free-Field Stress Gauges
Note: Overstress (in psi) indicated by numerals adjacent to plotted points

Fig. 27. Stress-Wave Velocity of the First Arrival Versus Initial Stress

resolved. Nevertheless, from the results it is apparent that fairly good agreement is obtained between the two sets of measurements.

Curve A in Fig. 27 is the relationship between initial stress and sound velocity for a rigid-pack Hertzian elastic response. Curve B, on the other hand, is the relationship between initial stress and sound velocity determined for an equation of state of the material wherein particle relocation occurs.* Both curves depict responses applicable to the test material. The experimental data for first arrivals, i.e., small-amplitude sound waves, would be expected to fall within these limits. It is of interest that the data are observed to fall closest to the rigid-pack Hertzian elastic response. Since the data fall very close to curve A, it might be inferred that the assemblage does appear initially as a rigid pack and that the magnitude of the difference in observed response from that calculated from the theory (shown graphically in Fig. 27) is dependent on the ability of the equipment to resolve extremely small amplitudes. Further observations indicate (to be shown later in Fig. 29, as evidenced by considerably slower wave velocities for the peak stress) that the assemblage does not continue to behave like a rigid pack even at amplitudes that are still very small and that this

---

* The particle-relocation consideration presented in the theory in Section 3 is based on a stress—strain curve characterized by $d^2\sigma/d\epsilon^2 > 0$. Specifically, this analytical relationship approximates the (σ - ϵ) behavior for the experimental data presented herein.

subsequent behavior is governed mainly by the particle relocation process.

Of course it is possible that the gauge threshold is too high for detecting sound waves and that the first detected disturbance is a shock wave propagating through the rigid pack. This would be limited by the lower curve of Fig. 3. That curve has been reproduced in Fig. 28 together with the above experimental data on precursor-front velocities. In addition these data are compared with other experimental data, i.e., the results of Lawrence's ultrasonic tests at MIT (Ref. 16). In addition, two values of precursor-front wave velocity, backfigured by measuring the initial tangent modulus on the two quasi-static stress–strain curves presented in Figs. 17 and 19, are plotted in Fig. 28.

Thus, laboratory tests with finite-amplitude waves, as reported here, indicate a relationship between the rigid-pack seismic, or Hertzian, velocities and what has been described as a precursor front. Consequently, seismic measurements have been placed in better perspective, insofar as stress–strain behavior is concerned, by showing them to be indicative of the initial-stress conditions.

It is, of course, valuable to be able to determine initial stress conditions by examining first arrivals, i.e., precursor fronts (seismic disturbances), but the major concern is to be able to determine response to rather large disturbances. To simplify this investigation, experimental

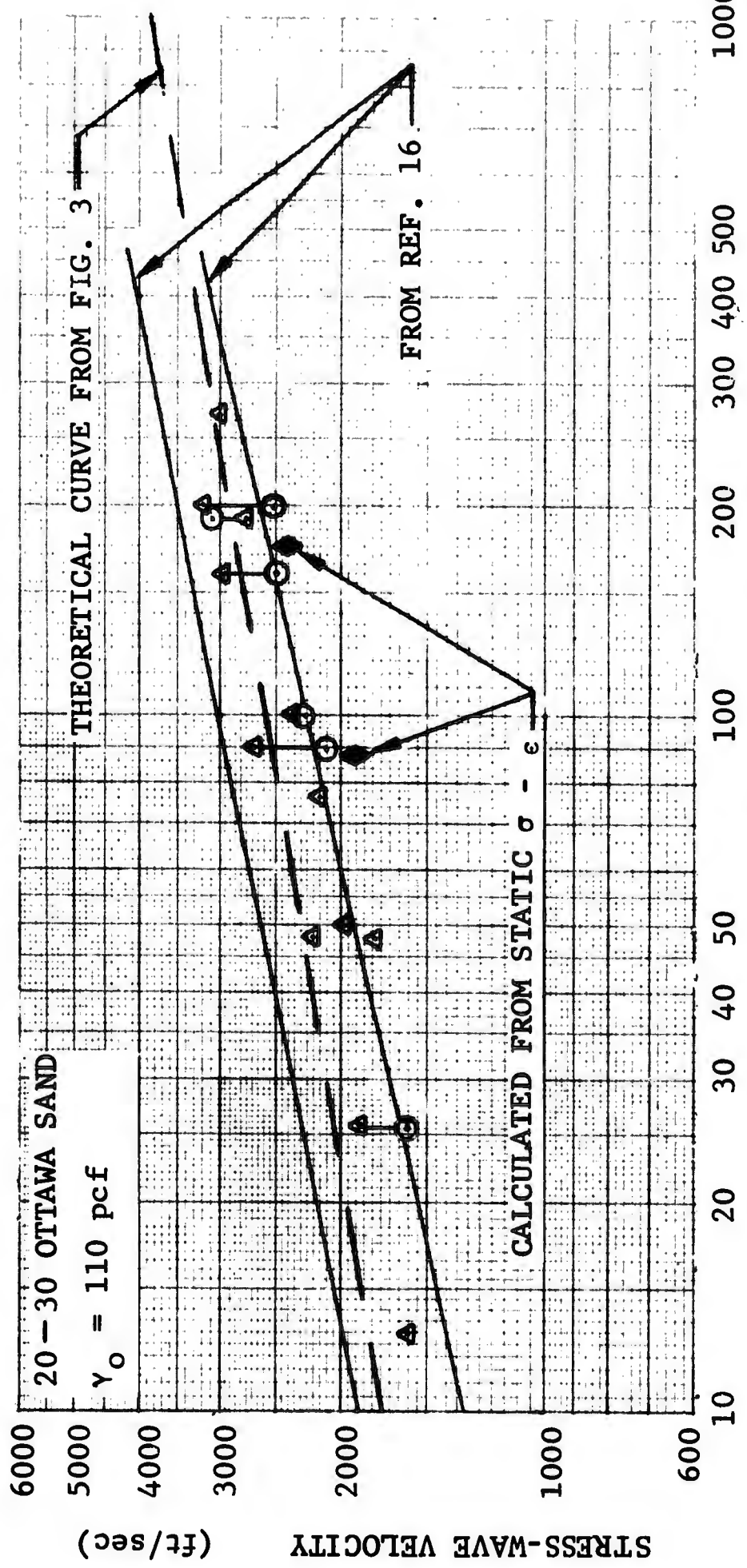

Δ Velocity of the First Arrival Measured Over the Total Sample Length
O Velocity of the First Arrival Measured Between Free-Field Stress Gauges

Fig. 28. Stress-Wave Velocity of the First Arrival Versus Total (Initial) Stress

studies have been made with constant conditions maintained ahead of and behind the wave front. Thus, the stress, strain, peak particle velocity and wave velocity resulting from large-magnitude impulsive loads were measured and compared fairly simply.

The results of such studies are summarized in Fig. 29, where wave velocities of the peak disturbance for various conditions of initial stress σ_o and dynamic stress increments $(\sigma - \sigma_o)$ are presented as a function of the total stress, σ. Also plotted in Fig. 29 are the curves of Fig. 7 representing sound and shock velocities determined from the theory of Section 3. It should be recalled that curve C in the figure represents the shock velocity as a function of stress behind the shock for an initially stress-free assemblage (zero initial stress), in which response is governed by particle relocations, and curve B is the corresponding sound velocity. Curve C is also the asymptote of all members of the family of curves of shock velocity when the assemblage is not stress-free initially, and curve B is the locus of the points of intersection of each member of the family, with the velocity of sound at the appropriate initial stress. It might be inferred that peak stress velocities of finite-amplitude waves that are large in magnitude relative to the initial stress would fall in the region of curve C and that finite-amplitude waves of small magnitude relative to the initial stress would have peak stress velocities which fall in the region of curve B. The initial stress condition has been indicated beside the plotted points to demonstrate this

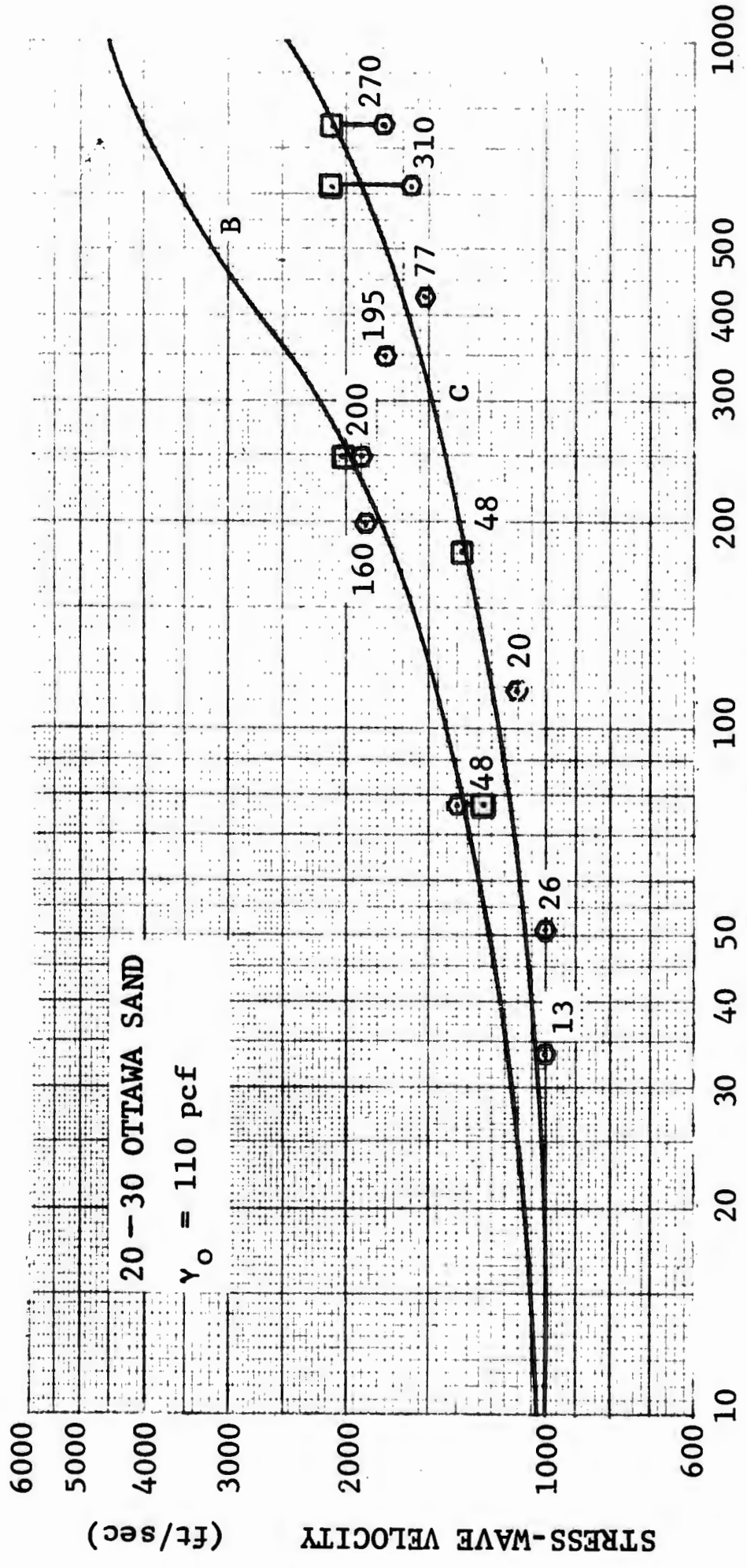

○ Velocity of the Peak Incident Stress Measured Over the Total Sample
□ Velocity of the Peak Incident Stress Measured Between Free-Field Stress Gauges
Note: Initial stress (in psi) indicated by numerals adjacent to plotted points

Fig. 29. Stress-Wave Velocity of the Peak Incident Stress Versus Total Stress

behavior. Within the experimental limits of error, it appears that when the ratio of the dynamic increment to the initial stress $(\sigma - \sigma_o)/\sigma_o$ exceeds 1, the points fall in the region of curve C and that it is not until the ratio is somewhat less than 1 that the peak stress velocities fall in the region of curve B. Response to the peak stress in all cases therefore corresponds to that portion of the theory presented (in Section 3) in which particle relocation was the governing behavior with regard to response to finite-amplitude waves.

The first disturbance velocities of Fig. 28, corresponding to different initial stresses, were obtained concurrently with the peak disturbance velocities of Fig. 29. The reader can easily see that first disturbance velocity is a straight line when plotted against its total stress on log-log paper, and the other is not. Hence the rigid pack response is quite different from that associated with particle relocation. Since this is true, the precursor velocity measured as a function of initial (or geostatic) stress is not at all a suitable index of the behavior of finite-amplitude waves as a function of depth and, therefore, of itself bears no relationship whatever to attenuation processes.

Furthermore, these observations preclude any belief that a single Hertzian (seismic) velocity measured for a particular initial condition could describe all the peak disturbance velocities of finite-amplitude waves of different magnitudes as some simple constant fraction (such as 1/2 or 2/3) of that one velocity.

Section 7
SUMMARY

Impulsive loadings with constant conditions ahead of and behind the wave front were applied to a dry granular cohesionless material under conditions characterized by a behavior such that $d^2\sigma/d\epsilon^2 > 0$. A general inspection of the stress-strain relationship under these conditions indicates three regions of behavior characterized chiefly by particle relocations, rigid-pack behavior, and particle fracturing. Studies of the relationship between characteristics of propagating stress waves and stress-strain-initial-stress conditions resulted in the following observations:

Primary Phenomena:

1. It appears as if particle relocations, rigid-pack behavior, and particle fracturing coexist throughout the entire stress range, but that the dynamic response to the loading front is dominated by the particle relocation behavior over a wide stress range.

2. Theoretical considerations and experimental observations indicate that when the initial stress conditions are those of zero stress, simple shock waves propagate.

3. These shock waves in granular media have finite rise times and are found to be rounded at the peak, but the rounding once formed is time independent.

4. The stress−strain relationship has been used as an applicable equation of state to determine the propagation velocity of the peak stress and the results found to agree suitably with the values measured in wave propagation tests.

5. Reflected waves propagating into material at an initial stress created by the incident wave behave as shock waves also.

6. Reflected wave-propagation velocities are also determinable from the stress−strain relationship.

Secondary Phenomena:

7. When a finite initial stress exists, the propagation of an overstress is governed by a local modification of the stress−strain curve, i.e., during the time the granular sample is held at the initial stress, the particles over-compact, so that upon application of the overstress the smallest elements of the overstress are observed to propagate as though the sample were a rigid pack at the same density.

8. As the overstress rises through the wave front, the smooth pattern of particle relocation appropriate to the typical stress−strain curve is again obtained.

   Thus

9. When the dynamic increment is large relative to the initial stress ($\Delta\sigma/\sigma_o \geq 3$), the peak stress is observed to propagate with a velocity approximating that of the pure shock according to 4 above, but a precursor traveling with the sound velocity of a rigid pack is seen to occur. It bears no constant relationship to the wave velocity of the peak disturbance.

   And

10. When the dynamic increment is small relative to the initial stress ($1/4 \leq \Delta\sigma/\sigma_o < 1$), the peak stress is observed to propagate with a velocity approximating that determined for a sound wave under conditions of particle relocation where Hertz type contact forces prevail. The precursor is still evident, propagating with the velocity of sound of the rigid pack. Again it bears no constant relationship to the wave velocity of the peak disturbance.

Interpretation:

11. When a granular medium is subjected to a dynamic as well as an initial stress, the finite wave of overstress will either propagate as a shock or as a two-element pulse. In the latter case, the first element, called the precursor, is of low amplitude, and the second element possesses properties characteristic of a shock. For example, the front of this second part of the wave has been observed to steepen with distance as it propagates.

12. Most important, the peak particle velocity and all other parameters pertinent to damage are associated with this second element. Since these two elements according to 9 above are not related linearly through overstress, no predictions of damage based on peak-disturbance velocities computed as a constant fraction of the first-disturbance velocity will be valid except by chance.

Section 8
CONCLUSIONS AND RECOMMENDATIONS

It is believed that the results of these dynamic loading studies lead to the following general conclusions:

1. Stress—strain behavior has been identified as a suitable equation of state for predicting wave-propagation behavior in a granular medium under a range of loading and boundary conditions.

2. This wave-propagation behavior includes defining the distribution of momentum necessary to design of protective construction. The procedure for conversion to deliverable impulse is implicit in the stress—strain relationship.

Thus, for a certain range of conditions, the stress—strain relationship has been correlated with measured and calculated wave and particle velocities to the extent that this relationship can be interpreted to make possible prediction of the delivered impulse. It might be inferred that this will also be possible under more general conditions.

By means of principles discussed herein, it is expected that samples of field material could be subjected to laboratory tests to determine the critical features of the material under a large impulsive loading—not originally accessible to a field study. Field seismic information might be used to determine initial conditions in situ. Thus, desirable information, as for example, input to the soil—structure interaction problem, could be determined. Nevertheless, there are still unresolved problems. Studies of unloading

processes, time-dependent effects of the initial stress condition, and variation in boundary conditions are necessary before stress–strain behavior of a cohesionless granular material will be related to deliverable impulse for most conditions of practical importance. When this is successfully completed, it is anticipated that these methods may be applied to deduce the more complex behavior of field media. Obviously, application of that information will be dependent on knowledge of the field loading condition and the applicable boundary conditions.

In order to resolve problems pertaining to the free-field input conditions required for soil–structure interaction studies, it would seem desirable to pursue all of the unanswered questions with further laboratory studies and then finally evaluate the results of these studies in the field.

Section 9
REFERENCES

1. Glasstone, S. et al., eds., The Effects of Atomic Weapons, Los Alamos Scientific Laboratories, Los Alamos, New Mexico, Sep 1950

2. Whitman, R. V., "The Behavior of Soils Under Dynamic Loadings, Final Report on Laboratory Studies," Journal of the Soil Mechanics and Foundations Division, ASCE, Vol. 87, No. SM3, Part 1, June 1961

3. Zaccor, J. V., H. G. Mason, and D. F. Walter,"Concepts, Equipment and Techniques for the Study of the Dynamic Behavior of Soils," Report 1, Study of the Dynamic Stress-Strain and Wave-Propagation Characteristics of Soils, URS 637-24, Contract No. DA-22-079-eng-373, United Research Services for the U.S. Army Engineer Waterways Experiment Station, Vicksburg, Mississippi, Nov 1964

4. Seaman, L. and R. V. Whitman, Stress Propagation in Soils, DASA 1266-4, Contract No. DA-49-146-XZ-018, SRI Project PHU-2917, for Defense Atomic Support Agency, June 1964

5. Selig, E. T., "Characteristics of Stress-Wave Propagation in Soil," Proceedings of the Symposium on Soil-Structure Interaction, University of Arizona, Tucson, Arizona, Sep 1964, pp. 27 – 61

6. Stoll, R. D. and I. A. Ebeido, Dynamic Response of Granular Soils, Technical Report No. 2, Columbia University for U.S. Naval Civil Engineering Laboratory, Port Hueneme, California, May 1964 (AD 451 015)

7. Duvall, G. E., "Concepts of Shock Wave Propagation," Bulletin of the Seismological Society of America, Vol. 52, No. 4, Oct 1962, pp. 869 – 893

8. Zaccor, J. V. and N. R. Wallace, Techniques and Equipment for Determining Dynamic Properties of Soils, Final Report URS 155-30, DASA 1421, Contract No. DA-49-146-XZ-019, United Research Services for the Defense Atomic Support Agency, Washington, D.C., Nov 1963

9. Zaccor, J. V., "Dynamic Behavior of Granular Media," Proceedings of the Symposium on Soil-Structure Interaction, University of Arizona, Tucson, Arizona, Sep 1964, pp. 62 – 72

10. Courant, R. and K. O. Friedrichs, Supersonic Flow and Shock Waves, Interscience Publishers, Inc., New York, 1948, p. 132

11. Hendron, A. J., Jr., R. E. Fulton, and B. Mohraz, The Energy Absorption Capacity of Granular Materials in One-Dimensional Compression, AFSWC-TDR-62-91, Department of Civil Engineering, University of Illinois, for Air Force Special Weapons Center, Kirtland Air Force Base, New Mexico, Jan 1963

12. Timoshenko, S. and J. N. Goodier, Theory of Elasticity, Second Edition, McGraw-Hill Company, Inc., New York, 1951, p. 372

13. Mindlin, R. D., "Compliance of Elastic Bodies in Contact," J. Appl. Mech., Vol. 16, 1949, pp. 259–268

14. Deresiewicz, H., "Mechanics of Granular Matter," Advances in Appl. Mech., Vol. V, 1958, pp. 233–306

15. Weidlinger, P. and A. T. Mathews, "Shock and Reflection Phenomena in a Nonlinear Medium," paper presented at American Society of Civil Engineers Structural Engineering Conference, New York, Oct 1964

16. Lawrence, F. V., Jr., "Propagation Velocity of Ultrasonic Waves Through Sand," The Response of Soils to Dynamic Loadings, Report No. 14, Contract No. DA-22-079-eng-224, Massachusetts Institute of Technology Report No. R63-8 for U.S. Army Engineers Waterways Experiment Station, Vicksburg, Mississippi, Mar 1963

17. Whitman, R. V. and G. B. Clark, Nuclear Geoplosics, Part II, DASA 1285(II), Contract Nos. DA-22-079-eng-224 and DA-49-146-XZ-030, Massachusetts Institute of Technology and Missouri School of Mines and Metallurgy for Defense Atomic Support Agency, Washington, D.C., May 1964

18. Durbin, W. L., "Measurements of Stress-Strain, Peak Particle Velocity and Wave-Propagation Velocity in Three Sands," Report 3, Study of the Dynamic Stress-Strain and Wave-Propagation Characteristics of Soils, URS 637-23, Contract No. DA-22-079-eng-373, United Research Services for U.S. Army Engineer Waterways Experiment Station, Vicksburg, Mississippi, Feb 1965

19. Durbin, W. L., "Correlation of Stress-Strain and Wave-Propagation Parameters in Shock-Loaded Dry Sands," Report 2, Study of the Dynamic Stress-Strain and Wave-Propagation Characteristics of Soils, URS 637-15, Contract No. DA-22-079-eng-373 Report No. 3-91, United Research Services for U.S. Army Engineer Waterways Experiment Station, Vicksburg, Mississippi, Nov 1964

20. Whitman, R. V., E. T. Miller, and P. J. Moore, "Yielding and Locking of Confined Sand," Journal of the Soil Mechanics and Foundations Division, ASCE, Vol. 90, No. SM4, Part 1, July 1964, p. 57

21. Jamieson, J. A. and M. Cann, "Grain Pressures in Deep Bins," Engineering News, Vol. 51, No. 10, Jan-June 1964, pp. 236-243

22. Tschebotarioff, G. P., Soil Mechanics, Foundations and Earth Structures, McGraw-Hill Civil Engineering Series, 1951, pp. 265-267

23. Jaky, Dr. J., "Earth Pressure - Pressure in Silos," Proceedings of the 2nd Interaction Conference on Soil Mechanics and Foundation Engineering, Sub-Section IF, Rotterdam, Holland, June 21 – 30, 1948

24. Janssen, H. A., "Versuche über Getreidedruck in Silozellen," Zeitschrift des Vereins deutscher Ingenieure, 1895, p. 1045

25. Seaman, L., G. N. Bycroft, and H. W. Kriebel, Stress Propagation in Soils, DASA 1266-3, Contract No. DA-49-146-XZ-018, SRI Project PHU-2917, for Defense Atomic Support Agency, May 1963

26. Terzaghi, Karl, Theoretical Soil Mechanics, John Wiley and Sons, New York, 1943

27. Mason, H. G., O. H. Criner, R. Waissar, and N. R. Wallace, A Study of the Dynamic Soil-Structure Interaction Characteristics of Real Soil Media, AFSWC-TDR-63-3075, URS 621-13, United Research Services for the Air Force Weapons Laboratory, Kirtland Air Force Base, New Mexico, Dec 1963

28. Lenczer, D., "An Investigation Into the Behavior of Sand in a Model Silo," The Structural Engineer, Vol. 41, No. 12, Dec 1963, pp. 389 – 398

29. Mason, H. G., V. W. Davis, and J. V. Zaccor, A Further Study of Stress-Wave Transmission, DASA 1364, URS 160-12, United Research Services for Defense Atomic Support Agency, Washington, D.C., Feb 1963

30. Rowe, P. W. and L. Barden, "Importance of Free Ends in Triaxial Testing," Journal of the Soil Mechanics and Foundations Division, ASCE, Vol. 90, No. SM1, Part 1, Jan 1964, pp. 1-29

31. Wiedermann, A. H., Static Experiments for the Study of the Interaction of Buried Structures With Ground Waves, AFSWC-TR-61-32, prepared by Armour Research Foundation for Air Force Special Weapons Center, Kirtland Air Force Base, New Mexico, Apr 1961

32. Liepmann, H. W. and A. E. Puckett, Introduction to Aerodynamics of a Compressible Fluid, John Wiley and Sons, Inc., New York, 1947

ACKNOWLEDGEMENTS

The work described here was done by the Soil and Structural Mechanics Division of URS. Technical guidance has been provided by Messrs. H. G. Mason, Manager, Soil and Structural Mechanics Division, and J. V. Zaccor, Project Manager. The work was done under the administrative leadership of Mr. A. B. Willoughby, General Manager, Burlingame Research Center. Mr. J. V. Zaccor, Project Manager, was supported by Messrs. W. L. Durbin, N. R. Wallace, D. F. Walter, and R. Rhoda. The cooperation and technical support of Mr. L. Schindler, WES Project Monitor, is gratefully acknowledged.

Appendix A
SIDEWALL FRICTION

In the history of soil mechanics research, investigators have been plagued by the problem of sidewall friction in their laboratory devices. Some investigators have assumed that a triangular zone, bounded on the top by the sample surface and on the sides by 45-deg lines extending toward the center from the intersection of the surface and the sidewalls, is unaffected by the friction of the sidewalls. Other investigators, not fully aware of the seriousness of the problem, have tended to ignore the influence. And still others (particularly those concerned with wave propagation) have taken steps to reduce the effects through use of friction-reducing materials or by the use of segmented boundaries. URS has taken such steps in the development of the fluid and ring boundaries. Nevertheless, from initial observations of the effects of sidewall friction, it was felt that the behavior could be used to advantage in providing a pseudo-longer sample,* and therefore additional observations and analyses were made. This appendix is a summary of this effort, including observations of other investigators.

---

* This concept is explained in more detail in Report 1, p. 91, where it is proposed to be used to reduce the rate of conversion of momentum to impulse to a very small amount in comparison with what occurs at a rigid end-boundary.

Some of the latter include observations made in grain silos and bins, which were made in an effort to gain, for design purposes, an understanding of stress distribution against the bin wall. These observations have been made on both models and on full-sized bins and have shown that the increase of load at the center of the bin on the bottom and against the sides of the bin at the bottom is not directly proportional to the height of the grain, but gradually increases to a maximum value above which additional height of grain causes no increase. Probably the best known of these tests, on full-sized bins, was reported by Jamieson in Ref. 21, Tschebatarioff (Ref. 22),in commenting on the past mathematical treatment of the problem of pressures in silos, refers to a paper by Dr. Jaky (Ref. 23) as being noteworthy. Jaky makes a complex analysis of the data taken by Jamieson and shows good agreement between his theoretical analysis and that data. However, it is believed that a simpler relationship can be shown to exist if one examines the problem in terms of Terzaghi's arching theory. A number of investigators have made such analyses for sidewall friction for their particular devices* in an effort to determine the influence sidewall friction will have on the stress distribution within the soil sample.

---

* References 11, 24, and 25.

Two major problems have made it difficult for them to check these analyses, one being the choice of values for the ratio of lateral to axial stress K and the other being a method of measuring the free-field stress in the container.

ACTIVE ARCHING

A simple review at this point of the analysis of the active arching conditions developed by Terzaghi (Ref. 26. p. 71) and the resulting equations will help to make the comparison with the data given later easier to follow.*

A simple equilibrium condition within the soil bin, with the sidewalls replaced by friction forces and the bottom of the container replaced by its reaction forces, is presented in Fig. A-1a. If one assumes** that the shear resistance in the soil is less than between soil and bin, then the failure will take place within the soil, and thus it will be found that the shear forces will be related to the angle of internal friction within the soil and to the ratio of lateral to axial stress K (taken at a point).

---

* A detailed discussion of the development of the equations is given in Refs. 26, p. 71, and 27.

** The support for the validity of this assumption is presented later in this section.

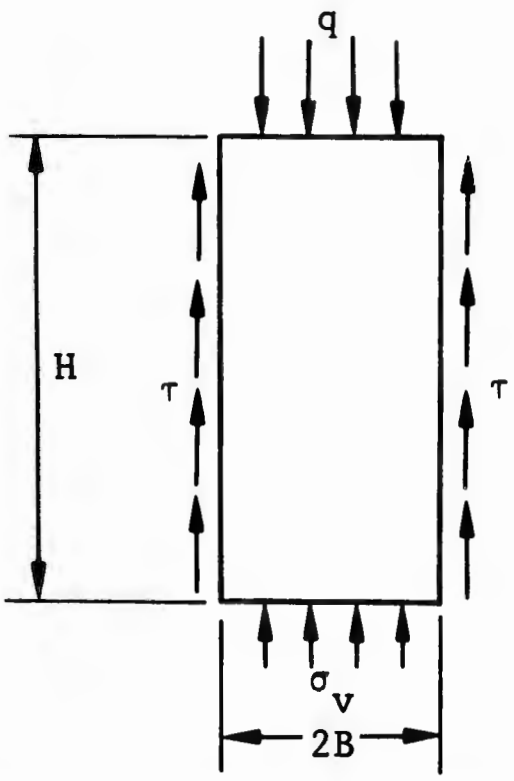

Fig. A-1a. Equilibrium Conditions for the Soil Within a Soil Bin

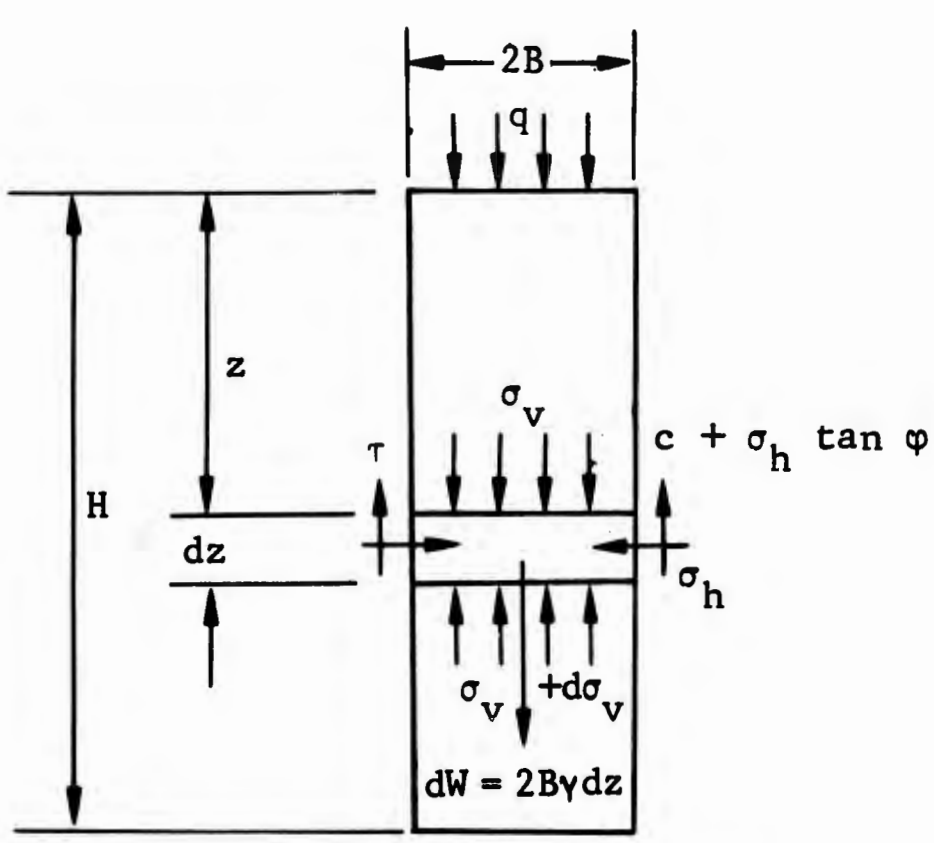

Fig. A-1b. Assumptions on Which Computation of Average Vertical Stress in Sand Between Two Vertical Surfaces of Sliding Is Based

Having made this assumption, one can then see from the following discussion the similarity between sidewall friction and the static active arching case as presented in Fig. A-1b.

In this application, the basic assumption of static active arching is that the model is comprised of the soil in the bin which compresses under its own weight and under a uniform surface pressure, if one exists. The differential straining between the soil and the container is assumed to be sufficient to develop the maximum shear forces along the failure plane.

Figure A-1b illustrates the assumptions that provide the basis for computation of stress in the soil between the two assumed* vertical surfaces of sliding in the static active case. Solution of the equations resulting from a summation of the vertical forces at equilibrium results in the following equation for the stress at a given depth Z:**

$$\sigma_v = \frac{B(\gamma - c/B)}{K \tan \varphi} \left(1 - e^{-\frac{Z}{B} K \tan \varphi}\right) + qe^{-\frac{Z}{B} K \tan \varphi} \qquad (A.1)$$

---

* Experimental evidence such as pictured in Fig. A-3 seems to support the concept of vertical surfaces of sliding of the soil, since as the soil was removed from the bottom of the container the soil at the top slid down. As can be seen from the curvature of the horizontal lines, the failure took place in the soil.

** The equation is developed for the case of a bin of unit thickness.

where

B = one-half the span of the container

γ = unit weight of the soil

c = cohesion

K = ratio of the horizontal (lateral) to the vertical (axial) stress

tan φ = coefficient of internal friction of the soil

σ_v = vertical stress on a horizontal section at depth Z

Z = depth of the soil

q = surcharge per unit area

This equation is for the solution of the two-dimensional condition. For a section having a circular cross section of radius B, or for a section having a square cross section of span 2B, Eq. (A.1) becomes

$$\sigma_v = \frac{B}{2K \tan \varphi}\left(\gamma - \frac{2c}{B}\right)\left(1 - e^{-\frac{2Z}{B} K \tan \varphi}\right) + qe^{-\frac{2Z}{B} K \tan \varphi} \qquad (A.2)$$

where all the terms are the same as in Eq. (A.1) except B, which is the radius or span of the container. If only the surcharge is considered, i.e., γ and c equal 0, these equations can be reduced to

$$\sigma_v = qe^{-\frac{Z}{B} K \tan \varphi} \qquad (A.1a)$$

$$\sigma_v = qe^{-\frac{2Z}{B} K \tan \varphi} \qquad (A.2a)$$

If only the weight of the material is considered, i.e.,q and c equal 0, these equations reduce to

$$\sigma_v = \frac{B\gamma}{K \tan \varphi}\left(1 - e^{-\frac{Z}{B} K \tan \varphi}\right) \qquad \text{(A.1b)}$$

$$\sigma_v = \frac{B\gamma}{2K \tan \varphi}\left(1 - e^{-\frac{2Z}{B} K \tan \varphi}\right) \qquad \text{(A.2b)}$$

COMPARISON WITH DATA OF RECORD

If we now compare these relationships with some of the data of record, we may be able to see the adequacy of the theory to predict the axial stress at any given depth. In order to compare the results with work like Jamieson's (Ref. 21), it is necessary to choose a K-value and a value for the angle of internal friction φ.

In his discussion of this work, Tschebatarioff (Ref.22) points out that the apparent ratio of lateral to axial stress K as determined from measurement at a fixed height increases with the height of the wheat in the bin. This increase is quite understandable when one considers that the axial stress σ_1 was measured at the center of the bin while the lateral stress σ_3 was measured at the edge of the bin at the same depth for the entire filling of the bin. Since the sidewall friction occurs at the edge of the sample, one can reason that the resultant redistribution of axial load through existence of shear forces would cause a nonuniform

distribution of the axial stress across the container. Consequently there is little merit to the concept of relating orthogonal stresses measured at two different locations in a material in which a nonuniform load distribution exists. If one visualized a horizontal row of grains, as in Fig. A-2a, it is then possible to define a set of forces as shown in Fig. A-2b. Force F_1 is the force applied to grain A by the grain above it. Force F_3 is the support given to grain A by the grain below it. Force F_2 is the frictional resistance provided by the wall. Force F_4 represents the friction force developed by grain B's tendency to move past grain A. If B slides, then frictional resistance is greater at the walls than in the sample body. Experiments generally verify this. Jaky (Ref. 23), for instance, while presenting contrary evidence in the form of shear data from laboratory devices states that "it is a well-known phenomenon [in] emptying the silo that material adheres to the wall: sliding occurs first in the interior of the granular material . . ." In Ref. 28, Lenczner reported some tests conducted in a glass-sided model silo, in which he placed colored sand in layers to observe the motion during emptying. Figure A-3 is a trace of the resulting motions of the horizontal lines showing the particles near the wall to have remained much more fixed than those in the center portion.

Among the items of URS equipment are containers which do have sidewall friction. Observations in these containers after the load–unload cycle show the material in the center to have been compressed more than that near the wall.

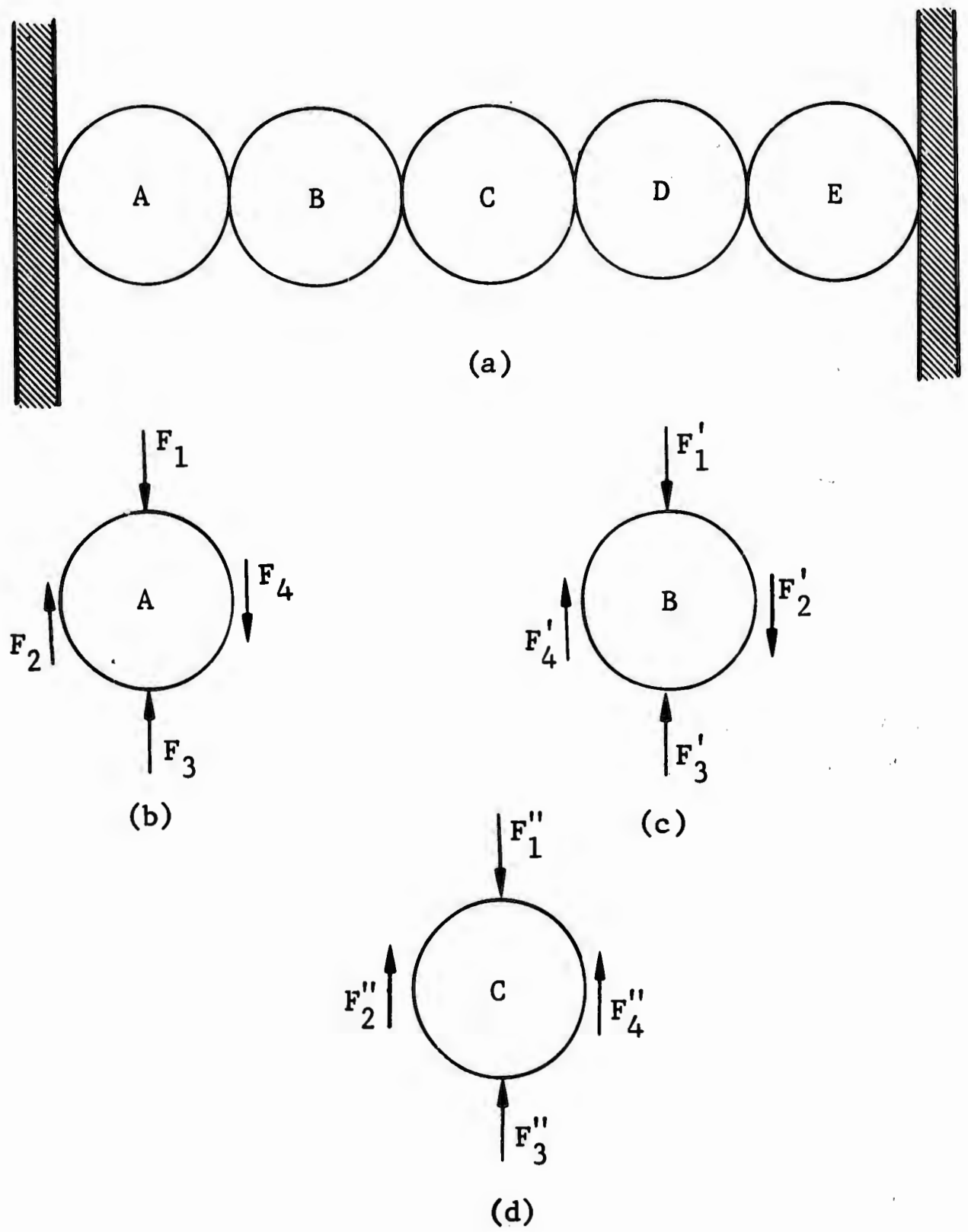

Fig. A-2. Assumption of Forces on Individual Grains Within the Sample

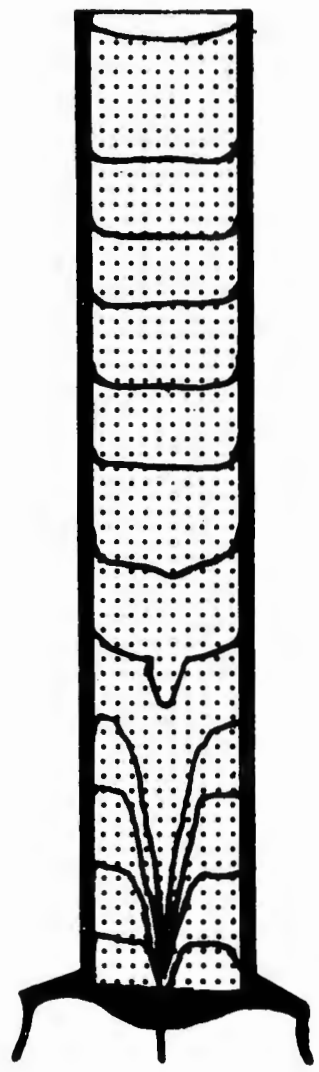

Note: The area of the door is small compared to the area of the silo.

Fig. A-3. Apparatus for Studying Flow Characteristics (Showing Effects of Greater Friction at the Wall. Taken from D. Lenczner.)

Thus, the material near the wall has shown very little displacement, while the center may show a differential displacement of over ½ in. The greater displacement at the center could either result from higher stress or higher effective compressibility as compared to the periphery.

Further consideration of the axial forces on the grains would indicate that if there is relative motion between particles, then the frictional resistance would cause a transfer of stress toward the walls. This in turn would result in a nonuniform stress distribution across the container. Therefore if the stress is larger nearer the edges, the observation of greater strains in the center must have been the result of the effective compressibility. Since it was all the same material, the difference in compressibility must result from the influence of the sidewalls. Two possible causes have been postulated: The first is that the sidewall frictional resistance itself would cause a resistance to axial motion for those grains adjacent to the wall. Motion of succeeding layers inward from the wall would be resisted by the reduced motion of the layers closer to the wall, and it would be a progressive effect, with the grain motion nearer the center approaching that which would occur if the wall effect were nonexistent. The second source of increased stiffness near the wall stems from the fact that, as implied in Section 3, granular

material becomes stiffer when particle relocation is inhibited. It is clear that a rigid wall is restrictive in this regard. A greater stiffness of material at the wall then would explain the increase of K (in the experiments discussed by Tschebatarioff) with an increase in height of the wheat, since the lateral stress measured at the wall would be associated with the higher axial stress at the wall and not with the axial stress measured at the center. It can be further reasoned that at greater depths in granular media more of this stress redistribution would have taken place and the greater would be the apparent K-value. With such nonuniformities in stress distribution, the necessary K-value should be determined from stresses measured at the same point. Since this was not done in the case discussed, it would therefore seem most reasonable to use a K-value associated with his shallower depths, i.e., at 7 ft 0.94/1.88 = 0.50 in the data presented in Ref. 21. Further, from the above considerations it can be seen that the friction angle that must be applicable is that in the medium, i.e., between grains where the failure occurs, since it must be a lower value. In the Jamieson tests, this value of φ was given as 28 deg.

In Fig. A-4, the test data for the bin having a 12- by 13.5-ft cross section is plotted as the depth of the wheat in the bin against both the vertical (axial σ_1) and horizontal (lateral σ_3) stress. Also plotted in this figure is the curve representing the results of Eq. (A.2b) for σ_v as a function of depth, using the values of the shallow

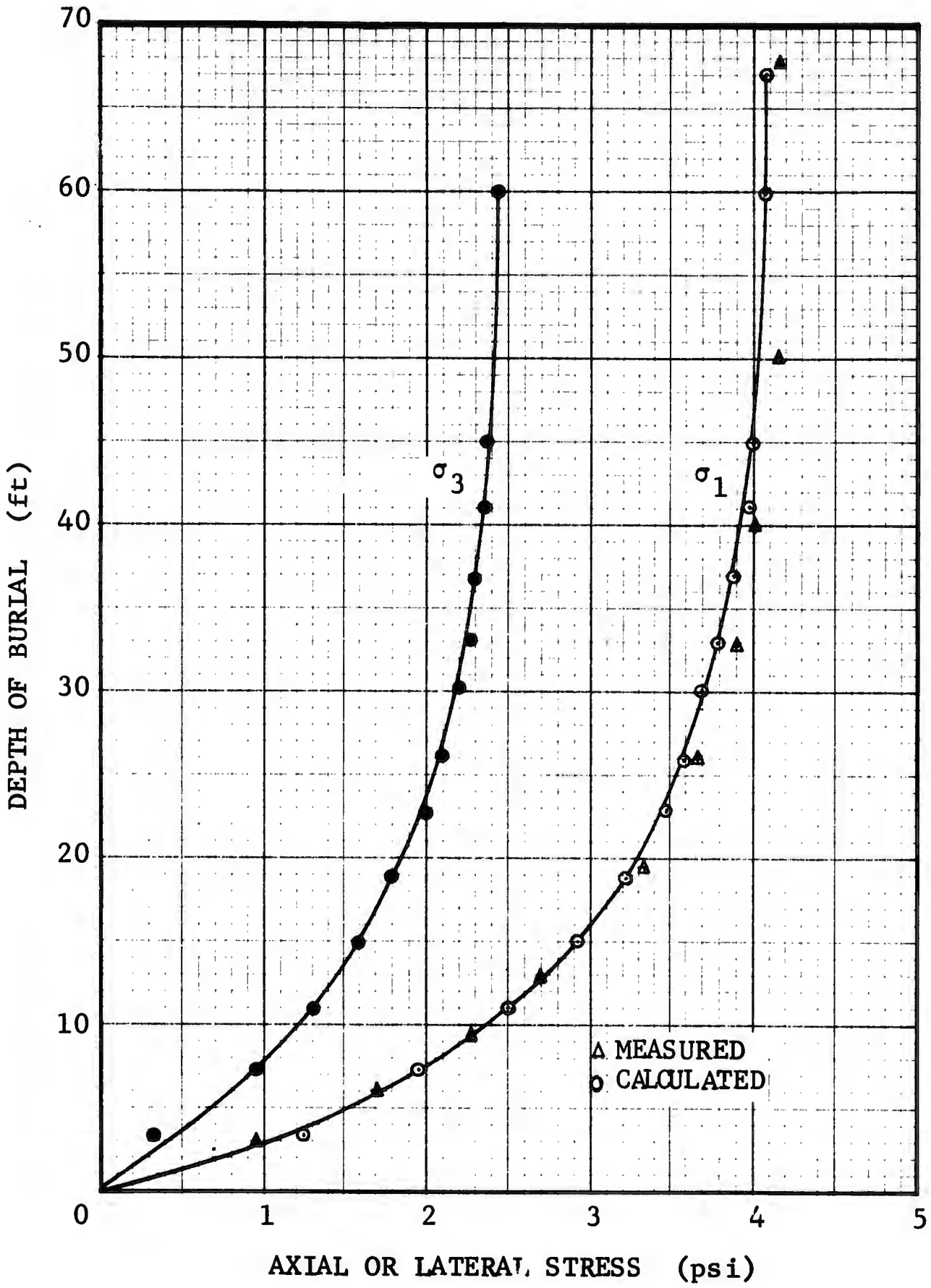

Fig. A-4. Axial and Horizontal Stresses at Bottom of a 12 x 13.5-ft Wheat Silo

depth K, the φ listed above, and assuming a B of 6.5 ft. The equation shows close agreement with the experimental data. In Fig. A-5 the same relationships are plotted for wheat in a bin having a 10- by 10-ft cross section and shows the same good agreement with Eq. (A.2b), using the appropriate values. In Fig. A-6, the same relations are plotted for sand in a model bin having a 12-in.-diameter cross section and again shows the same good agreement with the measured data. All the experimental data for the above examples are from the original work in Ref. 21. Since Eq. (A.2) has been observed to give the value of σ_1 at the bottom of the bin versus depth of fill, it appears applicable for determining the axial stress as a function of depth.

In the basic analysis the lateral stress can be obtained from the ratio K since it is constant throughout the sample. However, since it has been shown that the axial stress is not uniform across the entire cross section and since the equation gives only an average value for σ_v, the lateral stress will have some variation in its value. An evaluation of the magnitude of this variation can be obtained from the K-data in Jamieson's work, where it varies from 0.50 to 0.58. This would tend to indicate that axial stress at the edge might be as much as 16 percent higher than the average value.

COMPARISON WITH URS DATA (INCLUDING DYNAMIC EFFECT)

URS conducted some sidewall friction tests and reported the results in Ref. 29.

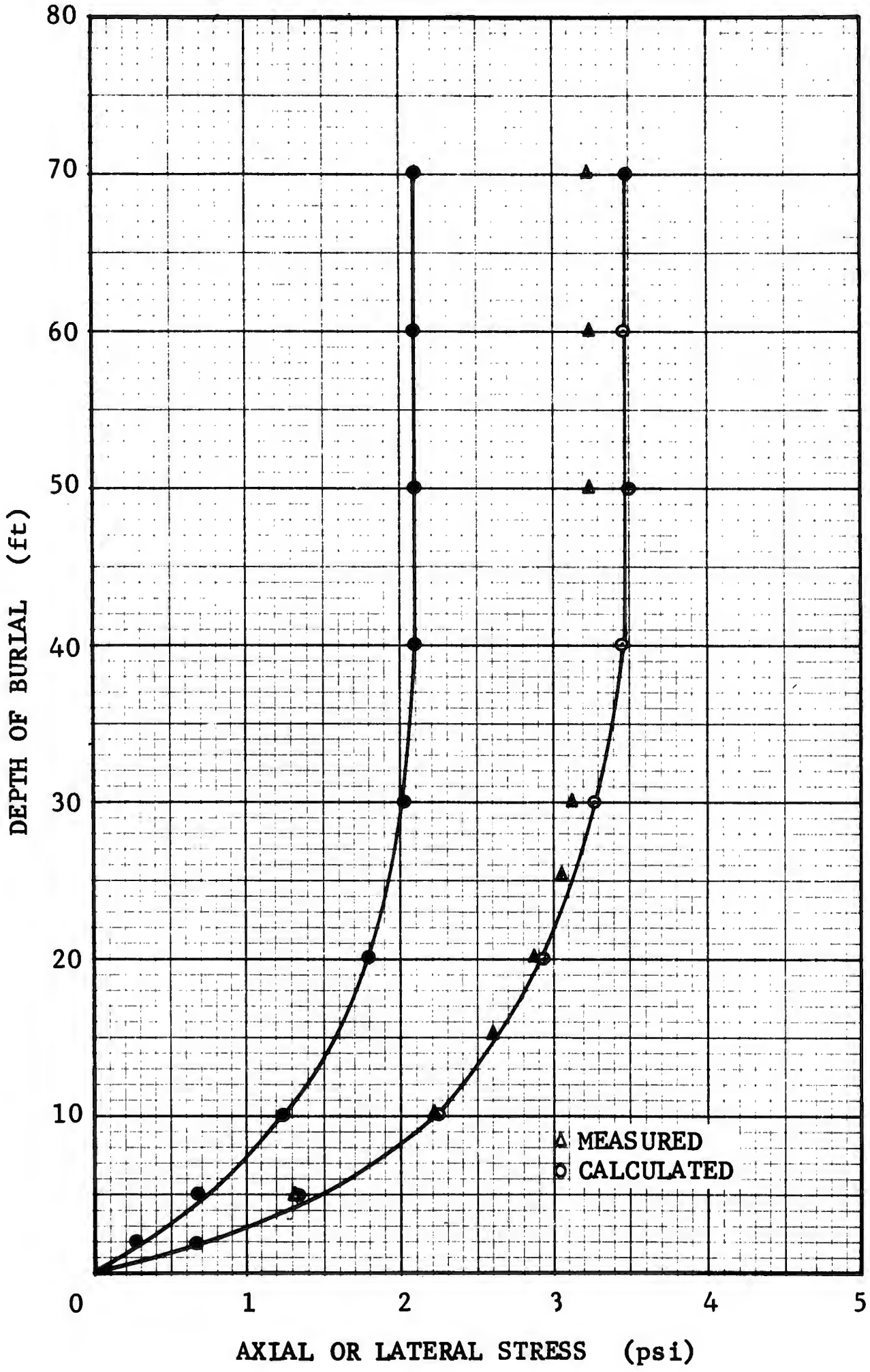

Fig. A-5. Axial and Horizontal Stress at the Bottom of a 10 x 10-ft Wheat Bin

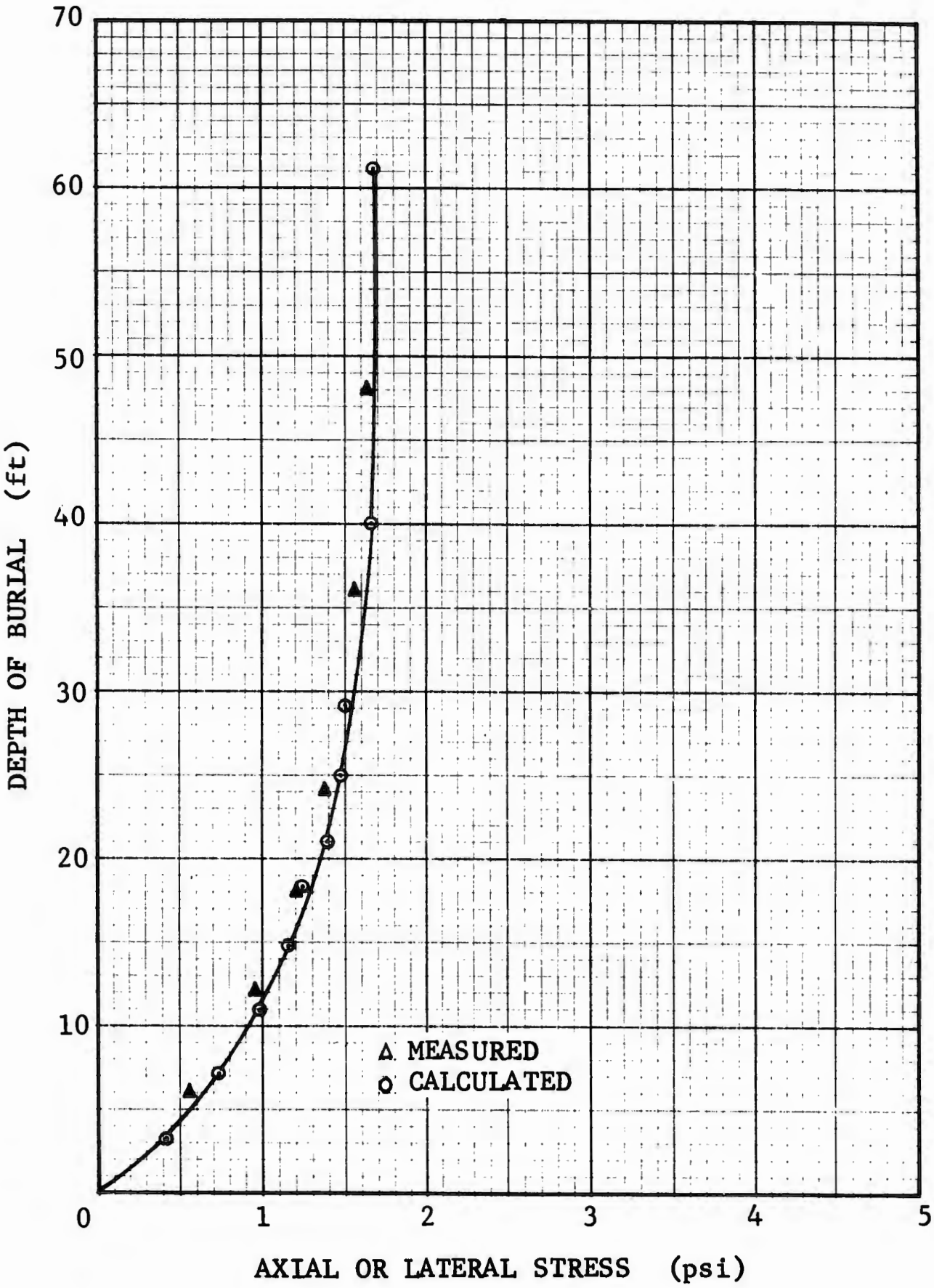

Fig. A-6. Axial Stress in a 12-in.-Diameter Sand Bin

In these tests a series of gauges was placed at various depths below the surface along the center lines of several containers. These containers varied in diameter (span in the case of a square container) from 1 to 19 in. Data from three of these tests are presented in Fig. A-7. The other results were taken in connection with other testing programs, and the data were checked against the curve. The data show the maximum discrepancy found. The container cross sections represented by the points presented in the figure are for a 4-in.^{2} container and 12-in. and 19-in. circular containers. The data presented represent the stress due to a dynamic surcharge, and since no dead-load readings were taken, Eq. (A.2a) is applicable, i.e., the buried condition represents zero load on the gauge.

In some of these tests, a gauge was placed with the face parallel to the axis of the container, which resulted in reading a K-value of 0.38. The 0.38 value was also measured in the fluid boundary and is representive of a sand having a density of between 100 and 105 lb/ft^3, which was about the density measured in some of the containers. URS tests conducted in the fluid boundary have shown that throughout the loading and during the equilibrium, K has a relatively constant value that seems related to initial density. The K-values range from 0.27 for the dense condition of Ottawa sand to approximately 0.6 for the loose sand.

By means of the relationship between K and φ of K = 1-sin φ, values for φ were obtained. They were 23.6 deg,

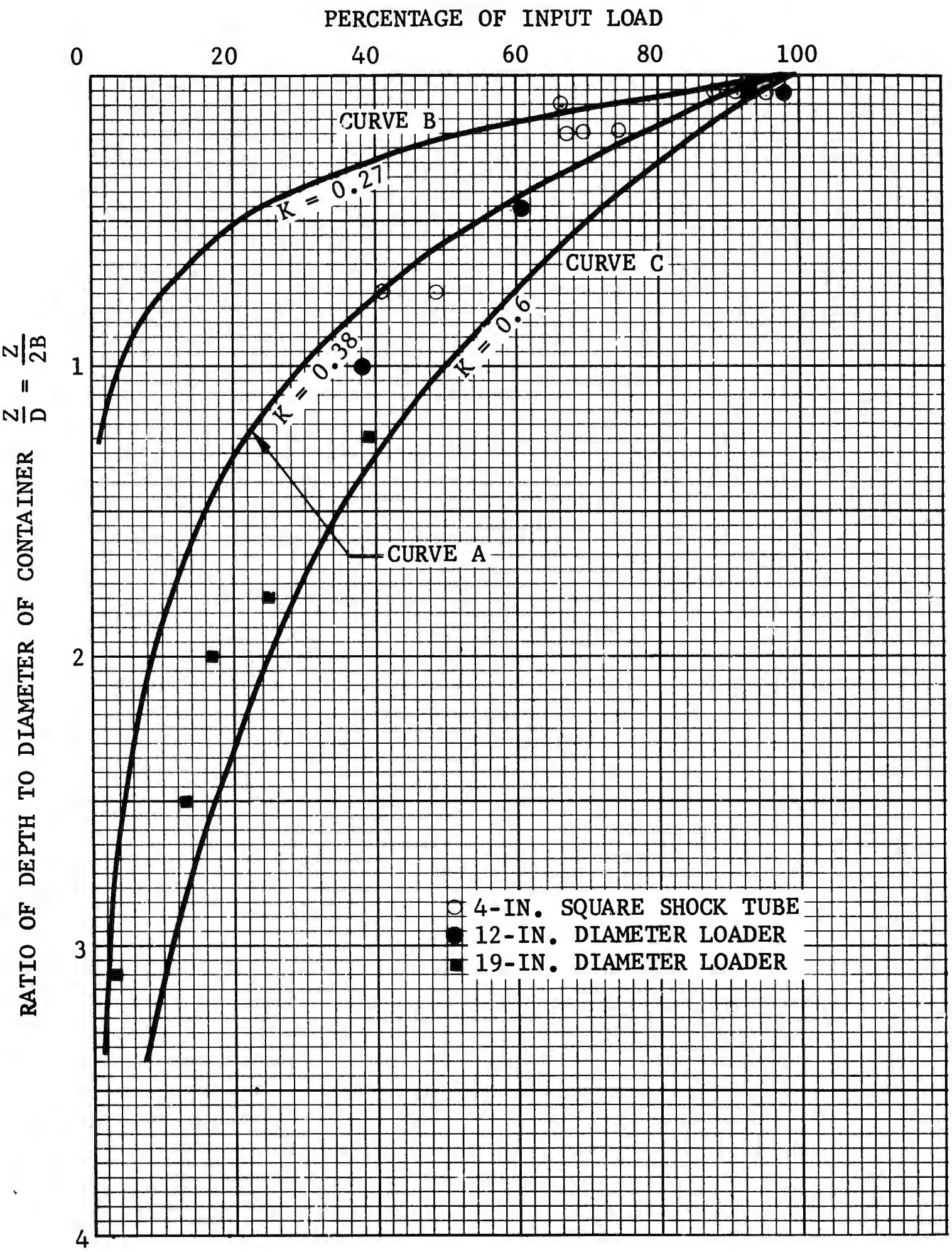

Fig. A-7. Stress As a Function of Depth Under Dynamic Load in a Steel Container

38.3 deg, and 46.9 deg for K-values of 0.6, 0.38 and 0.27, respectively. If the value for φ of 38.3 deg is used for the Ottawa sand having a K of 0.38, curve A on Fig. A-7 is obtained for equation (A.2a). Curves B and C on Fig. A-7 represent, respectively, curves for the dense and loose conditions employing the appropriate K and φ. It would seem that these curves would tend to bracket (with depth) all values for the axial stress measured along the centerline of a frictional container.

The above discussions have been really confined to the static or equilibrium condition. Much has been discussed about what effects a dynamic loading would have on sidewall friction; however, no known investigations have been conducted. In the URS tests discussed above, these loadings were with a step or square-wave pulse, but the values were read at equilibrium conditions. In the 4-in. square shock tube tests, the loading was that of an air shock (less than 10 μsec). Whereas these data fit the same curve as the data taken in the other devices having rise times around 1 ms, it was found that a type of dynamic effect was observable. At the 1/2-in. depth, the stress—time trace resembled that of the air input; however, at greater depths, a sharp spike appeared at the very front, as shown in Fig. A-8. It was discovered at very shallow depths that the peak was related to the air input. Behind this spike was located a flat, which also was related to the air input (taking into account the sidewall friction).

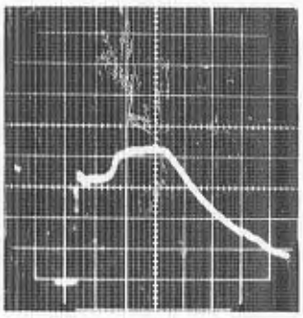

(a)

SCALES:

HORIZONTAL 2.0 ms/division
VERTICAL 13.7 psi/division

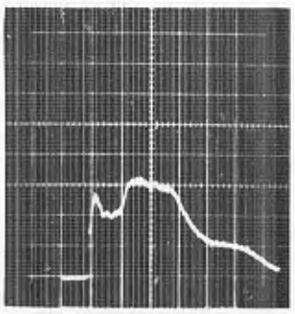

(b)

SCALES:

HORIZONTAL 2.0 ms/division
VERTICAL 5.0 psi/division

Note: The hump in these traces that arrives approximately 2 ms after the front is a characteristic disturbance in the air loading in this air shock tube and does not derive from soil behavior.

Fig. A-8. Stress—Time Traces at Depths of (a) 0.5 in. and (b) 3.0 in.

What appears to occur is that because the gauge is at the center of the sample, it first records the incident stress of the plane wave applied at the surface. This is then followed by an unloading or rarefaction wave propagated from the sidewall due to the friction there. A check of travel times of the waves correlates with this interpretation of these findings. The effect is more distinguishable at much greater depths, since the spike is all that remains at greater depths, although its magnitude is reduced. Unloading waves continue to be generated and will continue to decay the peak stress, even though a step pulse is introduced at the surface.

Some investigators have postulated that Eq. (A.2) is applicable only in deep bins or in shallow bins in which the bottom of the bin deflects enough to develop the shear resistance. It appears from the correlation for several conditions* that the equation may be applicable without these restrictions and that the compressibility of the soil under the dead weight or live load if there is one, may be sufficient to cause the straining required to develop the full shear resistance.

---

* This correlation was shown to be valid throughout the shallow as well as the deep heights of fill, where the media was resting on a rigid base. Since it showed the same validity for dynamic live loads near the surface in the URS tests, whose conditions might be considered those of a deep bin, it would seem that these restrictions may not be valid.

Those investigators who have recognized the importance of the sidewall-friction problem have attempted to solve it in a number of interesting ways. These have included segmented boundaries,* fluid boundaries** and teflon liners.

Segmented Boundary

The theory behind the segmented boundary is that the boundary is interrupted periodically so that an axial force cannot be transmitted over the entire length of the container.

A concept which explains the net effect of processes of sidewall friction in one segment of a segmented boundary is one involving a balance of axial forces. Sidewall friction is continually introducing an axial force into the wall. When this axial force gets large enough to overcome the frictional resistance between grains and wall, relative motion occurs. This motion of the wall past the grains will cause a transfer of axial stress, by means of shearing resistance, back into the soil, so that all the load is carried between segments as axial stress in the soil. If one then examines a simple balance of forces on the segment it is found that net shearing resistance along the

---

* Segmented boundaries include the ciliary and ring boundaries described in Report 1.

** Fluid boundary includes the so-called greased boundary.

top part of the segment is downward and along the lower part of the wall it is upward. Therefore the net change in the average free-field stress between a level at the top of the segment and one at the bottom is zero. The average axial free-field stress between these two levels decreases toward a minimum near mid-height of the segment. This behavior is due to the frictional resistance at the wall. From this mid-height level the stress increases until it reaches the same average stress as at the top level. The actual particle-by-particle shearing resistance may be much more complex, especially dynamically. In some instances the space between segments is filled with a compressible material which may transfer a small force down the column. This force is usually considered negligible. However, if this material becomes stiffer when laterally confined by the soil on one side (two other sides being confined by the rings), this force may be very large, and the effect may approach the rigid-wall conditions. Under dynamic conditions, the process of generating the axial force in the wall, which is due to the sidewall friction, will obviously generate an axial unloading wave in the soil, as discussed earlier. In addition, as the wall moves past the soil, the resulting sidewall friction will create a loading wave. The importance and influence of these waves is not known at this time but should be investigated in order to improve the understanding of behaviors in such devices.

The ring boundary described in Ref. 3 is an extreme condition of the segmented boundary, i.e., the segments are reduced to the thickness of an individual grain, thereby reducing the sidewall friction effects (since each ring moves with grains), so that there is no resistance to axial grain motion. The total loss in axial stress between the air loading and the opposite end of the sample is less than 5 percent. This is commensurate with the loss in the Wilson seals in the piston system. Dynamically the inertial effects of the rings may have an influence on the wave, causing a time-dependent resistance. This effect should be confined to the very front of the wave if the mass of the rings is small compared to the mass of the soil. This effect has not been fully evaluated at this time. It should be pointed out that an inertial effect will be prevalent in all segmented boundaries.

Fluid Boundary

Another approach to the sidewall friction problem has been to treat the sidewalls so that the ability of the surface to support the shear forces is reduced, i.e., to lower the coefficient of friction between the grains and the wall. In the previous discussion it was shown that, in all probability, the friction between the grains and the wall is greater than between grains. Therefore, anything that would reduce wall-to-grain friction to a value below that of grain-to-grain would reduce frictional losses.

The fluid or greased boundaries can be shown to be such treatment. In the case of the fluid boundary, a thin layer of fluid is placed between the sample and a rigid outer container. A rubber membrane between the fluid and the sample prevents the fluid from penetrating the sample. Since the fluid is unable to sustain shear forces, the loss to the sidewall is only that supportable by the stretch of the membrane. URS devices fitted with such a boundary have shown that the total loss in axial stress between the air loading and the opposite end of the sample was on the order of 12 percent. This was commensurate with the loss in the Wilson seals in the piston system at the input end.*

Another version of the fluid boundary concept is that of the greased boundary built on principles similar to those used by Rowe (Ref. 30) to reduce friction in the end platens of a triaxial shear device. This system is being used by several investigators at present, but no published reports are available to evaluate its ability to reduce the friction. It would, however, appear that for static tests this system should have the same effect. Nevertheless, the dynamic behavior may be different, since the grease would have a greater viscous effect.

Teflon Liners

Another system used by a number of investigators and which really falls into the treated-surface catagory is the use of Teflon liners. A number of investigators have used

---

* This boundary is described in detail in Ref. 29.

a single, thin layer of Teflon and come to the same conclusion as Rowe did in Ref. 30, in which he stated that "low-friction materials such as Teflon are so soft that sand grains cause deep scouring of the surface of the platen, which results in high sliding resistance." Probably the first investigator to see the effects of two layers of Teflon was Weiderman, as reported in Ref. 31, in which the addition of a second layer drastically reduced the sidewall friction.

URS conducted some tests in which single layers of Teflon up to 0.25 in. thick showed no variation from the curves in Fig. A-4, which represent the effects in rigid-walled steel and aluminum containers. However, when a second layer, 0.005 in. thick, was added, a reduction was observed. Using short overlapped lengths for the second layer caused further reduction. A similar effect could probably be obtained using even a thinner second layer. The effects of sidewall friction for the steel-wall containers (from Fig. A-7) without Teflon or with a single layer are compared in Fig. A-9 with those effects resulting from the two layers. Since K of the soil should be no different than in the case where there were no liners, the value of φ between the two layers of Teflon must be much lower than between the grains of soil. Computing the tangent of φ from Eq. (A.2a) from the measured value for σ_v at a given depth and a K of 0.38, one arrives at a φ-value of 12 deg. If Eq. (A.2a) is used to compute σ_v for various depths, one arrives at curve A' in Fig. A-9. Using

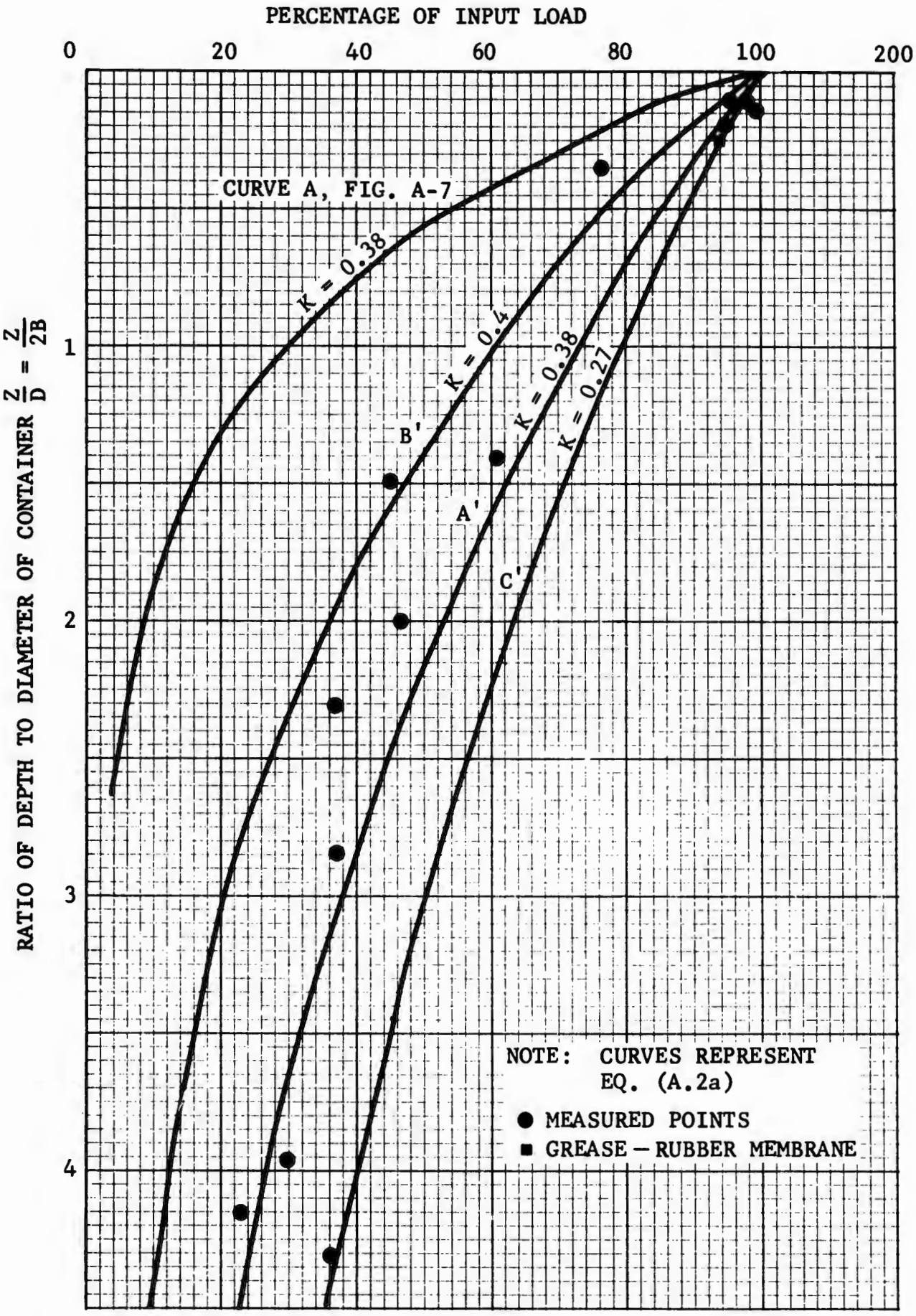

Fig. A-9. Stress As a Function of Depth Under Dynamic Load in a Teflon Lined Container

the possible spread in K for changes in density, as was done for Fig. A-7, curves B' and C' result.

Although the previous discussion shows that some knowledge of sidewall-friction behavior has been gained, it is also obvious that additional research is needed in this area. The implication of the possible effects on soil-structure interaction is also worthy of additional research.

Appendix B

EXPERIMENTAL IDENTIFICATION OF A STABLE SHOCK

An elastic wave propagating within the medium is not expected to fulfill the requirements that the wave form will propagate unchanged and with constant velocity. However, this is true of a stable shock, but a stable shock does not exist until a transition zone characteristic of the material and boundary conditions has been established. Discerning these conditions even in the laboratory requires a degree of sophistication in free-field-stress measuring technique quite beyond the ability to determine peak stress and general wave form because it cannot be discerned with a single stress gauge.* Specific experimental problems arise, where more than one gauge is required, because some variation can be expected simply from differences between gauges and differences between soil–gauge couplings. Differences such as these may be expected to alter the time required for transmission of all the necessary messages regarding particle relocation and gauge readjustment at the boundaries of each gauge as the wave front passes over the gauge. These gauge–soil adjustments are likely to be similar to the type of time-dependent process postulated

---

* In Section 3 it is brought out that the exact shape of a shock front in granular material is not describable on theoretical grounds.

earlier with regard to relaxation effects. Thus some differences might be expected in recorded rise times which are entirely local in nature. It is not easy to estimate the range of values of local variations to be expected, but it is obvious that the shorter the rise time the more likely it is that uncertainties in timing will be sizeable in comparison.

Although experimental studies of variations in free-field gauge rise times have not yet been made at URS, such observations have been reported by Seaman.* For a single test in which two gauges (of different types) were located at the same column depths, the measured rise times were approximately 300 and 500 μsec. Thus it is clear that where uncertainties in measured rise time are sizeable relative to the rise time itself, it could be difficult to discern that a constant wave form was propagating unchanged. However, because of the experimental variation, the reverse might reasonably be inferred, i.e., that differences in rise time less than some amount** do not clearly indicate any change in rise time. Barring consideration of small amplitude precursors, it is of interest that rise times observed by a number of investigators (Refs. 2–6) in various systems that are not influenced by sidewall friction are reasonably constant.***

---

* Reference 4, p. 53.

** The expected experimental variation.

*** This is true even though the tests were on various granular media and subject to differences in lateral restraint.

It seems something more than coincidental that all of the referenced studies demonstrate rise times (where shock fronts might reasonably be expected) in a range of 400 ± 200 μsec whether rise times of the applied loading are several microseconds or several milliseconds. Furthermore, data obtained at URS indicates decreasing rise times for material under ever-increasing initial pressures (up to pressures equivalent to overburdens of 500 ft). Thus the shock front or transition zone, is apparently a function of opportunities available for further particle adjustments. (A shock front in a rigid-pack of particles is likely the only condition in which the rise time is determined by the cut-off frequency for the size of particles in the array).

With regard to the question of identification of shocks (as distinquished from discerning their nature), it is also of interest that wave fronts have been observed to steepen under conditions of significant geostatic stress, i.e., where initial pressures have been on the order of 45 psi, equivalent to 65—70 ft of overburden. This has been observed where the applied overpressure has been as little as 135 psi (see Fig. 22). Therefore, even if free-field instrumentation currently lacks the desired sophistication for discerning unchanging wave forms with indisputable accuracy, it is possible to discern whether steepening of the front is followed by a constant wave velocity of the peak stress and a constant particle velocity behind the wave

front.* Of course measurement of wave velocities is directly dependent on reading time delays between corresponding points on two gauges, so that variations in apparent rise times may also be expected to produce corresponding (but not necessarily comparable) variations in apparent travel time. However, an increase in accuracy can be expected with this particular measure by increasing the distance and, hence, the travel time between stations, so that it is large with respect to rise time. In this fashion the problem of the wave-form variation, which cannot be so simply improved, may be circumvented when examining propagation velocities in order to discern behavior indicative of a propagating shock.

---

* Thus indicating a stable condition subsequent to "shocking-up", which is one of two ways of distinguishing shock behavior that is amenable to experimental detection. (The other involves observation of the degrading of a front that is steeper than a stable shock, as observed and reported by Stoll and Ebeido, Ref. 6)

Appendix C
EXPERIMENTAL FACILITIES AND SAMPLE PREPARATION

The apparatus used in this study and the techniques employed have been described in Report 1 so that only a brief description is given here.

CONFINEMENT

The applicable lateral boundary conditions provided in the laboratory tests were characterized by a stress − strain ($\sigma - \epsilon$) behavior such that $d^2\sigma/d\epsilon^2 > 0$. In order to reduce the effect of sidewall friction that accompanies most constrained compression tests in rigid-wall containers, the ring boundary shown in Fig. C-1 was used.* This boundary consists of a column of rings with an inside diameter of 1.500 in., an outside diameter of 1.680 in., and a thickness of 0.020 in. An air space of 0.003 to 0.005 in. is maintained between rings, which allows the soil and rings to displace axially without stress in the soil being transmitted axially through the rings. The rings are made of a high-strength aluminum alloy and have a unit mass roughly one-third that of the samples tested. A photograph of a portion of the rings in the Plexiglas holder (used for spacing) is presented in Fig. C-2. In the tests reported herein, the initial sample length, L_o, was 14.3 in.

---

* See Ref. 3.

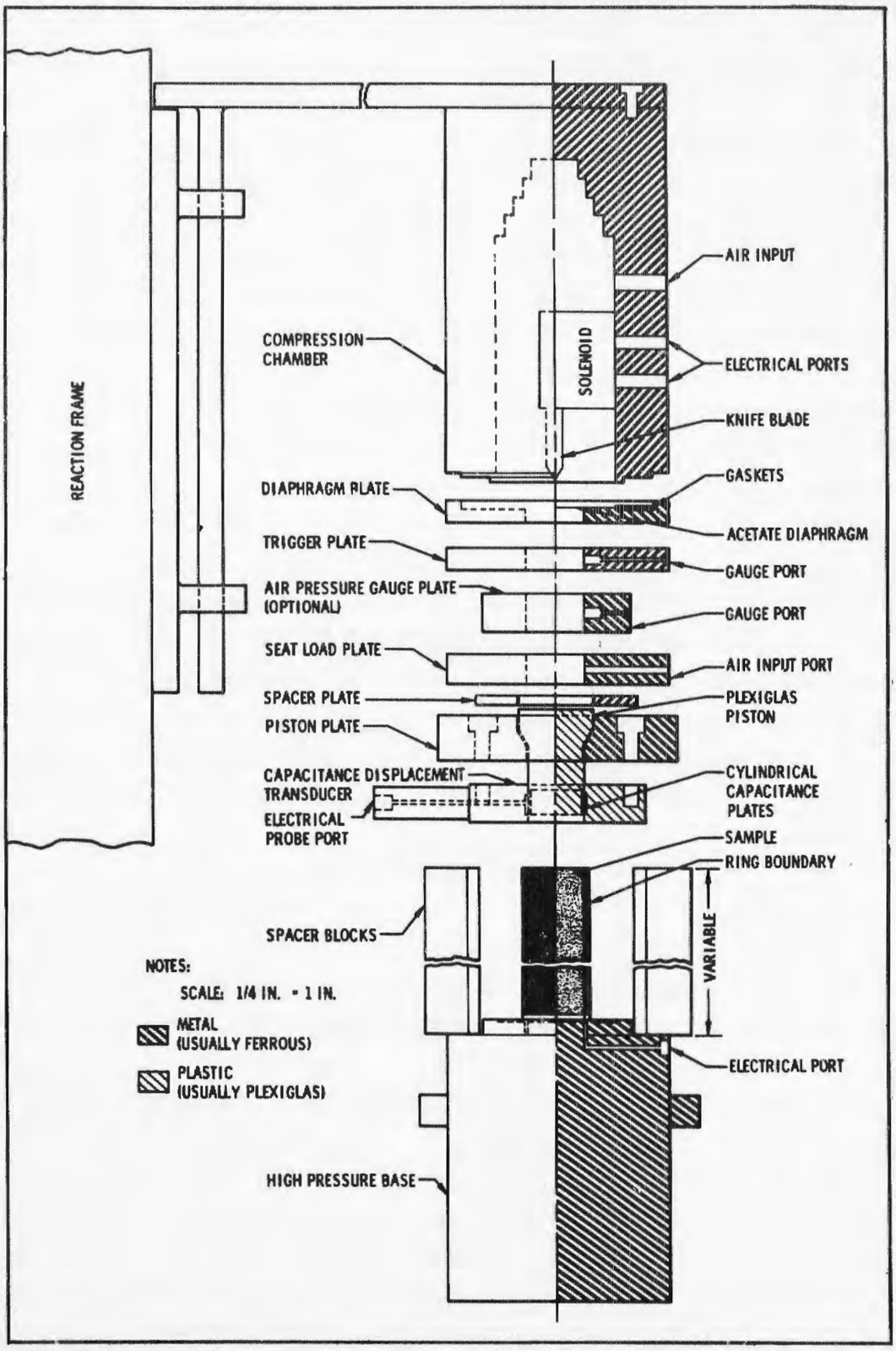

Fig. C-1. Ring Boundary Wave-Propagation Device With High-Pressure Loader

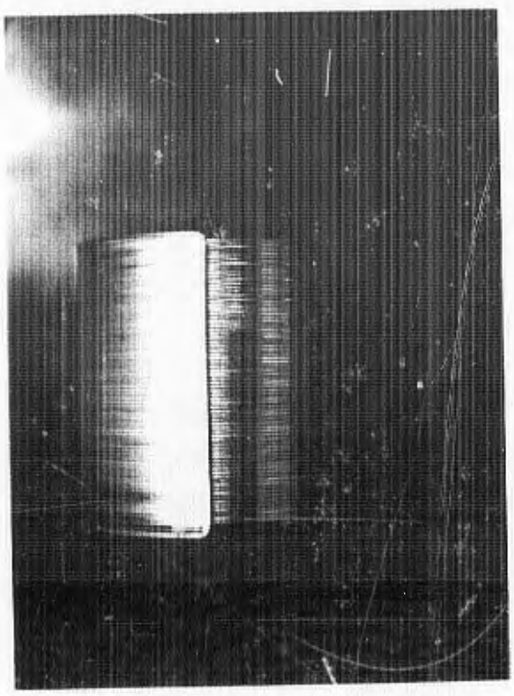

Fig. C-2. Aluminum Rings and Spacer System

The rings are assembled in the holder, the sand is placed, and the equipment completely assembled. The holders may then be removed, the rings being held in place by the friction between the sand grains and the rings. A seat load of about 5 to 10 psi was usually required to stabilize the column before removal of the holder. This seat load was then released before proceeding with the test.

LOADERS

The very fast loadings used in the wave-propagation tests were generated in a modified shock tube. The high-pressure loader (Fig. C-1) used with the ring boundary is capable of providing direct input loadings in excess of 2,000 psi, which can be increased substantially, if needed, by the use of a multiplier piston. This loading system is closed, so that a stepped pressure pulse can be applied to the sample. In addition, square-wave loadings can be generated by arresting the motion of the loading piston before the wave front propagates completely dowr the column. The rise time of the input air pressure as applied to the piston was about 200 to 300 μsec. This rise time was lengthened to about 400 to 500 μsec by the piston inertia before being reduced by shocking-up in the soil.

This same loading device was used for the quasi-static tests simply by omitting the bursting diaphragm (Fig. C-1) and controlling the rate of air input with a standard hand-operated air valve.

INSTRUMENTATION

In the quasi-static tests, stress was monitored by the piezoceramic crystal (RSG) located at the base of the sample, and displacement was monitored by a capacitance-type displacement transducer (CDT) at the top of the sample.

In the wave-propagation tests, stress was monitored as a function of time by the RSG which indicated the peak reflected stress and by free-field stress gauges located at interior points to indicate the incident stress. Displacement of the surface was monitored by the CDT. Specifications on equipment performance are given in Report 1.

TEST SAMPLE

The tests reported herein were conducted on 20 – 30 Ottawa sand at an initial density of 110 pcf. Ottawa sand is a uniform sand composed of rounded particles and has a specific gravity of 2.65. All tests were conducted on newly prepared samples placed in the following manner. Essentially, this technique consisted of allowing the sand grains to fall freely at a rate slow enough to insure reasonably dense samples.

The physical process of the technique, often referred to as a "raining" methcd, was as follows. The sand was placed in a funnel connected to a hand-held vibrator. A known weight of sand was placed in the funnel and the vibrator turned on to keep the sand flowing uniformly. A screen was attached at the base of the funnel to control the rate of emission.

Unclassified
Security Classification

DOCUMENT CONTROL DATA - R&D
(Security classification of title, body of abstract and indexing annotation must be entered when the overall report is classified)

1. ORIGINATING ACTIVITY *(Corporate author)*
United Research Services Incorporated
Burlingame, California

2a. REPORT SECURITY CLASSIFICATION
Unclassified

2b. GROUP

3. REPORT TITLE STUDY OF THE DYNAMIC STRESS-STRAIN AND WAVE-PROPAGATION CHARACTERISTICS OF SOILS: Report 4, CONCEPTS OF SHOCK BEHAVIOR IN A GRANULAR MEDIUM

4. DESCRIPTIVE NOTES *(Type of report and inclusive dates)*
Report 4 of a series of reports

5. AUTHOR(S) *(Last name, first name, initial)*
Zaccor, J. V. Wallace, N. R.
Durbin, W. L. Mason, H. G.

6. REPORT DATE	7a. TOTAL NO. OF PAGES	7b. NO. OF REFS
March 1965	157	32

8a. CONTRACT OR GRANT NO.
Contract No. DA-22-079-eng-373
b. PROJECT NO
c.
d.

9a. ORIGINATOR'S REPORT NUMBER(S)

9b. OTHER REPORT NO(S) *(Any other numbers that may be assigned this report)*
U. S. Army Engineer Waterways Experiment Station Contract Report No. 3-91

10. AVAILABILITY/LIMITATION NOTICES
Qualified requesters may obtain copies of this report from DDC.

11. SUPPLEMENTARY NOTES
Conducted for U. S. Army Engineer Waterways Experiment Station, Corps of Engineers, Vicksburg, Miss.

12. SPONSORING MILITARY ACTIVITY
Defense Atomic Support Agency

13. ABSTRACT This report summarizes current URS understanding of wave propagation in a cohesionless dry granular material in response to loadings suddenly applied and held at constant magnitude. Experimental studies of propagating waves were conducted in which measurements were made of stress and displacement, as a function of time and position along a column of granular material, so that the stress-strain relationship, and wave and particle velocities could be determined. The latter quantities, thus obtained from experimental measurements, have been compared with values obtained from applicable equations of state. A number of equations of state are considered. Two equations of state appropriate to rigid-pack conditions have been discussed. They apply to very different, but regular, packings of equi-radii elastic spheres where Hertz-type contact forces prevail and rearrangement of particles under loading is not allowed. These two equations of state were derived only from material properties of the individual particles and the packing arrangement. In addition, equations of state appropriate to conditions where particle relocations occur during loading have also been developed from the measured stress-strain relationship. From the equations of state, shock, sound, and particle velocities have been obtained as derived quantities and compared with those obtained from experiment. Excellent agreement has been found between experiment and theory. Experimentally it has been found that where no initial stress exists prior to dynamic loading, the behavior is governed entirely by particle-relocation phenomena. Where an initial-stress condition exists prior to loading, elements of response that are characteristic

(see attached continuation sheet)

DD FORM 1 JAN 64 1473

Unclassified
Security Classification

14. KEY WORDS	LINK A		LINK B		LINK C	
	ROLE	WT	ROLE	WT	ROLE	WT
Sand Shock waves Soils--Stresses Soils--Testing						

INSTRUCTIONS

1. ORIGINATING ACTIVITY: Enter the name and address of the contractor, subcontractor, grantee, Department of Defense activity or other organization *(corporate author)* issuing the report.

2*a*. REPORT SECURITY CLASSIFICATION: Enter the overall security classification of the report. Indicate whether "Restricted Data" is included. Marking is to be in accordance with appropriate security regulations.

2*b*. GROUP: Automatic downgrading is specified in DoD Directive 5200.10 and Armed Forces Industrial Manual. Enter the group number. Also, when applicable, show that optional markings have been used for Group 3 and Group 4 as authorized.

3. REPORT TITLE: Enter the complete report title in all capital letters. Titles in all cases should be unclassified. If a meaningful title cannot be selected without classification, show title classification in all capitals in parenthesis immediately following the title.

4. DESCRIPTIVE NOTES: If appropriate, enter the type of report, e.g., interim, progress, summary, annual, or final. Give the inclusive dates when a specific reporting period is covered.

5. AUTHOR(S): Enter the name(s) of author(s) as shown on or in the report. Enter last name, first name, middle initial. If military, show rank and branch of service. The name of the principal author is an absolute minimum requirement.

6. REPORT DATE: Enter the date of the report as day, month, year; or month, year. If more than one date appears on the report, use date of publication.

7*a*. TOTAL NUMBER OF PAGES: The total page count should follow normal pagination procedures, i.e., enter the number of pages containing information.

7*b*. NUMBER OF REFERENCES: Enter the total number of references cited in the report.

8*a*. CONTRACT OR GRANT NUMBER: If appropriate, enter the applicable number of the contract or grant under which the report was written.

8*b*, 8*c*, & 8*d*. PROJECT NUMBER: Enter the appropriate military department identification, such as project number, subproject number, system numbers, task number, etc.

9*a*. ORIGINATOR'S REPORT NUMBER(S): Enter the official report number by which the document will be identified and controlled by the originating activity. This number must be unique to this report.

9*b*. OTHER REPORT NUMBER(S): If the report has been assigned any other report numbers *(either by the originator or by the sponsor)*, also enter this number(s).

10. AVAILABILITY/LIMITATION NOTICES: Enter any limitations on further dissemination of the report, other than those imposed by security classification, using standard statements such as:

(1) "Qualified requesters may obtain copies of this report from DDC."

(2) "Foreign announcement and dissemination of this report by DDC is not authorized."

(3) "U. S. Government agencies may obtain copies of this report directly from DDC. Other qualified DDC users shall request through

_____."

(4) "U. S. military agencies may obtain copies of this report directly from DDC. Other qualified users shall request through

_____."

(5) "All distribution of this report is controlled. Qualified DDC users shall request through

_____."

If the report has been furnished to the Office of Technical Services, Department of Commerce, for sale to the public, indicate this fact and enter the price, if known.

11. SUPPLEMENTARY NOTES: Use for additional explanatory notes.

12. SPONSORING MILITARY ACTIVITY: Enter the name of the departmental project office or laboratory sponsoring *(paying for)* the research and development. Include address.

13. ABSTRACT: Enter an abstract giving a brief and factual summary of the document indicative of the report, even though it may also appear elsewhere in the body of the technical report. If additional space is required, a continuation sheet shall be attached.

It is highly desirable that the abstract of classified reports be unclassified. Each paragraph of the abstract shall end with an indication of the military security classification of the information in the paragraph, represented as *(TS)*, *(S)*, *(C)*, or *(U)*.

There is no limitation on the length of the abstract. However, the suggested length is from 150 to 225 words.

14. KEY WORDS: Key words are technically meaningful terms or short phrases that characterize a report and may be used as index entries for cataloging the report. Key words must be selected so that no security classification is required. Identifiers, such as equipment model designation, trade name, military project code name, geographic location, may be used as key words but will be followed by an indication of technical context. The assignment of links, rules, and weights is optional.

Abstract (continued)

of a rigid-pack condition may be found to be superimposed on the response associated with particle relocation. With regard to damage, the pertinent response is that governed by particle-relocation phenomena. Pertinent to the subject of sidewall friction, a number of observations have been made during the course of this study. These observations, and others drawn from the literature, have been summarized in an appendix in a form which provides a relationship between pressure and depth of cover for the static case. Observations of some of the effects of dynamic behavior of sidewall friction are discussed.